Interactions of cyanobacterial blooms with physical processes in lakes

By

Huaming Wu

Accepted Dissertation thesis for the partial fulfillment of the requirements for a

Doctor of Natural Sciences

Fachbereich: Natur- und Umweltwissenschaften

Rheinland-Pfälzische Technische Universität Kaiserslautern-Landau

Place and date of oral examination:

Landau, Oct. $07th$ 2024

This dissertation is based on the following manuscripts and publications (ordered by date):

1. **Huaming Wu**, Xingqiang Wu, Lorenzo Rovelli, Andreas Lorke. (2024) Selection of photosynthetic traits by turbulent mixing governs formation of cyanobacterial blooms in shallow eutrophic lakes. The ISME Journal. 18(1) doi:10.1093/ismejo/wrae021
2. **Huaming Wu**, Xingqiang Wu, Lorenzo Rovelli, Andreas Lorke. (2024). Dynamics of *Microcystis* surface scum formation under different wind conditions: the role of hydrodynamic processes at the air-water interface. Frontiers in Plant Science. 15:1370874 doi: 10.3389/fpls.2024.1370874
3. Yanxue Zhang[1], **Huaming Wu**[1], Xingqiang Wu, Hans-Peter Grossart, Andreas Lorke (2024). Intraspecific competition can promote cold-water cyanobacterial blooms: Revisiting cyanobacteria-temperature relationships based on traits. ([1]equally contribute, submitted to Ecology Letters).

Table of Contents

Abstract

Cyanobacterial harmful algal blooms (CyanHABs) are becoming increasingly frequent and intense across large geographic areas. These blooms disrupt aquatic ecosystems and pose risks to water usage due to the production of cyanotoxins by toxic strains like *Microcystis* spp. However, the interactions of cyanobacteria with physical environments (including their potential feedback effects on these environments), particularly at a deeper level (e.g., trait level), remain largely unknown.

In this thesis, laboratory experiments, field investigations, and a one-dimensional trait-based coupled hydrodynamic-phytoplankton model were used to explore the interactions of CyanHABs with physical drivers, including wind-driven hydrodynamics, turbidity, and temperature. The experiments showed that weak winds create stable conditions that increase the size of *Microcystis* colonies at the air-water interface, likely through capillary forces. *Microcystis* also reduce surface tension, decreasing surface flow velocity and potentially driving lateral surface convection, which promotes the reformation and expansion of surface scum. The coupled hydrodynamic-phytoplankton model further examined the effects of turbulence and turbidity on cyanobacterial populations at the trait level. It revealed that both turbulence and turbidity impact the photosynthetic capacity (P_{max}) of cyanobacterial populations through light competition. High diversity in P_{max} also accelerated the formation of surface blooms. This model, applied to a large shallow lake (Lake Dianchi, China), was also used to study the effect of temperature on CyanHABs, particularly how they occur under unfavorable cold-water conditions. The results showed that diversification in optimum growth temperature (T_{opt}) enhances psychrophilic strains, promoting cold-water blooms while mitigating summer blooms. T_{opt}-diverse populations exhibit an inverse relationship with summer temperatures, challenging the current cyanobacteria-temperature paradigm and indicating that environments can shape population responses in opposite directions based on trait diversity.

This thesis highlights previously unrecognized mechanisms (i.e., altering physical environments and trait distributions) by which cyanobacteria cope with varying conditions, emphasizing the need to integrate these processes into models to better understand how physical drivers will affect dynamics of CyanHABs under future climatic conditions.

1 Introduction

1.1 Cyanobacterial blooms: A global environmental issue

Harmful algal blooms (HABs) occur when harmful algae (e.g., cyanobacteria) grow excessively, often as a result of eutrophication. These blooms pose a significant global threat to the ecological integrity of inland and coastal waters, as well as to the ecosystem services they provide (Ho et al. 2019, Huisman et al. 2018, Paerl et al. 2016, Paerl and Otten 2013). HABs disrupt the functioning of aquatic ecosystems and impair water use, frequently producing toxic metabolites and malodorous compounds (Carmichael 1992, Carmichael 2001, de Figueiredo et al. 2004, Codd 1997).

The global extent, frequency, and persistence of HABs have been observed to increase in the context of climate change (Kosten et al. 2011, Mehnert et al. 2010, Paerl et al. 2016, Taranu et al. 2012). This trend underscores the growing importance of understanding driver promoting HABs in aquatic environments.

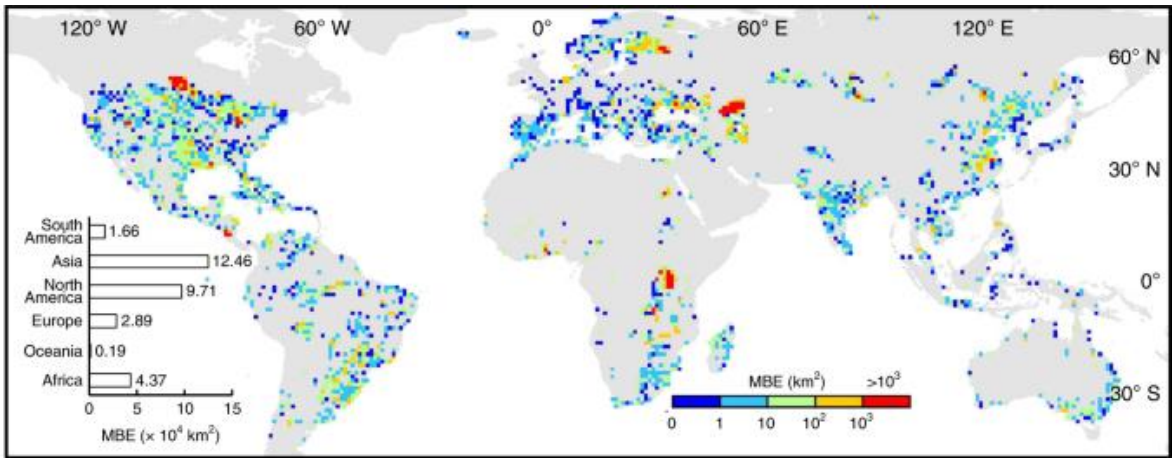

Fig. 1: Global patterns of algal blooms between 1982 and 2019, characterized by maximum bloom extent (MBE; representing the total area where algal blooms were detected at any time during the study period). Continental statistics (summarized MBE values) are presented in the panel. The bar in the middle shows the median, and the whiskers show the minimum and maximum values. Data from Hou et al. (2022).

Among bloom-forming phytoplankton, cyanobacteria are among the most common and ubiquitous groups. Many genera of cyanobacteria can form gas vesicles and colonies under natural conditions,

providing buoyancy and enabling them to maintain their position at the water surface. There, they accumulate in a scum layer to form water blooms (Huisman et al. 2018, Oliver 1994, Reynolds 1987). These surface blooms are associated with rapid deterioration of the underlying water body due to deoxygenation, resulting in fish kills, toxicity, nuisances, odors, and reduced aesthetic value of affected water bodies (Paerl 2003).

Beyond the buoyant capacity of cyanobacterial cells, biotic factors influencing bloom formation and development include colony formation mechanisms. Under natural conditions, many cyanobacterial species such as *Microcystis* spp., form colonies of varying sizes, with larger colonies playing a significant role in bloom occurrences due to their higher flotation velocities (Duan et al. 2018, Li et al. 2014, Xiao et al. 2018, Zhu et al. 2016). Larger colonies not only resist turbulent mixing but also serve as a survival strategy by reducing zooplankton grazing pressure and providing protection from heavy metals (Xiao et al. 2018).

Although mechanistic and empirical models have been developed to predict surface bloom formation, these models often fail to simulate the complex dynamics of cyanobacterial surface blooms in dynamic physical environments (this is reviewed below in more details). To improve the predictive performance of bloom models and enhance the implementation of mitigation measures and lake management strategies, it is crucial to advance our understanding of the interactions between cyanobacteria and the physical environments that control the formation, persistence, and decline of surface blooms in lakes, ponds, and reservoirs.

1.2 Effects of physical drivers on cyanobacterial blooms

Physical drivers, including turbulence, temperature, and light, play a significant role in the development and dynamics of cyanobacterial blooms (Aparicio Medrano et al. 2016a, Paerl and Ustach 1982, Soranno 1997, Wu et al. 2019). These factors shape the abiotic conditions that either promote or inhibit the growth of cyanobacteria, influencing the frequency, intensity, and spatial distribution of blooms in aquatic ecosystems. A thorough understanding of these physical drivers is essential for the prediction and management of cyanobacterial blooms.

1.2.1 Effect of wind-generated hydrodynamics on cyanobacterial blooms

Wind plays a significant role in the formation and dynamics of cyanobacterial blooms. While wind-generated large-scale motions, such as waves and circulation, are much larger than cyanobacterial cells, these motions influence the small-scale environment of phytoplankton cells through the turbulent cascade (Regel et al. 2004). By creating turbulent conditions over timescales ranging from days to months, wind affects the spatial distribution and growth-related physiological processes of cyanobacteria.

Wind-generated turbulence can vertically disperse surface scum to deeper depths when the wind speed exceeds a critical value (2.6-3 m s^{-1}, Cao et al. 2006, Wu et al. 2015). Below the critical wind speed, wind-generated flow leads to the accumulation of *Microcystis* in downwind areas of the basin (Chen et al. 2022). The intensity, frequency, and duration of wind-generated turbulence significantly impact bloom formation. Turbulence controls the vertical distribution of buoyant cyanobacterial cells or colonies (Paerl et al. 2006, Wang et al. 2016). Weak turbulence, associated with low wind speeds, often favors cyanobacterial blooms by providing calm conditions that allow cyanobacteria to float rapidly to the water surface. Studies have shown that in nutrient-rich and temperature-suitable waters, low turbulent mixing or shallow mixing depths often result in shifts in dominant phytoplankton species from diatoms to cyanobacteria (Huisman et al. 2004, Kang et al. 2019, Yu et al. 2017, Yu et al. 2018).

The size of *Microcystis* colonies mediates the effect of turbulence on their spatial distribution and determines their response to turbulent intensity. Large colonies (>500 μm) can overcome disturbances and float quickly, while smaller colonies (100-300 μm) tend to disperse throughout the mixed layer. Increased mixing strength leads to colony disaggregation (Liu et al. 2019), while intermittent disturbances of appropriate intensity enhance the size of *Microcystis* colonies. Continuous disturbance, on the other hand, inhibits their aggregation over longer periods (Zhao et al. 2020).

In addition to colony formation and flotation, turbulence affects the physiological activities and growth of cyanobacteria (Kang et al. 2019, Yu et al. 2018, Zhao et al. 2020, Zhou et al. 2016). Suitable turbulent intensity promotes the growth of cyanobacteria, whereas long-term intense turbulence inhibits their growth.

Small-scale turbulence significantly impacts photosynthesis, nutrient uptake, and the growth of *Microcystis* compared to stagnant conditions (Qin et al. 2018, Wilkinson et al. 2016, Xiao et al. 2016).

Moreover, wind-induced mixing is associated with the release of extracellular polysaccharides (EPS), which indirectly affect surface bloom formation by increasing the size and buoyancy of cyanobacteria colonies (Qin et al. 2018). Recent studies have demonstrated that EPS likely promotes the development of the scum layer by trapping colonies from the wind-stirred bulk water at the surface through the release of EPS (Wu et al. 2019).

1.2.2 Effect of temperature on cyanobacterial blooms

Temperature is a critical physical factor influencing cyanobacterial blooms. Numerous studies have shown a positive correlation between high temperatures and the occurrence of cyanobacterial blooms. High temperatures facilitate cyanobacterial growth in several ways. Laboratory experiments have demonstrated that many bloom-forming cyanobacteria species have higher optimum growth temperature (>25°C) compared to other phytoplankton species such as diatoms and green algae, giving cyanobacteria a competitive advantage as temperatures rise (Lürling et al. 2017, Paerl and Huisman 2008, Robarts and Zohary 1987).

However, growing evidence indicates that cyanobacterial blooms can also occur at low temperatures (e.g., < 15°C). Reinl et al. (2023) conceptually interpret the formation of cold-water blooms as a consequence of winter limnology and physiological adaptations. They propose three possible types of cold-water bloom formation: (i) cyanobacterial blooms initiated during warm conditions that persisted into winter; (ii) metalimnetic cyanobacterial blooms brought to the surface through turbulent mixing; and (iii) blooms formed in cold water temperatures, potentially due to psychrophilic or psychrotolerant cyanobacteria. However, the detailed mechanisms underlying these processes remain unclear.

Temperature also affects cyanobacterial blooms by altering hydrodynamic processes in lakes. Thermal stratification, particularly in deep lakes, can suppress wind shear and vertical mixing, thereby facilitating surface cyanobacterial blooms (Hozumi et al. 2019, Kumagai et al. 2000). Global warming is expected to enhance lake stratification, leading to earlier stratification in spring and later destratification in autumn

(Paerl and Huisman 2008). Cyanobacteria exploit stratified conditions due to their buoyancy, allowing them to accumulate in the upper layers with warmer conditions, thus extending their growth periods.

Cyanobacterial blooms can also influence water temperatures by intensely absorbing light and affecting thermal exchange between the upper and bottom layers. It has been found that water temperatures in areas covered by surface blooms can be at least 1.5°C higher than ambient waters (Ibelings et al. 2003, Kahru et al. 1993), creating a positive feedback loop that further enhances the dominance of buoyant cyanobacteria over nonbuoyant algal species.

Moreover, global warming significantly influences precipitation and drought patterns, which can enhance cyanobacterial dominance in aquatic ecosystems. Intense precipitation events lead to increased nutrient runoff into water bodies. As these freshwater discharges decrease and residence time extends during ensuing drought conditions, the retained and concentrated nutrients promote cyanobacterial blooms (Paerl and Huisman 2008).

1.2.3 Effect of light on cyanobacterial blooms

As photosynthetic organisms, cyanobacteria rely on light for photosynthesis, making the intensity and duration of light critical factors that directly impact their growth rate and buoyancy (Visser et al. 1997). Cyanobacteria typically thrive within a specific range of light intensity that optimizes their photosynthetic efficiency. Under ideal light conditions, cyanobacteria can proliferate rapidly (Tilzer 1987). Insufficient light (or high turbidity) slows photosynthesis, limiting the growth of cyanobacteria and their capacity to form blooms. Conversely, excessively high light intensity can cause photo-inhibition, damaging the photosynthetic apparatus and leading to reduced growth or even cell death (Whitelam and Codd 1983) .

In addition to light intensity, light quality (wavelength) plays a crucial role in the growth of cyanobacteria. Studies have shown that most cyanobacteria absorb both blue and red light but use blue light less efficiently than other wavelengths (Luimstra et al. 2018, Solhaug et al. 2014). Changes in water color can shift phytoplankton succession in lakes. Previous studies have demonstrated that cyanobacteria outcompete green algae under red light, whereas green algae dominate over cyanobacteria under blue light (Luimstra et al. 2020).

Light also affects the buoyancy regulation and vertical positioning of cyanobacteria in the water column through carbon-reserve metabolism (Kromkamp and Mur 1984). The mass density of cyanobacterial cells is modulated by the rate of carbohydrates produced through photosynthesis or consumed via respiration (Ibelings et al. 1991). This mechanism allows cyanobacteria to rise to well-lit surface waters by consuming intracellular ballast and to access nutrients at greater depths after storing sufficient carbohydrates. Consequently, these surface blooms overshadow nonbuoyant phytoplankton beneath them, thereby suppressing them through competition for light. This buoyancy regulation has been extensively used in predictive models for bloom dynamics and phytoplankton succession (Aparicio Medrano et al. 2013, Ranjbar et al. 2022).

The presence of cyanobacteria can reduce light availability by creating shading and blocking light. According to Wu et al. (2021), interactions between cyanobacteria and light constitute a positive feedback regulation, enabling cyanobacteria to float upward and form surface scum within several hours.

1.3 Current research gaps

While the effects of physical factors on cyanobacteria are well-studied, most research does not delve into trait level. Previous studies often assumed that an array of averaged trait properties adequately represents the population at any given time or location, overlooking the variability of observed traits in relation to population dynamics and environmental stressors. However, increasing evidence suggests that this simplified assumption under-represents the importance of individual variation and community structure in population ecology.

Intraspecific variation is fundamental in driving intraspecific competition and shaping population responses under environmental stressors. Selection favors traits that enhance individual fitness, leading to their increased prevalence under selective pressures and reshaping trait distributions. This is particularly true for cyanobacteria, whose short generation timescales (Lochte and Turley 1988), substantial intraspecific trait variations (Rossi et al. 2023, Wu et al. 2024), and high population densities offer significant potential for alterations in trait distribution and adaptive responses. The ability of cyanobacteria to form blooms under dynamic environmental conditions is potentially affected by the coexistence or competition of different

traits. For instance, variations in photosynthetic capacity allow cyanobacteria to have different floating velocities and growth rates, leading to divergent trajectories in the water column, driving selection, and potentially influencing surface bloom formation. Furthermore, variations in optimum growth temperature (T_{opt}) may drive the formation of cold-water CyanHABs by selecting strains with lower T_{opt}. These processes may be affected by physical factors such as turbulence, turbidity, and temperature, yet these effects remain rarely explored.

Additionally, the feedback of cyanobacteria on physical environments has often been neglected in previous studies. As an important habitat of cyanobacteria, the free-water surface has unique physicochemical and biological properties compared to the underlying water (Cunliffe et al. 2013, Vella and Mahadevan 2005). However, its role in surface bloom formation has rarely been linked. At the air-water interface, interactions between cyanobacterial blooms and physical processes such as hydrodynamics can occur, as phytoplankton can affect the physical properties of surface water. For example, Chronakis et al. (2000) found that low concentrations of proteins in the culture medium of phytoplankton are sufficient to reduce water surface tension. These proteins were likely a part of the extracellular polymeric substances (EPSs) released by phytoplankton. This process potentially plays a role in the two-way interactions between cyanobacteria and wind-generated hydrodynamic processes, yet these interactions have remained scarcely explored.

To improve our understanding and prediction of cyanobacterial harmful algal blooms, more detailed studies regarding the interactions between cyanobacteria and physical environments at a deeper, trait level are required.

2 Hypotheses and research questions

The primary objective of this thesis is to advance the mechanistic understanding of cyanobacterial bloom formation in lakes. To achieve this, it is essential to study the interactions between cyanobacterial blooms and physical environments, such as hydrodynamics, turbidity, and thermal processes, in greater detail. This thesis aims to address four research questions by testing the following corresponding hypotheses.

Question 1: Are the unique hydrodynamic processes at the air-water interface linked to cyanobacterial surface blooms? How do they affect cyanobacterial bloom formation?

Hypothesis 1: The air-water interface, as an important habitat for buoyant cyanobacteria, serves as a key meeting place for their encounter and aggregation. This process may be mediated by the unique physical processes at the air-water interface, which facilitate surface bloom formation.

Question 2: Can the formation of cyanobacterial surface blooms affect the physical properties of surface water and in turn, influence cyanobacterial blooms?

Hypothesis 2: Cyanobacteria influence surface tension, inducing related hydrodynamic processes, which in turn promote bloom formation.

Question 3: What is the role of intraspecific trait variation in the formation of cyanobacterial surface scum?

Question 3.1: Do turbulence and turbidity influence the formation of surface blooms by changing the composition of photosynthetic traits within the cyanobacterial population?

Hypothesis 3.1: As photosynthesis affects both the growth and buoyancy of cyanobacteria, turbulence and turbidity can select for strains with differing photosynthetic traits by affecting light competition. This selective process plays a crucial role in the formation of cyanobacterial blooms.

Question 3.2: Are cold-water cyanobacterial blooms related to the change in thermal traits distribution? What role does temperature play in this process?

Hypothesis 3.2: Seasonal temperature variations affect the distribution of thermal traits (i.e., optimum growth temperature) within cyanobacterial populations, altering thermal adaptation and contributing to bloom formation in cold water.

3 Outline

In this thesis, laboratory mesocosm experiments, full-lake scale field investigations, and a one-dimensional trait-based phytoplankton-hydrodynamics coupling model were employed to test the hypotheses and achieve the objective.

Three publications/manuscripts containing the primary findings supporting this thesis are included in the Appendices. A brief description of each part addressing the corresponding question is outlined below:

Part 1:

Laboratory mesocosm experiments conducted in six annular flumes were used to study the interactions between cyanobacterial blooms and wind-generated hydrodynamic processes at the air-water interface (Question 1 and Question 2). Video observations were used to measure the size and velocity of cyanobacterial colonies, as well as the areal coverage of the water surface by scum under different magnitude and frequency of wind disturbance. Correlation between cyanobacteria and water surface tension were examined in a supplementary experiment.

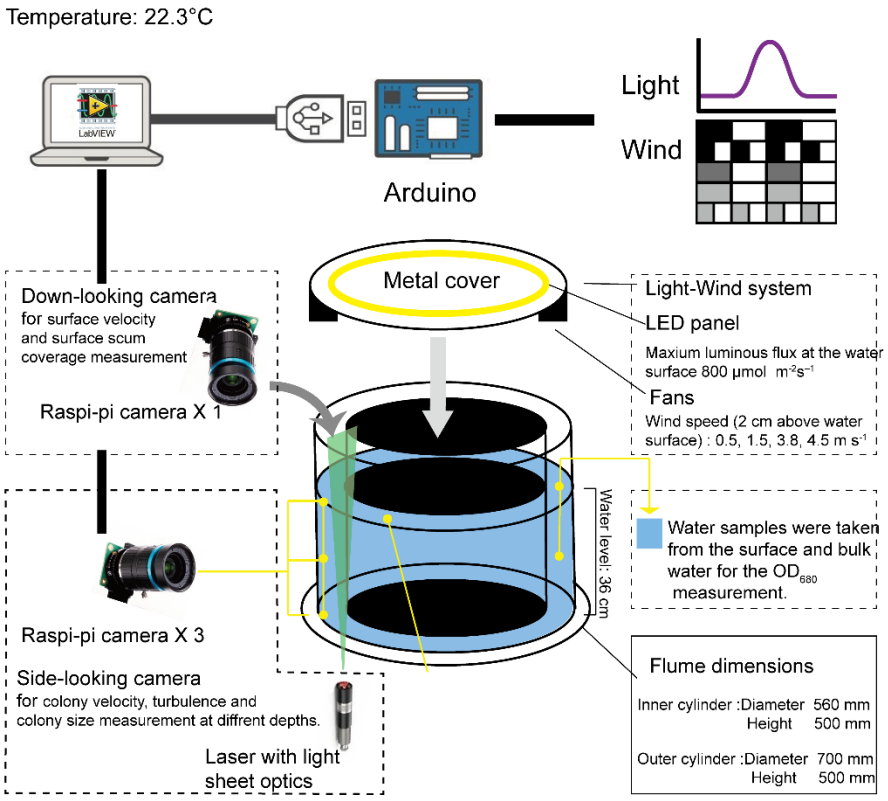

Figure 2: Laboratory mesocosms with controlled environmental conditions including wind-generated turbulence and detailed characterization of *Microcystis* colony size and velocity. The water flows between the inner and outer cylinders of the annular flume. The flow is generated by wind, provided by two diagonally arranged fans (5 cm diameter, 12 V maximum supply voltage) above the water surface. Illumination of algae is provided by the five Light-Emitting Diode (LED) panels installed on the lid. Colonies at the air-water interface are observed by a downward-looking camera. In the bulk water, colonies are observed by three side-looking cameras and vertically arranged laser light sheet illumination. The light intensity and wind speed are controlled by an Arduino microcontroller. The microcontroller, all cameras, and the laser illumination for all five flumes are controlled by a central computer using a LabView (community edition, National Instruments, USA) program.

Appendix I –

Huaming Wu, Xingqiang Wu, Lorenzo Rovelli, Andreas Lorke. (2024). Dynamics of *Microcystis* surface scum formation under different wind conditions: the role of hydrodynamic processes at the air-water interface. Frontiers in Plant Science. 15: 1370874. Doi: 10.3389/fpls.2024.1370874

Part 2:

A one-dimensional (1D) hydrodynamic model coupled with a trait-based phytoplankton model was employed to explore the effect of turbulent mixing and turbidity on the photosynthetic capacity of cyanobacterial populations and bloom formation (addressing Question 3.1). Additionally, by varying the diversity (range) of photosynthetic capacity, the impact of trait diversity on the formation of cyanobacterial blooms was examined.

Appendix II –

Huaming Wu, Xingqiang Wu, Lorenzo Rovelli, Andreas Lorke. (2024) Selection of photosynthetic traits by turbulent mixing governs formation of cyanobacterial blooms in shallow eutrophic lakes. The ISME Journal. 18(1). Doi: 10.1093/ismejo/wrae021

Part 3:

To study how cyanobacteria adapt to varying temperature conditions, particularly under climate change, and to investigate the mechanism of cold-water cyanobacterial blooms recently emerging in lakes worldwide (addressing Question 3.2), a full-lake scale field investigation was conducted in Lake Dianchi over one year. A one-dimensional hydrodynamic model coupled with a trait-based phytoplankton model focusing on thermal traits was applied to simulate the dynamics of cyanobacteria.

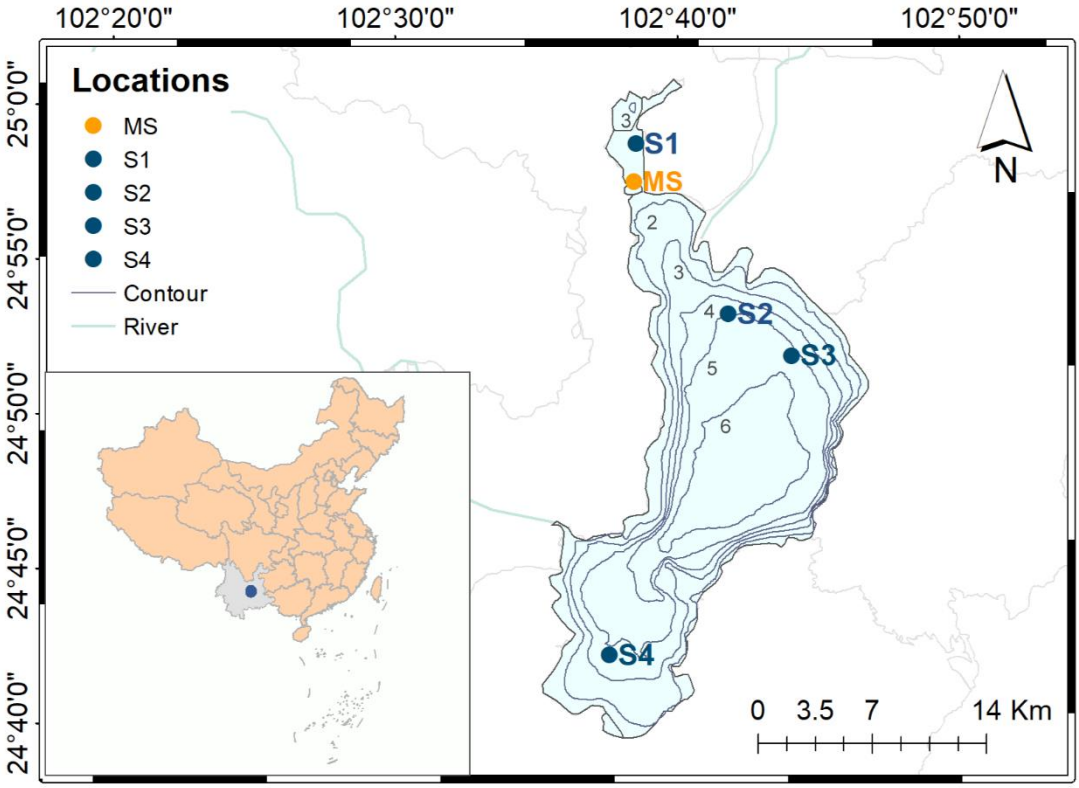

Figure 3: Bathymetry of the Lake Dianchi (light blue area) with the locations of sampling stations (S1-S4) and the meteorological station (MS). The blue solid lines denote the river and the light grey lines denote the district boundary in Lake Dianchi basin.

Appendix III –

Yanxue Zhang[1], Huaming Wu[1], Xingqiang Wu, Hans-Peter Grossart, Andreas Lorke (2024). Intraspecific competition can promote cold-water cyanobacterial blooms: Revisiting cyanobacteria-temperature relationships based on traits. ([1]equally contribute, submitted to Ecology Letters).

4. Discussion

This chapter presents the primary findings from three scientific manuscripts, enhancing the current understanding of the interactions between cyanobacterial blooms and physical processes, including processes related to hydrodynamics, light (turbidity) and temperature. The complete manuscripts and their respective supplementary materials are provided in Appendices I, II, and III, as previously mentioned. The overall results discussed in this chapter serve test the hypotheses raised and answer the scientific questions outlined in Chapter 2. Detailed discussions include laboratory mesocosm experiments focusing on the feedback of cyanobacteria to hydrodynamic conditions (section 4.1), a modeling exercise testing the effect of hydrodynamic conditions and turbidity on the selection of photosynthetic traits and bloom formation (section 4.2), and a full-lake scale field investigation, coupled with modeling (section 4.3), to explore the thermal effect on cyanobacteria and mechanism promoting cold-water blooms.

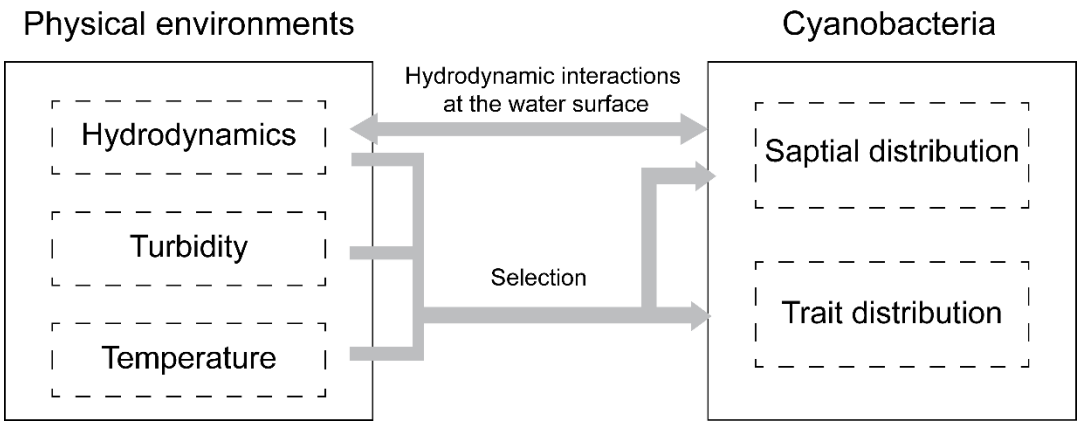

Figure 4: Schematic illustration depicting the interactions between physical environments and cyanobacteria, as presented in this thesis.

4.1 Interactions between hydrodynamics and cyanobacterial bloom at the air-water interface

Laboratory flume experiments, which implemented periodic wind disturbances, simulated the formation and disappearance of surface blooms, largely corresponding to wind speed patterns. Results indicated that the cyanobacterium *Microcystis* formed colonies or even larger aggregates at the water surface more rapidly than those in the bulk water (Appendices I). This highlights the crucial role of the air-water interface in *Microcystis* aggregation during low wind periods. Furthermore, larger *Microcystis* colonies in the bulk water during wind disturbances were significantly correlated with high areal coverage of surface blooms during preceding low wind periods (Appendices I, Fig. 6). This suggests that the surface scum layer is closely connected to the aggregation of cyanobacteria at the water surface. Previous studies suggest that these aggregates can result from cell adhesion via viscous extracellular polymeric substances (EPS) (Xiao et al. 2018, Xu et al. 2015). However, the prerequisite encounters among cells or small colonies, which facilitate this adhesion, remain unclear. This thesis argues that such encounter is facilitated by a unique physical process that only emerge at interface, that is capillary forces. Attractive forces arise in the vicinity of immersed buoyant particles, due to micro-deformation of the air-water interface (capillary immersion force, Kralchevsky and Nagayama 2000, Paunov et al. 1993). Capillary forces are an important mechanism for forming clusters of micrometer-scale to sub-meter-scale particles at the interface. For example, the common phenomenon that floating objects such as bubbles tend to clump together or cling to the sides of the container can also be driven by capillary forces (Vella and Mahadevan 2005). This process likely increases the encounter rate of *Microcystis*, leading to the aggregation of *Microcystis* into patches. This process represents a positive feedback mechanism that increases the colony size of cyanobacteria and shortens the timescale for subsequent surface bloom formation each time they accumulate at the air-water interface following periodic wind disturbances, supporting the Hypothesis 1.

In turn, supplementary laboratory experiments demonstrated a significant reduction in water surface tension with increasing *Microcystis* biomass (Appendices I, Fig. 9). This reduction in surface tension is expected to influence the physical environment of cyanobacteria, as surface tension plays a crucial role in

hydrodynamic processes. In flume experiments, normalized flow velocity decreased as scum coverage increased in the later phase (Appendices I, Fig. 8), indicating that the dense scum layer inhibited momentum transfer from wind to water. At low wind speeds, this reduction in momentum transfer can be explained by decreased water surface roughness, a result of lowered water surface tension and the suppression of capillary waves (Guseva et al. 2023, Wüest and Lorke 2003). The increased scum layer accounted for the observed decrease in water flow velocity generated by a constant wind speed over time in our experiments (Appendices I, Fig. S4) and in a previous study (Wu et al. 2019). These findings suggest that floating *Microcystis* can enhance the formation and persistence of surface scum by altering surface tension and counteracting wind-driven mixing. The reduced flow velocity due to the presence of scum layers further contributes to the increasing rate of surface scum reformation and development (Appendices I, Fig. 3) and potentially impacts hydrodynamics-related ecological processes in natural water bodies.

The reduced surface tension caused by *Microcystis* colonies can directly generate surface flows directed towards regions of higher surface tension, known as the Marangoni effect (Roché et al. 2014, Vinnichenko et al. 2018). This effect results in a lateral spreading motion towards *Microcystis*-free regions. Although we could not directly observe this flow in our experiments due to it being masked by wind-driven flow, the Marangoni effect is ubiquitously present in environmental flows (Scriven and Sternling 1960). Similar to the 'soap boat' visualization of Marangoni convection, we propose that the lateral gradient of surface tension near initial scum patches can drive their horizontal surface drift and redistribute them in the absence of external forces, such as weak wind forcing. This process may serve as a mechanism for the lateral expansion of surface scum and act as a strategy for floating cyanobacteria to alleviate competition during periods of low wind conditions.

4.2 Effects of hydrodynamics and turbidity on photosynthetic trait distribution and the resulting cyanobacterial bloom formation

Through a modeling exercise of a trait-based phytoplankton model coupled with the hydrodynamic model, how mixing dynamics and turbidity conditions select photosynthetic traits of *Microcystis* in eutrophic and shallow lakes was explored. The validity of the model was supported by the comparable

simulated cell density (up to 1.8 $\times 10^8$ cells mL^{-1}) (Ha et al. 1999, Saraf et al. 2018), timescale for bloom formation (26 – 180 days) (Duan et al. 2009, Huisman et al. 2018), and diel migration pattern (Ibelings et al. 1991) to natural cyanobacteria populations as well as the insensitive initial conditions (Appendices II). This model reveals important roles of both turbulence and turbidity in reshaping the population composition and the population-averaged photosynthetic capacity. Depending on the intensity, turbulence shifted the population-averaged photosynthetic capacity towards either a high or low photosynthetic rate through complex interactions of cyanobacteria with environments (Appendices II, Fig. 2). Differently, high turbidity accelerates the change in population-averaged photosynthetic capacity, likely by sharpening the competition for light (Appendices II, Fig. 3).

The plasticity in population-averaged photosynthetic capacity of *Microcystis* is attributed to the contrasting roles of photosynthetic capacity in migration and growth. *Microcystis* with lower photosynthetic capacity exhibit higher flotation velocities due to less accumulation of carbohydrate ballast (Appendices II, Fig. S7), positioning themselves at shallower depths to capture more light, albeit at the cost of a reduced growth rate. Conversely, *Microcystis* with high photosynthetic capacity have greater growth potential, but their excessive ballast hinders their access to the sunlit upper layers.

In *Microcystis* populations with diverse photosynthetic capacity, cyanobacteria with optimal photosynthetic traits can adjust the population composition to suit varying environmental conditions. This adaptation optimizes light resource utilization for growth. The flexibility observed in the photosynthetic capacity of cyanobacterial populations, provides novel insights into how turbulence and turbidity might affect population dynamics and primary production.

Additionally, owing to this flexibility, high diversity in photosynthetic traits within the seed population significantly promotes *Microcystis* bloom formation across a wide range of physical environmental conditions, particularly in high turbidity and low turbulence (Appendices II, Fig. 4). This diversity allows for better selection and more efficient use of available light, making it crucial for scum layer formation. In shallow eutrophic lakes, photosynthetic capacity diversity largely determines whether scum can form within a 180-day period (Appendices II, Fig. 6). A broad range of photosynthetic capacities accelerates dense scum

layer formation, reducing the development timescale by more than fourfold compared to narrower ranges (Appendices II, Fig. 6). These findings, brought to light by the modeling exercise, substantiate Hypothesis 3.1.

This model suggests that periodic moderate turbulence fosters a consistently dominant population characterized by low photosynthetic capacity (Appendices II, Fig. 2). This implies that artificial mixing techniques could be used to manipulate traits and their diversity within cyanobacterial populations as a potential bloom control measure. For instance, controlled moderate mixing can reduce the diversity of photosynthetic capacity, lower population resilience, and mitigate future blooms. This concept provides a new theoretical foundation for using artificial mixing to mitigate blooms (Visser et al. 2015).

4.3 Effect of temperature on thermal trait distribution and the cold-water cyanobacterial bloom formation

Focusing on thermal trait (optimum growth temperatures, T_{opt}) and cold-water cyanobacterial blooms, cyanobacteria dynamics in a large eutrophic shallow lake in China (Lake Dianchi) was simulated by a similar trait-based phytoplankton-hydrodynamics model as in the previous part. Compared to a narrow range or single T_{opt}, the results of simulation incorporating a wide range (T_{opt}) is closer to the observations, particularly for cold-water cyanobacterial blooms (CWCBs) in Lake Dianchi (Appendices III, Fig. 3). A broad range of T_{opt} profoundly increased the formation of cyanobacterial harmful algal blooms (CyanHABs) during cold-water periods (Appendices III, Fig. 3c). This is because a diverse T_{opt} range supports the persistence of psychrophilic cyanobacteria (Appendices III, Fig. 3d). This suggest that diversification of thermal traits, achievable through shifting selection pressures in response to environmental fluctuations (Driscoll et al., 2016), plays a crucial role in CWCBs (Hypothesis 3.2).

This rapid adaptation to temperature variations, facilitated by intraspecific competition and changes in trait distribution is similar to the findings by our previous section (section 4.2, Appendices III) and (Sandrini et al. 2016), in which environmental changes such as mixing conditions and elevated CO_2 induced adaptive phenotypic and genotypic changes in cyanobacteria over several month.

A wider range of T_{opt} unexpectedly reduced the peak amplitudes of bloom by around 10% compared to populations with narrower or single T_{opt} ranges (Appendices III, Fig. 3b). This is because the dominance of psychrophilic strains before temperature elevation subsequently hinders the growth of thermophilic strains through intraspecific competition for light. This finding suggests that populations can retain the memory of past thermal conditions by altering the distribution of T_{opt}, constituting an ecological memory—defined as 'the capacity of past experiences to influence present or future responses of a community' (Canarini et al. 2021, Letourneau et al. 2022, Padisak 1992). The lag in response to seasonally changing temperatures, owing to ecological memory and intraspecific competition, reduces bloom amplitudes and eventually homogenizes seasonal variations in cyanobacterial cell density.

Due to this ecological memory, cyanobacterial populations with varying T_{opt} ranges responded differently to changes in summer temperatures. The memory of a trait-diverse cyanobacterial population to previous low temperatures causes it to favor cooler summers over hotter ones, allowing for the accumulation of more psychrophilic strains that promote CWCBs during cold-water periods. Populations with a wide range of T_{opt} exhibited an inverse correlation with temperature, with -2°C reductions facilitating summer CyanHABs and CWCBs by up to twofold compared to 2°C increases (Appendices III, Fig. 4).

This finding challenges predictions from single-trait models and current cyanobacteria-temperature paradigms reported in previous studies (Beaulieu et al. 2013, Ho and Michalak 2019, Paerl and Huisman 2008), which implicitly neglect intraspecific variations and concluded that higher temperatures favor CyanHABs due to higher growth rates. However, it aligns with Anneville et al. (2015), who found that summertime heat waves inhibit rather than promote cyanobacterial blooms, and a global study showing that global warming has varied effects (both positive and negative) on phytoplankton blooms across 71 lakes worldwide (Ho et al. 2019). This counterintuitive phenomenon suggests that environmental conditions can elicit divergent outcomes in populations with varying intraspecific trait variations. It also demonstrates that highly diverse cyanobacterial populations can respond differently to current temperatures based on the thermal regimes they have experienced in the past, illustrating the cross-seasonal legacy effects of temperature on cyanobacteria blooms.

These results, along with those presented in the previous section (section 4.2) generally support Hypothesis 3 and are consistent with the paradigm suggesting that higher intraspecific trait diversity enhances population success across environmental gradients (Barrett and Schluter 2008, Brandenburg et al. 2018, Violle et al. 2012). The findings establish the previously unexplored link between this paradigm and cyanobacteria. Through simplified assumptions and a modeling approach, our results highlight the importance of intraspecific trait distribution in shaping cyanobacterial population dynamics. Specifically, diversification in P_{max} promotes the formation of CyanHABs and surface scum (Appendices II), while diversification in T_{opt} promotes cold-water blooms (Appendices III). Interestingly, this study shows that intraspecific competition among diverse T_{opt} can alter population responses to changing temperatures, underscoring the importance of these variations in population ecology (Des Roches et al. 2018).

4.4 Implications for future study

Laboratory experiments reveal that capillary forces and water surface tension-induced processes may impact the colony size and spatial distribution of *Microcystis* colonies (Appendices I). These findings suggest that water surface tension potentially plays a crucial yet largely unexplored role in enabling scum-forming cyanobacteria to shape their habitat in favorable ways. Therefore, further laboratory experiments and field investigations are needed to elucidate the detailed mechanisms underlying these processes and to comprehensively evaluate the dynamics of physical properties at the air-water interface and their effects on the spatial distribution of cyanobacteria. This should include quantifying the effect of capillary forces on colony aggregation at the water surface, the release rate of surface-active materials by cyanobacteria, and the extent to which these factors influence the vertical and horizontal migration of cyanobacteria. Taking these processes into account will enhance the understanding of cyanobacteria dynamics under more dynamic environmental conditions.

On the other hand, incorporating intraspecific trait variations into more complex models can describe cyanobacteria dynamics more accurately in dynamic and complex physical environments. This includes integrating additional ecological factors (e.g., nutrient limitation) and utilizing more sophisticated hydrodynamic models (Aparicio Medrano et al. 2016b), such as incorporating the interactions between

cyanobacteria, turbidity, temperature stratification, and turbulence. Future studies should also account for processes influencing cyanobacterial population dynamics that are currently unclear, such as the plastic photosynthetic capacity response of traits to the environment (e.g., temperature and nutrient), interactions among *Microcystis* colonies, and the interplay between colony size and the environment, including colony disaggregation and cell adhesion (Durham et al. 2013, Katherine R. O'Brien et al. 2004, Xiao et al. 2018).

Additional traits, such as nutrient uptake rates, vertical velocity, and the optimal light intensity of the *P-I* curve, may interact with each other, further influencing population dynamics, and should be included in future works. In deep lakes with stronger environmental gradients, cyanobacteria may experience more dynamic environmental variability. For instance, internal waves can entrain cyanobacteria within the thermocline (Cuypers et al. 2011), where strong temperature and light gradients may lead to simultaneous low-light and thermal adaptation. The interactions between gradients of temperature, light, turbulence, and nutrients, along with cyanobacterial traits, suggest an interesting possibility: cyanobacteria with varying T_{opt}, P_{max}, optimal light intensity, vertical velocity, and nutrient uptake rates may occupy their favorable depths, effectively differentiating niches throughout the water column, reducing niche overlap, and linking several independent traits. Cyanobacterial population with high diversity in different traits is expected to outperform those studied in this thesis, and have greater flexibility to cope with novel physical environments.

While this model uses literature-documented ranges of photosynthetic (Appendices II) and thermal traits (Appendices III), it would be advantageous to obtain the actual range of traits through extensive sampling and measurements prior to implementing a trait-based approach.

5 Conclusion

This thesis highlights the interactions of cyanobacteria with hydrodynamic processes at the air-water interface and examines how physical drivers like turbulence, turbidity, and temperature affect trait distribution within cyanobacterial populations and bloom formation. Several interesting findings were revealed, including: (1) the air-water interface plays an important role in the size dynamics of colonial cyanobacteria, potentially through hydrodynamic processes; (2) cyanobacteria can change the water surface tension, likely promoting the formation and horizontal expansion of cyanobacterial surface blooms; (3) turbulence and turbidity impact cyanobacterial populations and bloom formation by affecting photosynthetic trait distribution; and (4) the diversity of thermal traits determines the response of cyanobacteria to temperature fluctuations and the occurrence of cold-water cyanobacterial blooms. These findings advance the mechanistic understanding of the formation and development of cyanobacterial blooms in a dynamically changing world.

With ongoing anthropogenic climate change, underwater light attenuation is increasing, and physical variables such as temperature and wind speed are expected to become more variable. According to this thesis, these physical factors can profoundly impact cyanobacterial populations and bloom formation in previously unrecognized ways. Therefore, integrating the hydrodynamic interactions of cyanobacteria with the air-water interface and intraspecific variations into predictive models represents a key step toward understanding how future climatic conditions will affect the dynamics of cyanobacteria and aquatic ecosystems.

6 Reference

Anneville, O., Domaizon, I., Kerimoglu, O., Rimet, F. and Jacquet, S. (2015) Blue-Green Algae in a "Greenhouse Century"? New Insights from Field Data on Climate Change Impacts on Cyanobacteria Abundance. Ecosystems 18(3), 441-458.

Aparicio Medrano, E., Uittenbogaard, R.E., Dionisio Pires, L.M., van de Wiel, B.J.H. and Clercx, H.J.H. (2013) Coupling hydrodynamics and buoyancy regulation in *Microcystis* aeruginosa for its vertical distribution in lakes. Ecological Modelling 248, 41-56.

Aparicio Medrano, E., Uittenbogaard, R.E., van de Wiel, B.J., Dionisio Pires, L.M. and Clercx, H.J. (2016a) An alternative explanation for cyanobacterial scum formation and persistence by oxygenic photosynthesis. Harmful Algae 60, 27-35.

Aparicio Medrano, E., van de Wiel, B.J.H., Uittenbogaard, R.E., Dionisio Pires, L.M. and Clercx, H.J.H. (2016b) Simulations of the diurnal migration of *Microcystis* aeruginosa based on a scaling model for physical-biological interactions. Ecological Modelling 337, 200-210.

Barrett, R.D. and Schluter, D. (2008) Adaptation from standing genetic variation. Trends in Ecology and Evolution 23(1), 38-44.

Beaulieu, M., Pick, F. and Gregory-Eaves, I. (2013) Nutrients and water temperature are significant predictors of cyanobacterial biomass in a 1147 lakes data set. Limnology and Oceanography 58(5), 1736-1746.

Brandenburg, K.M., Wohlrab, S., John, U., Kremp, A., Jerney, J., Krock, B. and Van de Waal, D.B. (2018) Intraspecific trait variation and trade-offs within and across populations of a toxic dinoflagellate. Ecology Letters 21(10), 1561-1571.

Canarini, A., Schmidt, H., Fuchslueger, L., Martin, V., Herbold, C.W., Zezula, D., Gundler, P., Hasibeder, R., Jecmenica, M., Bahn, M. and Richter, A. (2021) Ecological memory of recurrent drought modifies soil processes via changes in soil microbial community. Nature Communications 12(1), 5308.

Cao, H.-S., Kong, F.-X., Luo, L.-C., Shi, X.-L., Yang, Z., Zhang, X.-F. and Tao, Y. (2006) Effects of Wind and Wind-Induced Waves on Vertical Phytoplankton Distribution and Surface Blooms of*Microcystis* aeruginosain Lake Taihu. Journal of Freshwater Ecology 21(2), 231-238.

Carmichael, W.W. (1992) Cyanobacteria secondary metabolites--the cyanotoxins. Journal of Applied Bacteriology 72(6), 445-459.

Carmichael, W.W. (2001) Health effects of toxin-producing cyanobacteria: “The CyanoHABs”. Human and Ecological Risk Assessment: An International Journal 7(5), 1393-1407.

Chen, H., Zhu, W., Wang, R., Feng, G. and Xue, Z. (2022) Rapid horizontal accumulation and bloom formation of the cyanobacterium *Microcystis* under wind stress. Hydrobiologia 850(1), 123-135.

Chronakis, I.S., Galatanu, A.N., Nylander, T. and Lindman, B. (2000) The behaviour of protein preparations from blue-green algae (Spirulina platensis strain Pacifica) at the air/water interface. Colloids and Surfaces A: Physicochemical and Engineering Aspects 173, 181-192.

Cunliffe, M., Engel, A., Frka, S., Gašparović, B., Guitart, C., Murrell, J.C., Salter, M., Stolle, C., Upstill-Goddard, R. and Wurl, O. (2013) Sea surface microlayers: A unified physicochemical and biological perspective of the air–ocean interface. Progress in Oceanography 109, 104-116.

Cuypers, Y., Vincon-Leite, B., Groleau, A., Tassin, B. and Humbert, J.F. (2011) Impact of internal waves on the spatial distribution of Planktothrix rubescens (cyanobacteria) in an alpine lake. ISME Journal 5(4), 580-589.

de Figueiredo, D.R., Azeiteiro, U.M., Esteves, S.M., Goncalves, F.J. and Pereira, M.J. (2004) Microcystin-producing blooms--a serious global public health issue. Ecotoxicology and Environmental Safety 59(2), 151-163.

Des Roches, S., Post, D.M., Turley, N.E., Bailey, J.K., Hendry, A.P., Kinnison, M.T., Schweitzer, J.A. and Palkovacs, E.P. (2018) The ecological importance of intraspecific variation. Nature Ecology & Evolution 2(1), 57-64.

Duan, H., Ma, R., Xu, X., Kong, F., Zhang, S., Kong, W., Hao, J. and Shang, L. (2009) Two-Decade Reconstruction of Algal Blooms in China's Lake Taihu. Environmental Science & Technology 43(10), 3522-3528.

Duan, Z., Tan, X., Parajuli, K., Upadhyay, S., Zhang, D., Shu, X. and Liu, Q. (2018) Colony formation in two *Microcystis* morphotypes: Effects of temperature and nutrient availability. Harmful Algae 72, 14-24.

Durham, W.M., Climent, E., Barry, M., De Lillo, F., Boffetta, G., Cencini, M. and Stocker, R. (2013) Turbulence drives microscale patches of motile phytoplankton. Nature Communications 4, 2148.

Codd, G.A., Ward, C.J. and Bell, S.G. (1997) Cyanobacterial toxins: Occurrence, modes of action, health effects and exposure routes. Archives of Toxicology Supplement 19, 399-410.

Guseva, S., Armani, F., Desai, A.R., Dias, N.L., Friborg, T., Iwata, H., Jansen, J., Lükő, G., Mammarella, I., Repina, I., Rutgersson, A., Sachs, T., Scholz, K., Spank, U., Stepanenko, V., Torma, P., Vesala, T. and Lorke, A. (2023) Bulk Transfer Coefficients Estimated From Eddy-Covariance Measurements Over Lakes and Reservoirs. Journal of Geophysical Research: Atmospheres 128(2).

Ha, K., Cho, E.-A., Kim, H.-W. and Joo, G.-J. (1999) *Microcystis* bloom formation in the lower Nakdong River, South Korea: importance of hydrodynamics and nutrient loading. Marine and Freshwater Research 50, 89-94.

Ho, J.C. and Michalak, A.M. (2019) Exploring temperature and precipitation impacts on harmful algal blooms across continental U.S. lakes. Limnology and Oceanography 65(5), 992-1009.

Ho, J.C., Michalak, A.M. and Pahlevan, N. (2019) Widespread global increase in intense lake phytoplankton blooms since the 1980s. Nature 574(7780), 667-670.

Hou, X., Feng, L., Dai, Y., Hu, C., Gibson, L., Tang, J., Lee, Z., Wang, Y., Cai, X., Liu, J., Zheng, Y. and Zheng, C. (2022) Global mapping reveals increase in lacustrine algal blooms over the past decade. Nature Geoscience 15(2), 130-134.

Hozumi, A., Ostrovsky, I., Sukenik, A. and Gildor, H. (2019) Turbulence regulation of *Microcystis* surface scum formation and dispersion during a cyanobacteria bloom event. Inland Waters 10(1), 51-70.

Huisman, J., Codd, G.A., Paerl, H.W., Ibelings, B.W., Verspagen, J.M.H. and Visser, P.M. (2018) Cyanobacterial blooms. Nature Reviews Microbiology 16(8), 471-483.

Huisman, J., Sharples, J., Stroom, J.M., Visser, P.M., Kardinaal, W.E.A., Verspagen, J.M.H. and Sommeijer, B. (2004) Changes in Turbulent Mixing Shift Competition for Light between Phytoplankton Species. Ecology 85(11), 2960-2970.

Ibelings, B.W., Vonk, M., Los, H.F.J., van der Molen, D.T. and Mooij, W.M. (2003) Fuzzy Modeling of Cyanobacterial Surface Waterblooms: Validation with Noaa-Avhrr Satellite Images. Ecological Applications 13(5), 1456-1472.

Kahru, M., Leppanen, J.-M. and Rud, O. (1993) yanobacterial blooms cause heating of the sea surface. Marine Ecology Progress Series 101, 1-7.

Kang, L., He, Y., Dai, L., He, Q., Ai, H., Yang, G., Liu, M., Jiang, W. and Li, H. (2019) Interactions between suspended particulate matter and algal cells contributed to the reconstruction of phytoplankton communities in turbulent waters. Water Research 149, 251-262.

Katherine R. O'Brien, David L. Meyer, Anya M. Waite, Ivey, G.N. and Hamilton, D.P. (2004) Disaggregation of *Microcystis* aeruginosa colonies under turbulent mixing: laboratory experiments in a grid-stirred tank. Hydrobiologia 519, 143–152.

Kosten, S., Huszar, V.L.M., Bécares, E., Costa, L.S., van Donk, E., Hansson, L.A., Jeppesen, E., Kruk, C., Lacerot, G., Mazzeo, N., De Meester, L., Moss, B., Lürling, M., Nõges, T., Romo, S. and Scheffer, M. (2011) Warmer climates boost cyanobacterial dominance in shallow lakes. Global Change Biology 18(1), 118-126.

Kralchevsky, P.A. and Nagayama, K. (2000) Capillary interactions between particles bound to interfaces, liquid films and biomembranes. Advances in Colloid and Interface Science 145, 192.

Kromkamp, J.C. and Mur, L.R. (1984) Buoyant density changes in the cyanobacterium *Microcystis* aeruginosa due to changes in the cellular carbohydrate content. FEMS Microbiology Letters 25(105-109).

Kumagai, M., Nakano, S.-i., Jiao, C., Hayakawa, K., Tsujimura, S., Nakajima, T., Frenette, J.-J. and Quesada, A. (2000) Effect of cyanobacterial blooms on thermal stratification. Limnology 1:191–195.

Letourneau, J., Holmes, Z.C., Dallow, E.P., Durand, H.K., Jiang, S., Carrion, V.M., Gupta, S.K., Mincey, A.C., Muehlbauer, M.J., Bain, J.R. and David, L.A. (2022) Ecological memory of prior nutrient exposure in the human gut microbiome. ISME Journal 16(11), 2479-2490.

Li, M., Zhu, W., Dai, X., Xiao, M., Appiah-Sefah, G. and Nkrumah, P.N. (2014) Size-dependent growth of *Microcystis* colonies in a shallow, hypertrophic lake: use of the RNA-to-total organic carbon ratio. Aquatic Ecology 48(2), 207-217.

Liu, M., Ma, J., Kang, L., Wei, Y., He, Q., Hu, X. and Li, H. (2019) Strong turbulence benefits toxic and colonial cyanobacteria in water: A potential way of climate change impact on the expansion of Harmful Algal Blooms. Science of the Total Environment 670, 613-622.

Lochte, K. and Turley, C.M. (1988) Bacteria and cyanobacteria associated with phytodetritus in the deep sea. Nature 333, 67–69.

Luimstra, V.M., Schuurmans, J.M., Verschoor, A.M., Hellingwerf, K.J., Huisman, J. and Matthijs, H.C.P. (2018) Blue light reduces photosynthetic efficiency of cyanobacteria through an imbalance between photosystems I and II. Photosynth Res 138(2), 177-189.

Luimstra, V.M., Verspagen, J.M.H., Xu, T., Schuurmans, M. and Huisman, J. (2020) Changes in water color shift competition between phytoplankton species with contrasting light-harvesting strategies. Ecology 101(3), e02951.

Lürling, M., Van Oosterhout, F. and Faassen, E. (2017) Eutrophication and Warming Boost Cyanobacterial Biomass and Microcystins. Toxins 9(2).

Mehnert, G., Leunert, F., Cires, S., Johnk, K.D., Rucker, J., Nixdorf, B. and Wiedner, C. (2010) Competitiveness of invasive and native cyanobacteria from temperate freshwaters under various light and temperature conditions. Journal of Plankton Research 32(7), 1009-1021.

Oliver (1994) Floating and sinking in gas-vacuolate cyanobacteria. Journal of Phycology 30, 161-173.

Padisak, J. (1992) Seasonal succession of phytoplankton in a large shallow lake (Balaton, Hungary) - a dynamic approach to ecological memory, its possible role and mechanisms. Journal of Ecology 80, 217-230.

Paerl, H.W. (2003) Nuisance phytoplankton blooms in coastal, estuarine, and inland waters1. Limnology and Oceanography 33(4part2), 823-843.

Paerl, H.W., Gardner, W.S., Havens, K.E., Joyner, A.R., McCarthy, M.J., Newell, S.E., Qin, B. and Scott, J.T. (2016) Mitigating cyanobacterial harmful algal blooms in aquatic ecosystems impacted by climate change and anthropogenic nutrients. Harmful Algae 54, 213-222.

Paerl, H.W. and Huisman, J. (2008) Blooms Like It Hot. Science 320(4).

Paerl, H.W. and Otten, T.G. (2013) Harmful cyanobacterial blooms: causes, consequences, and controls. Microbial Ecology 65(4), 995-1010.

Paerl, H.W. and Ustach, J.F. (1982) Blue-green algal scums: An explanation for their occurrence during freshwater blooms1. Limnology and Oceanography 27(2), 212-217.

Paerl, H.W., Valdes, L.M., Peierls, B.L., Adolf, J.E. and Harding, L.J.W. (2006) Anthropogenic and climatic influences on the eutrophication of large estuarine ecosystems. Limnology and Oceanography 51(1part2), 448-462.

Qin, B., Yang, G., Ma, J., Wu, T., Li, W., Liu, L., Deng, J. and Zhou, J. (2018) Spatiotemporal Changes of Cyanobacterial Bloom in Large Shallow Eutrophic Lake Taihu, China. Frontiers in Microbiology 9, 451.

Ranjbar, M.H., Hamilton, D.P., Etemad-Shahidi, A. and Helfer, F. (2022) Impacts of atmospheric stilling and climate warming on cyanobacterial blooms: An individual-based modelling approach. Water Research 221.

Regel, R.H., Brookes, J.D., Ganf, G.G. and Griffiths, R.W. (2004) The influence of experimentally generated turbulence on the Mash01 unicellular *Microcystis* aeruginosa strain. Hydrobiologia 517, 107–120.

Reinl, K.L., Harris, T.D., North, R.L., Almela, P., Berger, S.A., Bizic, M., Burnet, S.H., Grossart, H.P., Ibelings, B.W., Jakobsson, E., Knoll, L.B., Lafrancois, B.M., McElarney, Y., Morales-Williams, A.M., Obertegger, U., Ogashawara, I., Paule-Mercado, M.C., Peierls, B.L., Rusak, J.A., Sarkar, S., Sharma, S., Trout-Haney, J.V., Urrutia-Cordero, P., Venkiteswaran, J.J., Wain, D.J., Warner, K., Weyhenmeyer, G.A. and Yokota, K. (2023) Blooms also like it cold. Limnology and Oceanography Letters 8(4), 546-564.

Reynolds, C.S. (1987) Cyanobacterial water-blooms. Advances in botanical research, 1987, 13: 67-143.

Robarts, R.D. and Zohary, T. (1987) Temperature effects on photosynthetic capacity, respiration, and growth rates of bloom-forming cyanobacteria. New Zealand Journal of Marine and Freshwater Research 21(3), 391-399.

Roché, M., Li, Z., Griffiths, I.M., Le Roux, S., Cantat, I., Saint-Jalmes, A. and Stone, H.A. (2014) Marangoni Flow of Soluble Amphiphiles. Physical Review Letters 112(20).

Rossi, S., Carecci, D. and Ficara, E. (2023) Thermal response analysis and compilation of cardinal temperatures for 424 strains of microalgae, cyanobacteria, diatoms and other species. Science of The Total Environment 873, 162275.

Sandrini, G., Ji, X., Verspagen, J.M., Tann, R.P., Slot, P.C., Luimstra, V.M., Schuurmans, J.M., Matthijs, H.C. and Huisman, J. (2016) Rapid adaptation of harmful cyanobacteria to rising CO2. The Proceedings of the National Academy of Sciences 113(33), 9315-9320.

Saraf, S.R., Frenkel, A., Harke, M.J., Jankowiak, J.G., Gobler, C.J. and McElroy, A.E. (2018) Effects of *Microcystis* on development of early life stage Japanese medaka (Oryzias latipes): Comparative toxicity of natural blooms, cultured *Microcystis* and microcystin-LR. Aquatic Toxicology 194, 18-26.

Scriven, L.E. and Sternling, C.V. (1960) The Marangoni effects. Nature 187, 186-188.

Solhaug, K.A., Xie, L. and Gauslaa, Y. (2014) Unequal allocation of excitation energy between photosystem II and I reduces cyanolichen photosynthesis in blue light. Plant and Cell Physiology 55(8), 1404-1414.

Soranno, P.A. (1997) Factors affecting the timing of surface scums and epilimnetic blooms of blue-green algae in a eutrophic lake. Canadian Journal of Fisheries and Aquatic Sciences 54(9), 1965-1975.

Taranu, Z.E., Zurawell, R.W., Pick, F. and Gregory-Eaves, I. (2012) Predicting cyanobacterial dynamics in the face of global change: the importance of scale and environmental context. Global Change Biology 18(12), 3477-3490.

Tilzer, M.M. (1987) Light-dependence of photosynthesis and growth in cyanobacteria: Implications for their dominance in eutrophic lakes. New Zealand Journal of Marine and Freshwater Research 21(3), 401-412.

V.N.Paunov, P.A.Kralchevsky, N.D.Denkov and K.Nagayama (1993) Lateral Capillary Forces between Floating Submillimeter Particles. Journal of Colloid and Interface Science 157(1), 100-112.

Vella, D. and Mahadevan, L. (2005) The 'Cheerios effect'. American Journal of Physics 73, 817–825.

Vinnichenko, N.A., Plaksina, Y.Y., Baranova, K.M., Pushtaev, A.V. and Uvarov, A.V. (2018) Mobility of free surface in different liquids and its influence on water striders locomotion. Environmental Fluid Mechanics 18(5), 1045-1056.

Violle, C., Enquist, B.J., McGill, B.J., Jiang, L., Albert, C.H., Hulshof, C., Jung, V. and Messier, J. (2012) The return of the variance: intraspecific variability in community ecology. Trends in Ecology and Evolution 27(4), 244-252.

Visser, P.M., Ibelings, B.W., Bormans, M. and Huisman, J. (2015) Artificial mixing to control cyanobacterial blooms: a review. Aquatic Ecology 50(3), 423-441.

Visser, P.M., Passarge, J. and Mur, L.R. (1997) Modelling vertical migration of the cyanobacterium*Microcystis*. Hydrobiologia 349, 99–109.

W.Ibelings, B., R.Mur, L. and E.Walsby, A. (1991) Diurnal changes in buoyancy and vertical distribution in populations of *Microcystis* in two shallow lakes. Journal of Plankton Research 13(2), 419-436.

Wang, H., Zhang, Z., Liang, D., du, H., Pang, Y., Hu, K. and Wang, J. (2016) Separation of wind's influence on harmful cyanobacterial blooms. Water Research 98, 280-292.

Whitelam, G.C. and Codd, G.A. (1983) Photoinhibition of photosynthesis in the eyanobacterium Microc ystis aeruginosa. Planta 157, 561-566.

Wilkinson, A., Hondzo, M. and Guala, M. (2016) Effect of Small-Scale Turbulence on the Growth and Metabolism of <i>*Microcystis* aeruginosa</i&gt. Advances in Microbiology 06(05), 351-367.

Wu, H., Wu, X., Rovelli, L. and Lorke, A. (2024) Selection of photosynthetic traits by turbulent mixing governs formation of cyanobacterial blooms in shallow eutrophic lakes. ISME Journal 18(1).

Wu, H., Wu, X., Yang, T., Wang, C., Tian, C., Xiao, B. and Lorke, A. (2021) Feedback regulation of surface scum formation and persistence by self-shading of *Microcystis* colonies: Numerical simulations and laboratory experiments. Water Research 194, 116908.

Wu, T., Qin, B., Brookes, J.D., Shi, K., Zhu, G., Zhu, M., Yan, W. and Wang, Z. (2015) The influence of changes in wind patterns on the areal extension of surface cyanobacterial blooms in a large shallow lake in China. Science of the Total Environment 518-519, 24-30.

Wu, X., Noss, C., Liu, L. and Lorke, A. (2019) Effects of small-scale turbulence at the air-water interface on *microcystis* surface scum formation. Water Reseach 167, 115091.

Wüest, A. and Lorke, A. (2003) Small-scale hydrodynamics in lakes. Annual Review of Fluid Mechanics 35(1), 373-412.

Xiao, M., Li, M. and Reynolds, C.S. (2018) Colony formation in the cyanobacterium *Microcystis*. Biological reviews of the Cambridge Philosophical Society 93(3), 1399-1420.

Xiao, Y., Li, Z., Li, C., Zhang, Z. and Guo, J. (2016) Effect of Small-Scale Turbulence on the Physiology and Morphology of Two Bloom-Forming Cyanobacteria. PLoS One 11(12), e0168925.

Xu, F., Zhu, W., Xiao, M. and Li, M. (2015) Interspecific variation in extracellular polysaccharide content and colony formation of *Microcystis* spp. cultured under different light intensities and temperatures. Journal of Applied Phycology 28(3), 1533-1541.

Yu, Q., Chen, Y., Liu, Z., Zhu, D. and Wang, H. (2017) Longitudinal variations of phytoplankton compositions in lake-to-river systems. Limnologica 62, 173-180.

Yu, Q., Liu, Z., Chen, Y., Zhu, D. and Li, N. (2018) Modelling the impact of hydrodynamic turbulence on the competition between *Microcystis* and Chlorella for light. Ecological Modelling 370, 50-58.

Zhao, G., Gao, X., Zhang, C. and Sang, G. (2020) The effects of turbulence on phytoplankton and implications for energy transfer with an integrated water quality-ecosystem model in a shallow lake. Journal of Environmental Management 256, 109954.

Zhou, J., Qin, B. and Han, X. (2016) Effects of the magnitude and persistence of turbulence on phytoplankton in Lake Taihu during a summer cyanobacterial bloom. Aquatic Ecology 50(2), 197-208.

Zhu, W., Zhou, X., Chen, H., Gao, L., Xiao, M. and Li, M. (2016) High nutrient concentration and temperature alleviated formation of large colonies of *Microcystis*: Evidence from field investigations and laboratory experiments. Water Research 101, 167-175.

Author contributions

This thesis is based on four original research articles provided in Appendix I-IV which were conceived by all of the authors. I am the lead author of all articles and the contributions of all authors are explained in the following:

Appendix I –

Huaming Wu, Xingqiang Wu, Lorenzo Rovelli, Andreas Lorke. (2024). Dynamics of *Microcystis* surface scum formation under different wind conditions: the role of hydrodynamic processes at the air-water interface. Frontiers in Plant Science. doi: 10.3389/fpls.2024.1370874

Conceptualization: H. Wu, X. Wu and A. Lorke

Investigation: H. Wu

Methodology: L. Rovelli and A. Lorke

Formal analysis: H. Wu and A. Lorke

Writing the manuscript: H. Wu

Revising the manuscript: H. Wu, X. Wu, L. Rovelli, and A. Lorke

Appendix II –

Huaming Wu, Xingqiang Wu, Lorenzo Rovelli, Andreas Lorke. (2024) Selection of photosynthetic traits by turbulent mixing governs formation of cyanobacterial blooms in shallow eutrophic lakes. The ISME Journal. doi:10.1093/ismejo/wrae021

Conceptualization: H. Wu and A. Lorke

Model design: H. Wu and A. Lorke

Data acquisition: H. Wu

Formal analysis: H. Wu and A. Lorke

Writing the manuscript: H. Wu

Revising the manuscript: H. Wu, X. Wu, L. Rovelli, and A. Lorke

Appendix III –

Yanxue Zhang, Huaming Wu, Xingqiang Wu, Hans-Peter Grossart, Andreas Lorke (2024). Intraspecific competition promotes cold-water cyanobacterial blooms: Revisiting cyanobacteria-temperature relationships based on traits. (submitted to Ecology Letters).

Conceptualization: Y. Zhang, H. Wu and A. Lorke

Investigation: Y. Zhang

Methodology Y. Zhang and X. Wu

Model design: H. Wu and A. Lorke

Data acquisition: Y. Zhang and H. Wu

Formal analysis: Y. Zhang, H. Wu and A. Lorke

Writing the manuscript: H. Wu and Y. Zhang

Revising the manuscript: Y. Zhang, H. Wu, X. Wu, H.P. Grossart, and A. Lorke

Declaration

I hereby declare that the thesis entitled “Interactions of cyanobacterial blooms with physical processes in lakes” is the result of my own work except where otherwise indicated. It has not been submitted for any other degree at another university or scientific institution.

Landau, 8 October 2024 ……

Huaming Wu

Curriculum Vitae

Huaming Wu

Since August 2021	PhD candidate, Institute for Environmental Sciences, University of Kaiserslautern-Landau (RPTU), Germany
September 2017 – July 2020	MSc, Institute of Hydrobiology, Chinese Academy of Sciences, China
September 2013 – July 2017	BSc, School of Life Sciences and Technology, Jinan University, China
September 2010 – July 2013	Senior High School of Zhanjiang No.2, China

Acknowledgements

First and foremost, I want to express my heartfelt gratitude to my supervisor, Professor Andreas Lorke, for the incredible opportunity to join the Environmental Physics family and embark on this PhD journey. His support, valuable guidance, and insightful feedback have been crucial to completing this thesis. I am truly thankful for his patience, encouragement, and the freedom to explore my research interests at the University of Kaiserslautern-Landau. His excellent research skills and passion for scientific inquiry will benefit me throughout my life.

I am also deeply thankful to my colleagues for creating a stimulating academic environment. Special thanks to Dr. Lorenzo Rovelli for his expertise and constructive criticism, which greatly improved the quality of my work. I appreciate Christoph Bors, our former technician, for his support with the complex laboratory experiments. Angelika Holderle, our group's secretary, has been invaluable in resolving both work-related and personal issues. I am grateful to Lediane Marcon, Michael Schwarz, Jose Schreckinger, Simon Rudolph, Hao Xue, Xingxing Zhao, Clara Mendoza Lera, Fateme Gholami, and Abdullah Rumi Shishir for their contributions and companionship. Their collaboration and countless hours of discussion have enriched my research and made my PhD journey memorable. My life in Landau has been enjoyable, not only because of the environment but also because of the good memories shared with everyone.

I would also like to extend my sincere thanks to my former supervisor, Professor Xingqiang Wu, for his expertise and constructive feedback. I deeply appreciate his willingness to always be available for discussions and his commitment to my academic development. I am also grateful for his help and care during my field investigation in Lake Dianchi, China. Additionally, many thanks to Yanxue Zhang, my Chinese colleague and friend, who helped me complete the third manuscript. Without her assistance, this thesis would not have been finished on time.

Lastly, I am deeply grateful to my family for their unwavering support, love, and understanding. They have been my pillars of strength. To my parents, for their sacrifices and encouragement, and to my sister, for her

patience and faith in me, I am profoundly thankful. This thesis is dedicated to them for their constant belief in my potential and their endless support in all my endeavors.

Appendices

Appendices I

Dynamics of *Microcystis* surface scum formation under different wind conditions: the role of hydrodynamic processes at the air-water interface

Huaming Wu[a], Xingqiang Wu[b], Lorenzo Rovelli[a,c], Andreas Lorke[a]

[a]Institute for Environmental Sciences, University of Kaiserslautern-Landau (PRTU), Landau 76829, Germany

[b]Key Laboratory of Algal Biology of Chinese Academy of Sciences, Institute of Hydrobiology, Chinese Academy of Sciences, Wuhan 430072, China

[c]now at the Department of Ecology, Federal Institute of Hydrology - BfG, Koblenz 56068, Germany

Please click the following link to read the publication

https://www.frontiersin.org/journals/plant-science/articles/10.3389/fpls.2024.1370874/full

Dynamics of *Microcystis* surface scum formation under different wind conditions: the role of hydrodynamic processes at the air-water interface

Huaming Wu[1], Xingqiang Wu[2], Lorenzo Rovelli[1,3], Andreas Lorke[1]

[1]*Institute for Environmental Sciences, University of Kaiserslautern-Landau (PRTU), Landau 76829, Germany*

[2]*Key Laboratory of Algal Biology of Chinese Academy of Sciences, Institute of Hydrobiology, Chinese Academy of Sciences, Wuhan 430072, China*

[3]*now at the Department of Ecology, Federal Institute of Hydrology - BfG, Koblenz 56068, Germany*

Number of figures: 9

Number of tables:1

Abstract

Due to climate change, *Microcystis* blooms occur at increasing frequencies in aquatic ecosystems worldwide. Wind-generated turbulence is a crucial environmental stressor that can vertically disperse the *Microcystis* surface scum, reducing its light availability. Yet, the interactions of *Microcystis* scum with the wind-generated hydrodynamic processes, particularly those at the air-water interface, remain poorly understood. Here, we explore the response of *Microcystis* (including colony size and migration dynamics) to varying magnitudes and durations of intermittent wind disturbances in a mesocosm system. The flow velocities, size of *Microcystis* colonies, and the areal coverage of the water surface by scum were measured through video observations. Our results demonstrate that low wind speeds increase colony size by providing a stable condition where *Microcystis* forms a scum layer and aggregates into large colonies at the air-water interface. In contrast, wind disturbances disperse scum and generate turbulence, resulting in smaller colonies with higher magnitudes of wind disturbance. We observed that surface scum can form rapidly following a long period (6 h) of high-magnitude (4.5 m s^{-1}) wind disturbance. Furthermore, our results indicate reduced water surface tension caused by the presence of *Microcystis*, which can decrease surface flow velocity and counteract wind-driven mixing. The reduced surface tension may also drive lateral convection at the water surface. These findings suggest that *Microcystis* reduces surface tension, likely by releasing surface-active materials, as an adaptive response to various wind conditions. This could result in an increased rate of surface scum re-formation under wind conditions and potentially facilitate the lateral expansion of scum patches during weak wind periods. This study reveals new insights into how *Microcystis* copes with different wind conditions and highlights the importance of the air-water interface for *Microcystis* scum dynamics.

Keywords: Aquatic ecosystems; Cyanobacterial blooms; Wind disturbance; Surface tension; Biological-physical interactions; Capillary force

Highlights

1. Larger colony size of *Microcystis* at low wind speed

2. Rapid formation of scum after strong wind disturbances
3. Increasing re-formation rate of surface scum during recurring disturbances
4. Increasing biomass of *Microcystis* leads to reduction of water surface tension
5. Reduced surface tension can be advantageous for *Microcystis* surface scum

Introduction

Cyanobacterial blooms have been becoming a globally relevant threat to the ecological integrity of inland and coastal waters (Ho et al., 2019; Huisman et al., 2018). As one of the most common and ubiquitous cyanobacterial genera, *Microcystis* spp. can float upward to the water surface and form dense surface scum, i.e., visible mucilaginous cyanobacteria accumulating at the water surface (Oliver, 1994), disrupting the functioning of aquatic ecosystems.

Buoyancy regulation is an important cellular feature that enables *Microcystis* spp. to maintain their position at the water surface and form surface scum (Oliver, 1994; Reynolds, 1987). The buoyancy of *Microcystis* can be modulated by (i) the carbon-reserve metabolism, i.e., the accumulation of intracellular carbohydrates (Visser et al., 1997), (ii) the synthesis and collapse of gas-vesicles in the cells (Dunton and Walsby, 2005), (iii) the formation of colonies, i.e., aggregations of *Microcystis* cells embedded in a mucilaginous matrix, and (iv) trapping of gas bubbles within the colonies (Aparicio Medrano et al., 2016; Dervaux et al., 2015). The colony size of *Microcystis* is considered an important factor for surface scum formation as their floatation velocity increases with increasing colony size (Wu et al., 2020; Xiao et al., 2018).

Disturbances induced by wind are among the most important stressors that counteract scum formation (George and Edwards, 1976). Wind-generated turbulence can vertically disperse surface scum to deeper depths and reduce the light availability for *Microcystis* when the wind speed exceeds a critical value (2.6-3 m s^{-1}) (Cao et al., 2006; Wu et al., 2015). Below the critical wind speed, wind-generated flow leads to the accumulation of *Microcystis* in downwind areas of the basin (Chen et al., 2023). Although the flows generated by wind, including basin-scale circulation, waves and turbulent eddies exceed the size of *Microcystis* colonies by far, these motions are coupled through the turbulent cascade to the small-scale viscous environment of cells and colonies (Regel et al., 2004). Although wind disturbances at appropriate magnitudes can promote the aggregation of *Microcystis* colonies, continuous wind disturbances act as stressors by inhibiting growth and their aggregation through shear forces (Liu et al., 2019; O'Brien et al., 2004; Zhao et al., 2020).

The above studies have primarily focused on bulk water, without considering the presence of a free-water surface, i.e., the air-water interface. The physicochemical and biological properties at the water surface are measurably distinct from those in the underlying water, and various physical processes, such as momentum transfer from wind to water, wind-generated wave, and capillary effect can occur (Cunliffe et al., 2013; Vella and Mahadevan, 2005). For example, current knowledge focuses on how wind-generated turbulence in the water column affects colony size dynamics, but often overlooks the frequent aggregation of *Microcystis* at the water surface during low wind periods. This is due to a lack of understanding of aggregation mechanisms at the water surface and their role in colony size dynamics. Neglecting the aggregation of colonies at the water surface may lead to an overestimation of the role of colony size in surface scum formation, as larger colonies in the epilimnion are often considered as a cause (Zhu et al., 2014), instead of being the consequence of surface scum formation.

Current understandings of the interactions between *Microcystis* and wind-generated hydrodynamic processes are largely one-way, neglecting the potential feedback of *Microcystis* on hydrodynamics. Studies have revealed that phytoplankton can affect the physical properties of water; Dervaux et al. (2015) observed non-Newtonian behavior of algal suspensions at low shear stress, with viscosity increasing by three orders of magnitude. Additionally, proteins extracted from algae can reduce interfacial tension at the air-water interface, even at relatively low bulk concentrations (Chronakis et al., 2000). They attributed these findings to the release of extracellular polymeric substances (EPSs) by phytoplankton. The alteration in physical properties of water resulting from the released EPSs could be a response of phytoplankton to stressors, constituting two-way interactions between *Microcystis* and wind-generated hydrodynamic processes. However, these interactions have rarely been studied.

As a result of climate change, wind speeds are expected to decrease in some regions under future climates (Ranjbar et al., 2022; Vautard et al., 2010), necessitating the testing of how *Microcystis* responds to different magnitudes and durations of intermittent wind disturbances. In this study, we conducted laboratory experiments in annular flumes, in which wind-driven flow was simulated by controlled air circulation above the water surface. Different magnitudes of wind forcing (0.5, 1.5, 3.8, and 4.5 m s^{-1}) and durations of their

periodic occurrence (3 and 6 h) were used to simulate the periodic formation, development, dissipation and re-formation of surface scum over a period of seven days. We hypothesized that *Microcystis* surface scum can interact with the hydrodynamic processes at the air-water interface by affecting the physical properties of water, i.e., water surface tension. The experiments aimed at (i) studying the response of colony size and surface scum dynamics of *Microcystis* to wind-generated turbulence, and (ii) exploring the effect of *Microcystis* surface scum on hydrodynamic processes mediated by surface tension. The results of this study are expected to be instrumental in the mechanistic and process-based understanding of surface scum dynamics.

Materials and methods

2.1 Source of material

A stock of phytoplankton (approximately 90% of the phytoplankton was *Microcystis aeruginosa* by microscopic observation) was collected from the Moselle River in southwest Germany on 9 August 2022 during a heavy *Microcystis* bloom. Colonies were collected from the water surface using a silk plankton net with a 40 μm mesh size. To select predominantly *Microcystis* colonies, the samples were first filtered through a 500 μm sieve to remove large particles and then through a 40 μm sieve. The filtered *Microcystis* colonies with sizes between 40 and 500 μm were stored and cultured at 20 ± 1 ºC and photosynthetically active radiation (PAR) of 15 μmol photons s^{-1} m^{-2}.

2.2 Experimental design

2.2.1 Flume experiments

The dynamics of *Microcystis* colonies under different wind conditions were studied in five annular flumes with outer and inner diameters of 700 and 560 mm (Supplementary Figure S1). The light intensity and wind speed were varied in individual flumes. Flow velocities and *Microcystis* colonies were observed in video recordings with digital cameras (Raspberry Pi HQ Camera, United Kingdom, 1080p, 30 fps) at the water surface and at three different depths (near the water surface at 0 – 6 cm depth, in a middle layer at 12 – 18 cm depth and close to the flume bottom at 24 – 30 cm depth). All operations, including environmental settings (i.e., wind and light) and video recordings (i.e., cameras and laser light sheet for underwater illumination) were fully automated and computer-controlled (see Supplementary Figure S1 for details).

Before the experiment, all flumes were sterilized for 30 min using an ozone generator. The flumes were then filled with distilled water (volume: ~ 41.5 L, water height: ~ 30 cm) before a nutrient stock solution (BG-11, see Supplementary Table S1 for details) and *Microcystis* colonies were added to the five flumes. The final concentration of nutrients in the flumes was 10% (v/v) of BG-11 medium. Optical density at a wavelength of 680 nm (OD_{680}) was used as a proxy for *Microcystis* biomass (Lv et al., 2018; Wu et al., 2019) and measured by a spectrophotometer (Novaspec II, Amersham Pharmacia Biotech Inc, UK). The initial optical density (at 680 nm) of *Microcystis* in the flumes was 0.05 ± 0.01, which corresponds to an approximate cell density of 7.9×10^5 cells mL^{-1} (Lv et al., 2018).

During the following 7-day experimental period, different magnitudes (0.5, 1.5, 3.8, 4.5 m s^{-1}) and durations (3 and 6 h) of intermittent wind forcing were applied in the flumes at a constant water temperature of 22.3 ± 1.0 ℃. The chosen temperature is within the range of water temperatures for which *Microcystis* blooms were observed under field conditions (18 - 24 ℃, Feng et al., 2019). No temperature difference between the water surface, the middle layer and the bottom of the flume was observed. Two different wind forcing (high wind speed and low wind speed) were applied alternately for two different durations. The wind speed was measured 2 cm above the water surface at a location between the two fans using a hot-wire anemometer (Testo 425, Germany). The high wind speed in the flumes F1 – F5 was 4.5, 4.5, 3.8, 1.5, and 1.5 m s^{-1}, respectively, whereas a wind speed of 0.5 m s^{-1} was used in all flumes during the low wind periods (Figure 1). The high wind speed periods were defined as wind disturbances. Due to a technical issue, the experiment in F4 started at 11:00 on Day 2. Surface waves were observed in our experiment during wind disturbances; the amplitudes of the waves were determined to be < 8 mm through visual estimates using video footage. Due to the differing aerodynamic characteristics between the flume and the atmosphere, it is not easy to directly compare the airflow generated in the flumes with wind velocities measured in the atmospheric boundary layer above water surfaces. We estimated an equivalent wind speed in the atmospheric boundary layer at a standard height of 10 m (U_{10}) from observed surface flow velocities (U_0, described below) using a fixed wind factor (the ratio of wind speed at 10 m to the surface flow velocity of water, f = 0.01, (Wu, 1975)) as $U_{10}=U_0/f$.

We applied a diurnal light cycle (12:12 h light: dark periods) to all flumes. To simulate the light conditions in the field, the irradiance at the water surface was modulated as a sinusoidal function with a maximum irradiance of 800 μmol photons m^{-2} s^{-1} and truncated to zero for the nights (18:00 – 6:00) in induvial flumes (Figure 1). We defined the period 0:00 – 12:00 as stage I and the period 12:00 – 24:00 as stage II.

Videos were recorded at hourly intervals for estimating the surface flow velocity and areal coverage of the water surface with *Microcystis*. In addition, flow velocities and size of *Microcystis* colonies were observed at three different depths in the bulk water. The biomass of *Microcystis* colonies at the water surface and in the bulk water (~15 cm depth) were daily measured during 9:00- 11:00 am (low wind periods).

2.2.2 Supplementary experiment

Due to the sampling difficulties caused by strong heterogeneity in the surface scum layer and dispersal of surfactant molecules during sampling, surface tension measurements could not be conducted under the prevailing flow conditions in the flume experiment. Consequently, we conducted an additional experiment to investigate the relationship between surface tension and *Microcystis* biomass. We measured the OD_{680} (as described above) and surface tension (using the Wilhelmy plate method with a tensiometer (TC1, Lauda Scientific, Germany)) of various *Microcystis* samples at different dilution factors (0%,1.5%, 3%, 6%, 9%, 15%, 75% and 100%). To ensure the OD_{680} did not exceed the detection limit of the spectrophotometer, the OD_{680} of algal samples higher than 0.3 were diluted 10 – 50 times, and then the OD_{680} of algal samples was calculated from OD_{680} of the diluted samples multiplied by the dilution factor.

2.3 Parameters of *Microcystis* and hydrodynamics measurements

Time-resolved observations of *Microcystis* colonies were obtained from video observations of the water surface using a down-looking digital camera (for the observation of surface scum and velocities of *Microcystis*) and of the bulk water (at depths of 0 – 4 cm, 12 – 16 cm and 26 – 30 cm) using side-looking cameras (for the observation of colony size and velocities of *Microcystis*). Videos of 90 s duration were hourly recorded. During the recordings at the water surface, illumination was provided by an LED spotlight, while during the recordings of the side-looking cameras, illumination in the bulk water was provided by a vertically oriented laser light sheet, which illuminated a central plane of the flow channel using a continuous-

wave line laser (InLine HP, MediaLas, Germany; output power: 500 mW, green, 532 nm). Colonies within the approximately 3 mm thick light sheet were observed using three digital cameras in a perpendicular arrangement (Supplementary Figure S1). The resolution and field of view of the videos recorded by the cameras used in the experiments are shown in Supplementary Table S2.

Individual *Microcystis* colonies were detected in each image based on intensity thresholds during automated image processing. The analysis provided surface areal coverage of *Microcystis* (SAC, calculated as the percentage of water surface that was covered by colonies) for down-looking cameras, the equivalent spherical diameter of colonies for side-looking cameras, as well as colony velocities estimated using particle tracking velocimetry (Kelley and Ouellette 2011). We estimated and summed up the area covered by the colonies for each frame, which was then divided by the camera's field of view to calculate the SAC. The change rate of surface areal coverage (dSAC/dt) during low wind periods, representing the reformation rate of surface scum, was estimated by the difference of mean SAC between subsequent recordings. The volumetric median colony diameter (D_{v50}, i.e., the colony size corresponding to the 50th percentile of observed colony volumes) was used to characterize the average colony size as described in Wu et al. (2019) and Wu et al., (2020). More than 300 colonies on each of the videos were used to estimate D_{v50}. The rate of change of colony size (dD_{v50}/dt) was used to characterize the aggregation or disaggregation of colonies. Since surface scum formed during low wind periods and was dispersed during wind disturbances, the D_{v50} near the water surface at the beginning of a wind disturbance, when the surface scum layer was dispersed, was considered as a representative colony size at the water surface. To compare the colony size dynamics at the water surface and in the bulk water, dD_{v50}/dt in the bulk water was estimated as the difference of mean D_{v50} near the water surface during wind disturbances between subsequent recordings. The dD_{v50}/dt at the water surface was estimated by the ratio of the difference of mean D_{v50} near the water surface between the beginning of the wind disturbance and the end of the preceding wind disturbance to the duration of the wind disturbance.

The mean velocities of colonies at the water surface and in the bulk water were estimated by observing the displacement of identified colonies via particle tracking velocimetry, using the predictive tracking

algorithm described by Kelley and Ouellette (2011).

We did not observe a consistent size-dependence of colony velocities (Supplementary Figure S2) and therefore considered the observed colony velocities as a proxy for flow velocity.

We use root-mean-square velocity fluctuations (U_{rms}) as the measure of the intensity of turbulence, which scales with the square root of turbulence kinetic energy, and is calculated as:

$$U_{rms} = \sqrt{\frac{1}{2}(\overline{(u')^2} + \overline{(v')^2})} \qquad (1)$$

where the fluctuating velocity components of the horizontal (u') and vertical (v') flow velocities are the difference between the instantaneous and the temporarily averaged velocities (Reynolds decomposition: $u' = u - \bar{u}$ and $v' = v - \bar{v}$). The temporarily averaged velocity was calculated by averaging the velocities of all colonies in each video.

2.4 Statistical analyses

Shapiro-Wilk test was used to assess the normality of data. A post hoc LSD (least significant difference) test with one-way ANOVA was used to compare the surface areal coverage (SAC) and the flow velocity during low wind periods at different depths at both stages among the different flumes if the data were normally distributed with homogeneous variance, otherwise, Kruskal-Wallis tests were used. The differences in D_{v50} of colonies among different flumes as well as the difference between the rate of colony size change (dD_{v50}/dt) at the water surface and in the bulk water were compared using the student *t*-test. The relationships between mean SAC and D_{v50}, mean SAC and dD_{v50}/dt, normalized flow velocity and SAC as well as between rate of change in SAC and time were fitted by linear regressions. All statistical analyses were performed using the software package SPSS 27.0 (IBM Corp, USA). Data are presented as mean ± standard deviation and were tested for statistical significance at a significance level (p) of 0.05 unless stated otherwise.

3. Results

3.1 Dynamics of *Microcystis* surface scum formation

Surface scum layers developed during low wind periods and disappeared during wind disturbance over the seven-day experimental period (Figure 2). During wind disturbances (1.5 – 4.5 m s^{-1}), the areal coverage

of the water surface with *Microcystis* colonies was generally < 1%, whereas it increased during low wind period (0.5 m s^{-1}) gradually from 0.1 to 25 % from Day 1 to Day 7. The observed rates of change in SAC (dSAC/dt) and rates of change in SAC per unit biomass (dSAC / (OD_{680} dt)) during low wind speed linearly increased over time ($p < 0.05$, Figure 3), suggesting that the surface scum recovered from wind disturbances at increasing rates. Similar to surface coverage, the biomass of *Microcystis* colonies in the thin surface layer showed a 2 - 6 fold increase from Day 1 to Day 7 (Supplementary Figure S3A).

The formation of surface scum followed a diurnal pattern with the average surface coverage during low wind periods in the afternoon (stage II) being reduced by 87.7%, 36.6%, 31.3%, 44.5% and 51.1% (for F1 – F5) in comparison to that in the morning (stage I) (Figure 2).

The dynamics of surface scum formation varied in dependence on wind conditions (Figure 2). The prolonged duration of low wind periods promoted scum formation: the surface coverage in flumes F1 and F4 was significantly higher than that in F2 and F5 in most cases ($p < 0.05$). Wind magnitudes of 4.5 and 1.5 m s^{-1} promoted the subsequent surface scum formation, in comparison to the intermediate magnitude of 3.8 m s^{-1}: In most cases, the surface areal coverage in F1 and F4 was higher than that in F3 ($p < 0.05$).

3.2 Dynamics of *Microcystis* colony size

The colony size showed temporal trends during the 7-day experiment (Figure 4). In the upper layer near the water surface, Dv_{50} increased from the beginning to Day 7 by a factor of 2.4, 3.1, 2.4, 4.4 and 2.7 in F1-F5, respectively. During the increase of Dv_{50}, we observed the peaks in Dv_{50} of *Microcystis* colonies near the water surface at times when the wind speed changed from low to high from Day 3 – Day 7 (Figure 4). Through visual observations, we found that such larger colonies suddenly appearing in the bulk water resulted from wind-induced entrainment of surface scum patches forming during preceding low wind periods.

The mean rate of change in colony size (dDv_{50}/dt) at the water surface and in the bulk water is -0.12 and 0.14 mm h^{-1}, respectively. In each flume, the dDv_{50}/dt at the water surface is significantly higher than that in the bulk water ($p < 0.05$, Figure 5). At the beginning of wind disturbances, both Dv_{50} and dDv_{50}/dt increased linearly with increasing SAC during the preceding low wind period (Figure 6).

The median diameter of *Microcystis* colonies (Dv_{50}) was affected by the different wind conditions (Figure 4). Dv_{50} increased with decreasing magnitude of wind disturbances regardless of their duration (Figure 4). The response of Dv_{50} to the duration of the wind disturbance was dependent on its magnitude, with longer duration of high-magnitude wind disturbances leading to decreased Dv_{50} (F1 < F2, Figure 4), whereas Dv_{50} increased for longer durations of low-magnitude wind disturbances (F4 > F5, Figure 4). The order of mean Dv_{50} of *Microcystis* colonies near the water surface was F4>F5>F3>F2>F1 when combining all measurements ($p < 0.05$).

3.3 Hydrodynamics under different wind conditions

At the beginning of the experiment, the surface flow velocities increased nearly linearly with the applied wind speed resulting in equivalent wind speeds in the atmospheric boundary layer (U_{10}) of 2.0 m s^{-1} under low wind speed conditions and 2.8 to 5.3 m s^{-1} during the simulated disturbances (Table 1).

The surface flow velocity and underwater flow velocities (at three depths) observed at a particular wind speed generally decreased from Day 1 to Day 7 (Supplementary Figure S4). The normalized flow velocity (defined as the ratio of flow velocity to wind speed) at the water surface and in the bulk water generally decreased linearly over time ($p < 0.05$, Supplementary Figure S5 and Table S3). In all flumes, the surface flow velocity and underwater flow velocities during low wind periods decreased to approximately 1 mm s^{-1} on Day 7 (Figure 7).

At the applied wind speed of 0.5 m s^{-1} (low wind periods), significant differences in surface flow velocity among different flumes were observed (p <0.05, Figure 7). No consistent dependence of surface flow velocity on the duration of the intermittent wind disturbance was observed, while surface flow velocity during low wind periods generally increased with increasing preceding magnitudes of wind disturbance: The order of surface flow velocity during low wind periods was F1>F3>F4, except for Day 6 stage I and Day 7. Unlike the surface flow velocity, the underwater flow velocities during low wind periods did not differ significantly between different flumes in most cases (Supplementary Figure S6).

3.4 Relationship between *Microcystis* and hydrodynamic parameters

Higher SAC was primarily observed at low surface flow velocities (< 5 mm s^{-1}). However, it is noteworthy

that SAC at moderate surface flow velocities (5-12 mm s^{-1}) on Day 3 – Day 6 could also surpass some SAC at low surface flow velocities (Supplementary Figure S7). Neither Dv_{50} of colonies nor (dDv_5/dt) were linearly related to the root-mean-square velocities of colonies in the bulk water (U_{rms}) when combining all measurements (Supplementary Figure S8). However, the proportion of dDv_{50}/dt being smaller than -1 mm h^{-1} (indicating colony disaggregation) increased with increasing U_{rms}. Conversely, the proportion of dDv_{50}/dt larger than 0.5 mm h^{-1} (colony aggregation) decreased with increasing U_{rms} when U_{rms} exceeded 3 mm $s^{-1}$and increased with increasing U_{rms} when U_{rms} was smaller than 3 mm s^{-1} (Supplementary Figure S9).

The presence of *Microcystis* affected the hydrodynamic parameters: In the flumes experiment, from Day 1 to Day 4, no linear relationships between the normalized flow velocity and SAC were found, but from Day 5 to Day 7, the normalized flow velocity decreased with increasing SAC ($p < 0.05$, Figure 8). The results of our supplementary dilution experiment showed that the surface tension decreased with the increasing optical density of *Microcystis* (Figure 9).

4. Discussion

4.1 The response of colony size and scum of *Microcystis* to wind-generated hydrodynamics

Our experiments successfully reproduced the periodical formation and dispersion of *Microcystis* surface scum under intermittent wind disturbances (Figure 2). During low wind periods (0.5 m s^{-1}), we observed gradually increased surface scum in all the flumes. Surprisingly, we found that scum was forming more rapidly following prolonged duration of high-magnitude wind disturbances compared to that following moderate magnitudes (F1, Figure 2). The differences in scum coverage in varying flumes can be attributed to the flow conditions, as they govern the migration of *Microcystis*. However, we found significant differences in flow velocities among flumes were only evident for the surface (Supplementary Figure S6 & Figure 7), suggesting that the surface flow field likely played a pivotal role in modulating the response of scum formation to preceding wind disturbances.

Higher scum coverage can be observed at moderate surface flow velocities (5 - 12 mm s^{-1}) compared to lower surface flow velocities in some cases (Supplementary Figure S7). This result implies potential mechanisms for surface scum formation under moderate flow velocities, considering that surface scum is

typically associated with lower flow conditions (Wu et al., 2015). Webster and Hutchinson (1994) suggested the trapping mechanisms of colonies by viscous sublayer. A possible explanation we proposed is the strong vertical velocity gradient within the viscous sublayer, where the higher flow velocities near the water surface result in lower static pressure and a net upward lift force on the colonies, of which the magnitudes depend on the colony size and morphology. Although this process was not resolved in our study due to the lack of small tracer particles, we speculate that these complex interactions may account for the higher scum coverage observed at moderate flow velocities following a prolonged period (6 h) of high-magnitude wind disturbance. Future studies should include a more detailed characterization of the hydrodynamic conditions at the water surface (e.g., adding additional small seeding particles to perform particle image velocimetry) to better understand this mechanism.

The observed increase in surface scum also led to more frequent aggregations among colonies at the air-water interface. The developing scum significantly increased the colony size (Figure 6), thereby explaining the higher rates of change in colony size at the surface compared to in the bulk water (Figure 5). Given the limited attention to these aggregations, the underlying mechanism is unclear. Here we proposed capillary forces could be a driver for the formation of *Microcystis* aggregations at the water surface. In the vicinity of immersed buoyant particles, attractive forces arise due to micro-deformation of the air-water interface (capillary immersion force, Kralchevsky and Nagayama, 2000 & Paunov et al., 1993). The common phenomenon that floating objects such as bubbles tend to clump together or cling to the sides of the container is driven by capillary forces (Vella and Mahadevan, 2005). We speculate that capillary forces partly increase the encounter rate of *Microcystis* at the water surface during prolonged periods of low wind speed, which promotes their accumulation and aggregation.

During wind disturbance, surface scums were dispersed throughout the bulk water, in which the hydrodynamics was governed by turbulent flow. Our study showed that moderate wind-generated turbulence promoted the aggregation of *Microcystis* into larger colonies, whereas high wind-generated turbulence favored their disaggregation (Supplementary Figure S9). This dual effect can be explained by the opposing effects of turbulence in increasing the collision frequency of cells and colonies and by

increasing shear forces (Liu et al., 2019; Njobuenwu and Fairweather, 2018; O'Brien et al., 2004; Yao and Capecelatro, 2021). The latter likely limited the colony size in our experiments, which consistently decreased for increasing magnitudes of wind disturbances, regardless of disturbance duration (Figure 4). The duration of wind disturbances thus affects colony size by controlling the duration of interactions of colonies with turbulence, which may explain the magnitude-dependent effect of wind disturbance duration on colony size.

Periodic wind disturbances shifted the habitat of *Microcystis* between the air-water interface and the bulk water, during which the surface aggregation of *Microcystis* and the combination of their collision and disaggregation in the bulk water were alternating. In our experiments, such cycles constituted a positive feedback regulation between colony size and formation of surface scum, by which the size of suspended colonies and re-formation rate of scum continuously increased (Figure 3). It should be noted that colony size can also be affected by *Microcystis* growth (Xiao et al., 2018). However, the growth of *Microcystis* did not show notable differences among different flumes. In addition, the D_{v50} changed in accordance with the wind conditions, with the peak in D_{v50} occurring after the start of the disturbances (Figure 4), suggesting that the colony size dynamics were likely governed by the hydrodynamic conditions rather than by growth.

4.2 The effect of *Microcystis* surface scum on hydrodynamics under different wind conditions

We found a pronounced reduction in water surface tension with increasing *Microcystis* biomass with our supplementary experiment (Figure 9), which can have important consequences for the hydrodynamic processes at the air-water interface. We found that the normalized flow velocity decreased with increasing scum coverage at the later phase of our experiment (Figure 8), suggesting that the dense scum layer suppressed the momentum transfer from wind to water. At low wind speed, the reduction in momentum transfer can be explained by low water surface roughness, which is a consequence of low water surface tension (suppression of capillary waves, Wüest and Lorke, 2003). The increasing scum layer explained the decrease in water flow velocity generated by a given wind speed over time in our experiments (Supplementary Figure S5) and in a previous study (Wu et al. 2019). These findings implied that floating *Microcystis* can promote the formation and persistence of surface scum by altering surface tension and

counteracting wind-driven mixing. Such reduced flow velocity caused by the presence of scum layers additionally contributed to the increasing re-formation rate of surface scum (Figure 3). The lack of direct measurements of surface tension in the flumes does not negate the surface tension-mediated hydrodynamic interactions between *Microcystis* and the air-water interface during the flume experiments, as indicated by the observed reduction in flow velocity.

The reduced surface tension caused by *Microcystis* colonies can also directly generate surface flows being directed towards regions of high surface tension (Marangoni effect, (Vinnichenko et al., 2018; Roché et al., 2014), i.e., a spreading towards *Microcystis*-free regions. Although we could not directly observe this flow in our experiment as the Marangoni flow was masked by the wind-driven flow, it is ubiquitously present in environmental flows (Scriven and Sternling, 1960). Similar to the 'soap boat' (a well-known visualization of Marangoni convection), we propose that the lateral gradient of surface tension in the vicinity of initial scum patches can drive their horizontal surface drift and reshape their distributions in the absence of external force (e.g., weak wind forcing).

4.3 The environmental relevance and limitations of the experiment

We scaled the wind speeds measured in the flumes to representative wind velocities at a standard measurement height of 10 m (U_{10}, see Supplementary Table S3). In our experiment, the low wind speed (U_{10} of 2 m s^{-1}) corresponds to the wind magnitude during weak wind periods, while the wind disturbances (U_{10} of 2.8 – 5.3 m s^{-1}) correspond to amplitudes of periodic wind forcing frequently observed over lakes (Fernández Castro et al. 2021, Saber et al. 2018). The chosen 6 h and 12 h periods of wind disturbances represent the lower and the upper range of field observations over lakes (Fernández Castro et al., 2021).

Surface scum formed during low wind periods and was dispersed during wind disturbances, which is in line with field investigation that showed an upper threshold of U_{10} for scum persistence is 2.6 - 3 m s^{-1} (Cao et al., 2006; George and Edwards, 1976; Qi et al., 2018). Moreover, light-induced changes in the buoyancy of *Microcystis,* commonly observed in the field (Ibelings et al., 1991), were successfully reproduced (Figure 2). These observations further demonstrate the validity of our experimental design.

The water depth in our study was limited by the dimensions of the flume to 30 cm, which is smaller than

the amplitude of vertical migration of *Microcystis* in natural lakes. Consequently, the formation rates of surface scum that we observed in the flumes may be higher than those found in the field. In addition, the low water depth restricted vertical mixing at high wind speeds, exposing *Microcystis* in the bulk water to higher irradiance than in deeper water. However, the focus of this study was on the hydrodynamic interactions of surface scum with the air-water interface, which is not expected to be linked to the scale of the experimental setup or to water depth. As the light intensity affects both the growth and the buoyancy production of *Microcystis,* we utilized relatively high irradiance levels, as they often persist in surface waters in the field. Initially, our experiments also included the configuration of the low duration (3 h) and median-magnitude (3.8 m s^{-1}) wind disturbances. That data, however, had to be excluded due to technical issues with the flume operation. Future experiments should be conducted at higher resolutions (e.g., analyzing finer gradients of disturbance magnitude and duration) in order to provide a more comprehensive understanding of the partly non-linear interactions of wind with surface scum. Furthermore, buoyancy-driven migration could not be resolved in our measurements, as the flow velocity (generally exceeding 1 mm s^{-1}) surpasses the floatation velocity of most colonies (< 1 mm s^{-1}, Wallace et al., 2000).

Our study reveals the close connection between *Microcystis* dynamics and the air-water interface. The air-water interface emerges as a crucial habitat increasing colony size during scum formation (typically under low wind speeds), surpassing the impact of bulk water (Figure 5). Recent studies have shown that the wind has declined in some regions over the past few decades (Ranjbar et al., 2022; Vautard et al., 2010). Consequently, this study indicates that the projected decrease in wind speed under future climate conditions will result in larger colonies and facilitate the recovery of surface scum upon wind disturbance. Additionally, our finding of denser scum after prolonged periods of high wind speeds may have implications for early warning of blooms during windy conditions.

Our study also suggests that *Microcystis* reduces surface tension, likely through the excretion of surface-active substances. This process constitutes a dispersion-avoidance mechanism under wind conditions, allowing *Microcystis* to persist at well-lit depths. Furthermore, reduced surface tension potentially drives lateral convection, facilitating the expansion of *Microcystis* and mitigating competition for resources during

weak wind periods. These processes may represent adaptive responses of *Microcystis* to wind stressors, suggesting that water surface tension, affected by *Microcystis*, may be an important mediator by which scum-forming cyanobacteria shape their habitat in favorable directions. Given the oversight of the aggregation of *Microcystis* at the air-water interface and their hydrodynamic interactions in current studies, it is important to consider these processes appropriately for a more accurate prediction of *Microcystis* scum dynamics in future climatic conditions.

Conflict of Interest

The authors declare that the research was conducted in the absence of any commercial or financial relationships that could be construed as a potential conflict of interest.

Author Contributions

Huaming Wu: Investigation, formal analysis, writing – original draft preparation. **Xingqiang Wu: Conc**eptualization, writing – review & editing, funding acquisition. **Lorenzo Rovelli**: Methodology, writing – review and editing. **Andreas Lorke**: Conceptualization; methodology, writing – review & editing, funding acquisition. All authors approved the final submitted manuscript.

Funding

This study was financially supported by the German Research Foundation (grant no. LO 1150/18) and the National Natural Science Foundation of China (grant nos. 42061134013).

Acknowledgments

We thank Christoph Bors (University of Kaiserslautern-Landau, Institute for Environmental Sciences) for his help with the experimental setup and measurements, and acknowledge the open-source scripts for particle tracking provided by the Environmental Complexity Lab (Stanford University, https://web.stanford.edu/~nto/software_tracking.shtml).

Data Availability Statement

The raw data supporting the conclusions of this article will be made available by the authors, without undue reservation.

References

Aparicio Medrano, E., Uittenbogaard R. E., Van De Wiel B. J. H., Dionisio Pires L. M., and Clercx H. J. H. (2016). An alternative explanation for cyanobacterial scum formation and persistence by oxygenic photosynthesis. *Harmful Algae* 60, 27-35. doi: 10.1016/j.hal.2016.10.002

Cao, H.S., Kong F.X., Luo L.C., Shi X.L., Yang Z., Zhang X.F., et al. (2006). Effects of wind and wind-induced waves on vertical phytoplankton distribution and surface blooms of *Microcystis* aeruginosa in Lake Taihu. *Freshw. Ecol.* 21, 231e238. doi: 10.1080/02705060.2006.9664991

Chen, H., Zhu W., Wang R., Feng G., and Xue Z. (2023). Rapid horizontal accumulation and bloom formation of the cyanobacterium *Microcystis* under wind stress. *Hydrobiologia* 850, 123-135. doi: 10.1007/s10750-022-05048-8

Chronakis, I. S., Galatanu A. N., Nylander T., and Lindman B. (2000). The behaviour of protein preparations from blue-green algae (Spirulina platensis strain Pacifica) at the air/water interface. *Colloids Surf., A Physicochem. Eng. Asp.* 173, 181-192. doi: 10.1016/S0927-7757(00)00548-3

Cunliffe, M., Engel A., Frka S., Gašparović B., Guitart C., Murrell J.C., et al. (2013). Sea surface microlayers: A unified physicochemical and biological perspective of the air–ocean interface. *Prog. Oceanogr.* 109, 104-116. doi: 10.1016/j.pocean.2012.08.004

Dervaux, J., Mejean A., and Brunet P. (2015). Irreversible Collective Migration of Cyanobacteria in Eutrophic Conditions. *PLoS One* 10, e0120906. doi: 10.1371/journal.pone.0120906

Dunton, P.G., and Walsby A.E. (2005). The diameter and critical collapse pressure of gas vesicles in *Microcystis* are correlated with GvpCs of different length. *FEMS Microbiol. Lett.* 247, 37-43. doi: 10.1016/j.femsle.2005.04.026

Feng B., Wang C., Wu X., Tian C., Zhang M., Tian Y., Xiao B. (2019). Spatiotemporal dynamics of cell abundance, colony size and intracellular toxin concentrations of pelagic and benthic *Microcystis* in Lake Caohai, China. *J. Environ. Sci*. 84, 184-196

Fernández Castro B., Sepúlveda Steiner O., Knapp D., Posch T., Bouffard D., and Wüest A. (2021). Inhibited vertical mixing and seasonal persistence of a thin cyanobacterial layer in a stratified lake. *Aquat. Sci.* 83, 1-22. doi: 10.1007/s00027-021-00785-9

George, D., and Edwards R. (1976). The effect of wind on the distribution of chlorophyll a and crustacean plankton in a shallow eutrophic reservoir. *J. Appl. Ecol.* 667-690. doi: 10.2307/2402246

Ho, J.C., Michalak A.M., and Pahlevan N. (2019). Widespread global increase in intense lake phytoplankton blooms since the 1980s. *Nature* 574, 667-670. doi: 10.1038/s41586-019-1648-7

Huisman, J., Codd G.A., Paerl H.W., Ibelings B.W., Verspagen J.M.H., and Visser P.M. (2018). Cyanobacterial blooms. *Nat. Rev. Microbiol.* 16, 471-483. doi: 10.1038/s41579-018-0040-1

Ibelings, B.W., Mur L.R., and Walsby A.E. (1991). Diurnal changes in buoyancy and vertical distribution in populations of *Microcystis* in two shallow lakes. *J. Plankton Res.* 13, 419–436. doi: 10.1093/plankt/13.2.419

Kelley, D.H., and Ouellette N.T. (2011). Using particle tracking to measure flow instabilities in an undergraduate laboratory experiment. *Am. J. Phys.* 79, 267-273. doi: 10.1119/1.3536647

Kralchevsky, P.A., and Nagayama K. (2000). Capillary interactions between particles bound to interfaces, liquid films and biomembranes. *Adv. Colloid Interface Sci.* 85, 145-192. doi: 10.1016/S0001-8686(99)00016-0

Liu, M., Ma J., Kang L., Wei Y., He Q., Hu X., et al. (2019). Strong turbulence benefits toxic and colonial cyanobacteria in water: A potential way of climate change impact on the expansion of Harmful Algal Blooms. *Sci. Total. Environ.* 670, 613-622. doi: 10.1016/j.scitotenv.2019.03.253

Lv, L., Zhang X., and Qiao J. (2018). Flocculation of low algae concentration water using polydiallyldimethylammonium chloride coupled with polysilicate aluminum ferrite. *Environ. Technol.* 39, 83-90. doi: 10.1080/09593330.2017.1296028

Njobuenwu, D.O., and Fairweather M. (2018). Large eddy simulation of particle agglomeration with shear breakup in turbulent channel flow. *Phys. Fluids* 30, 063303. doi: 10.1063/1.5037174

O'Brien K.R., Meyer D.L., Waite A.M., Ivey G.N., and Hamilton D.P. (2004). Disaggregation of *Microcystis* aeruginosa colonies under turbulent mixing: laboratory experiments in a grid-stirred tank. *Hydrobiologia* 519, 143–152. doi: 10.1023/B:HYDR.0000026501.02125.cf

Oliver R.L. (1994). Floating and sinking in gas-vacuolate cyanobacteria. *J.Phycol.* 30, 161-173. doi: 10.1111/j.0022-3646.1994.00161.x

Qi, L., Hu, C., Visser, P.M., Ma, R., (2018). Diurnal changes of cyanobacteria blooms in Taihu Lake as derived from GOCI observations. *Limnol. Oceanogr*. 63, 1711e1726.

Paerl, H.W., and Ustach J.F. (1982). Blue-green algal scums: An explanation for their occurrence during freshwater blooms1. *Limnol. Oceanogr.* 27, 212-217. doi: 10.4319/lo.1982.27.2.0212

Paunov, V.N., Kralchevsky P.A., Denkov N.D., and Nagayama K. (1993). Lateral capillary forces between floating submillimeter particles. *J. Colloid Interface Sci.* 157, 100-112. doi: 10.1006/jcis.1993.1163

Ranjbar, M. H., Hamilton, D. P., Etemad-Shahidi, A., and Helfer, F. (2022). Impacts of atmospheric stilling and climate warming on cyanobacterial blooms: An individual-based modelling approach. *Water Res.*221, 118814.

Regel, R. H., Brookes J. D., Ganf G. G., and Griffiths R. W. (2004). The influence of experimentally generated turbulence on the Mash01 unicellular *Microcystis* aeruginosa strain. *Hydrobiologia* 517, 107–120. doi: 10.1023/B:HYDR.0000027341.08433.32

Reynolds, C.S. (1987). Cyanobacterial Water-Blooms. *Adv. Bot. Res.* 13, 67-143. doi: 10.1016/S0065-2296(08)60341-9

Roché, M., Li Z., Griffiths I.M., Le Roux S., Cantat I., Saint-Jalmes A., et al. (2014). Marangoni Flow of Soluble Amphiphiles. *Phys. Rev. Lett.* 112, 208302. doi: 10.1103/PhysRevLett.112.208302

Saber, A., James D.E., and Hayes D.F. (2018). Effects of seasonal fluctuations of surface heat flux and wind stress on mixing and vertical diffusivity of water column in deep lakes. *Adv. Water Resour.* 119, 150-163. doi: 10.1016/j.advwatres.2018.07.006

Scriven, L. E., and Sternling C. V. (1960). The Marangoni effects. *Nature* 187, 186-188. 10.1038/187186a0

Soranno, P.A. (1997). Factors affecting the timing of surface scums and epilimnetic blooms of blue-green algae in a eutrophic lake. *Can. J. Fish. Aquat.* 54, 1965-1975. doi: 10.1139/f97-10

Vautard, R., Cattiaux, J., Yiou, P., Thépaut, J. N., and Ciais, P. (2010). Northern Hemisphere atmospheric stilling partly attributed to an increase in surface roughness. *Nat. Geosci.* 3(11), 756-761.

Vella, D., and Mahadevan L. (2005). The "cheerios effect". *Am. J. Phys.* 73, 817-825. doi: 10.1119/1.1898523

Vinnichenko, N.A., Plaksina Y.Y., Baranova K.M., Pushtaev A.V., and Uvarov A.V. (2018). Mobility of free surface in different liquids and its influence on water striders locomotion. *Environ. Fluid Mech.* 18, 1045-1056. doi: 10.1007/s10652-018-9577-9

Visser, P. M., Passarge J., and Mur L.R. (1997). Modelling vertical migration of the cyanobacterium *Microcystis*. *Hydrobiologia* 349, 99–109. doi: 10.1023/A:1003001713560

Wallace, B.B., Bailey M. C., and Hamilton D. P. (2000). Simulation of vertical position of buoyancy regulating *Microcystis aeruginosa* in a shallow eutrophic lake. *Aquat. Sci.* 62(4), 320–333.

Webster, I.T., and Hutchinson P.A. (1994). Effect of wind on the distribution of phytoplankton cells in lakes revisited. *Limnol. Oceanogr.* 39, 365e373. doi: 10.4319/lo.1994.39.2.0365

Wu, J. (1975). Wind-induced drift currents. *J. Fluid Mech.* 68, 49-70. doi: 10.1017/S0022112075000687

Wu, T., Qin B., Brookes J. D., Shi K., Zhu G., Zhu M., et al. (2015). The influence of changes in wind patterns on the areal extension of surface cyanobacterial blooms in a large shallow lake in China. *Sci. Total Environ.* 518-519, 24-30 doi: 10.1016/j.scitotenv.2015.02.090

Wu, X., Noss C., Liu L., and Lorke A. (2019). Effects of small-scale turbulence at the air-water interface on *Microcystis* surface scum formation. *Water Res.* 167, 115091. doi: 10.1016/j.watres.2019.115091

Wu, X., Yang T., Feng S., Li L., Xiao B., Song L., et al. (2020). Recovery of *Microcystis* surface scum following a mixing event: Insights from a tank experiment. *Sci. Total. Environ.* 728, 138727. doi: 10.1016/j.scitotenv.2020.138727

Wüest, A., and Lorke A. (2003). Small-scale hydrodynamics in lakes. *Annu. Rev. Fluid Mech.* 35, 373e412. doi: 10.1146/annurev.fluid.35.101101.161220

Xiao, M., Li M., and Reynolds C.S. (2018). Colony formation in the cyanobacterium *Microcystis*. *Biol. Rev. Camb. Philos. Soc.* 93, 1399-1420. doi: 10.1111/brv.12401

Yao, Y., and Capecelatro J. (2021). Deagglomeration of cohesive particles by turbulence. *J. Fluid Mech.* 911, A10 doi: 10.1017/jfm.2020.1020

Zhao, G., Gao X., Zhang C., and Sang G. (2020). The effects of turbulence on phytoplankton and implications for energy transfer with an integrated water quality-ecosystem model in a shallow lake. *J. Environ. Manage.* 256, 109954. doi: 10.1016/j.jenvman.2019.109954

Zhu, W., Li M., Luo Y., Dai X., Guo L., Xiao M., et al. (2014). Vertical distribution of *Microcystis* colony size in Lake Taihu: its role in algal blooms. *J. Gt. Lakes Res.* 40, 949–955. doi: 10.1016/j.jglr.2014.09.009

Figure legend

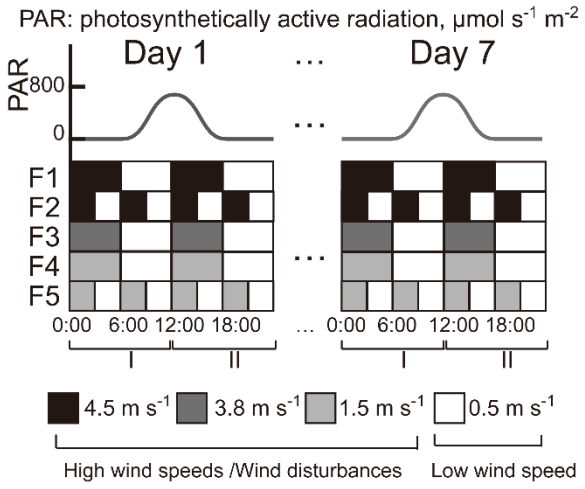

Figure 1. Diurnal variations of photosynthetically active radiation (PAR, upper panel) and wind speed (lower panel) in the five flumes (F1 – F5) during the 7-day experiment. The morning period (0:00 to 12:00) was defined as stage I and the afternoon (12:00 to 24:00) was defined as stage II. The wind speeds of 4.5, 3.8 and 1.5 m s^{-1} were defined as high wind speeds and the wind speed of 1.5 m s^{-1} was defined as low wind speed

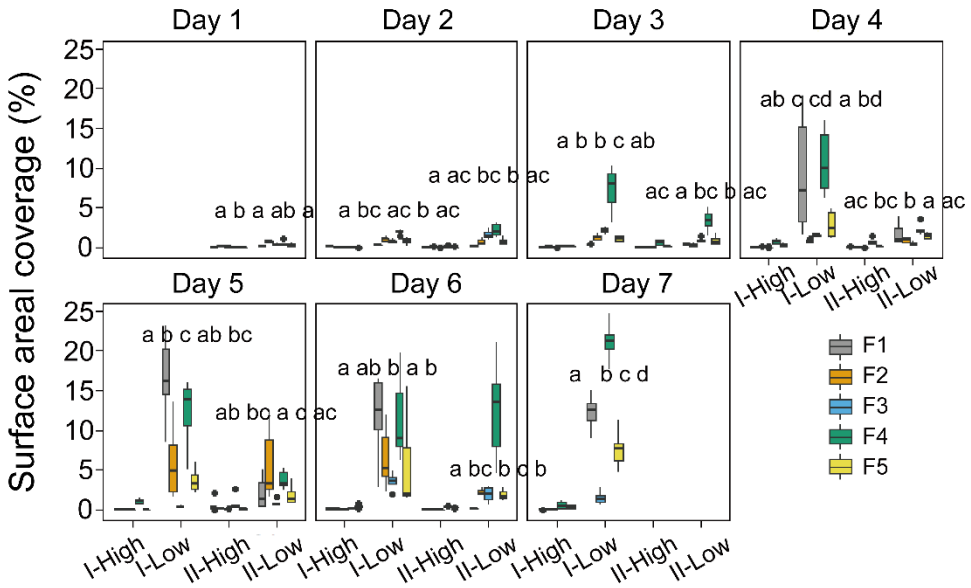

Figure 2. Temporal dynamics of the surface areal coverage of *Microcystis* colonies in different stages (I and II) and experimental flumes (F1 – F5, see legend for color assignment). High and Low represent the periods of high wind speed (wind disturbances, 4.5 m s^{-1} for F1 and F2, 3.8 m s^{-1} for F3, 1.5 m s^{-1} for F4 and F5) and low wind speed (0.5 m s^{-1}), respectively. Different panels denote the time (day) after the start of the experiment. Each box plot shows the mean surface areal coverage observed in the hourly video observations (n=6). Different letters on top of the box plots indicate significant differences ($p < 0.05$) in surface areal coverage during low wind periods between different groups at each stage, while the same or no letter indicates no significant difference (Kruskal-Wallis tests). F1: 6 h of high-magnitude (4.5 m^{-1}) wind disturbance; F2: 3 h of high-magnitude wind disturbance; F3: 6 h of moderate-magnitude (3.8 m^{-1}) wind disturbance; F4: 6 h of low-magnitude (1.5 m^{-1}) wind disturbance; F5: 3 h of low-magnitude wind disturbance.

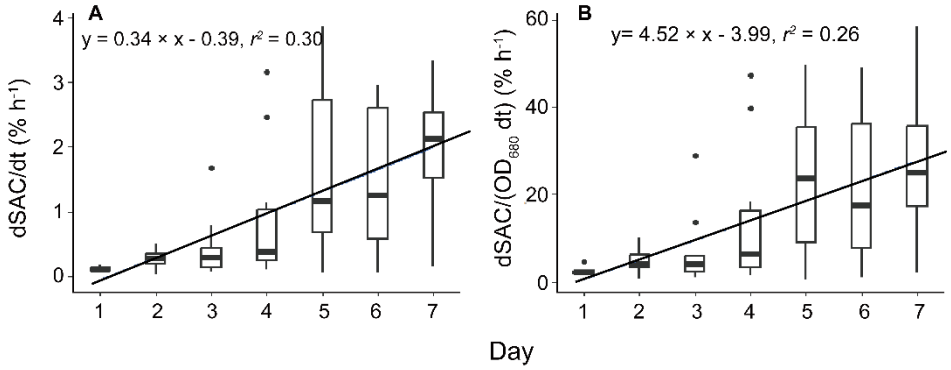

Figure 3. The temporal change of the rate of change in scum areal coverage (**A**, dSAC/ dt) and the rate of change in scum areal coverage per unit biomass (**B**, dSAC/ (OD_{680} dt)). Significant linear relationships between dSAC/ dt as well as dSAC/ (OD_{680} dt) and time were observed ($p < 0.05$). Each box plot shows the dSAC/ dt or dSAC/ (OD_{680} dt). Both solid lines represent linear regressions based on the equations provided in the legend, with a significance level of $p < 0.05$. F1: 6 h of high-magnitude (4.5 m^{-1}) wind disturbance; F2: 3 h of high-magnitude wind disturbance; F3: 6 h of moderate-magnitude (3.8 m^{-1}) wind disturbance; F4: 6 h of low-magnitude (1.5 m^{-1}) wind disturbance; F5: 3 h of low-magnitude wind disturbance.

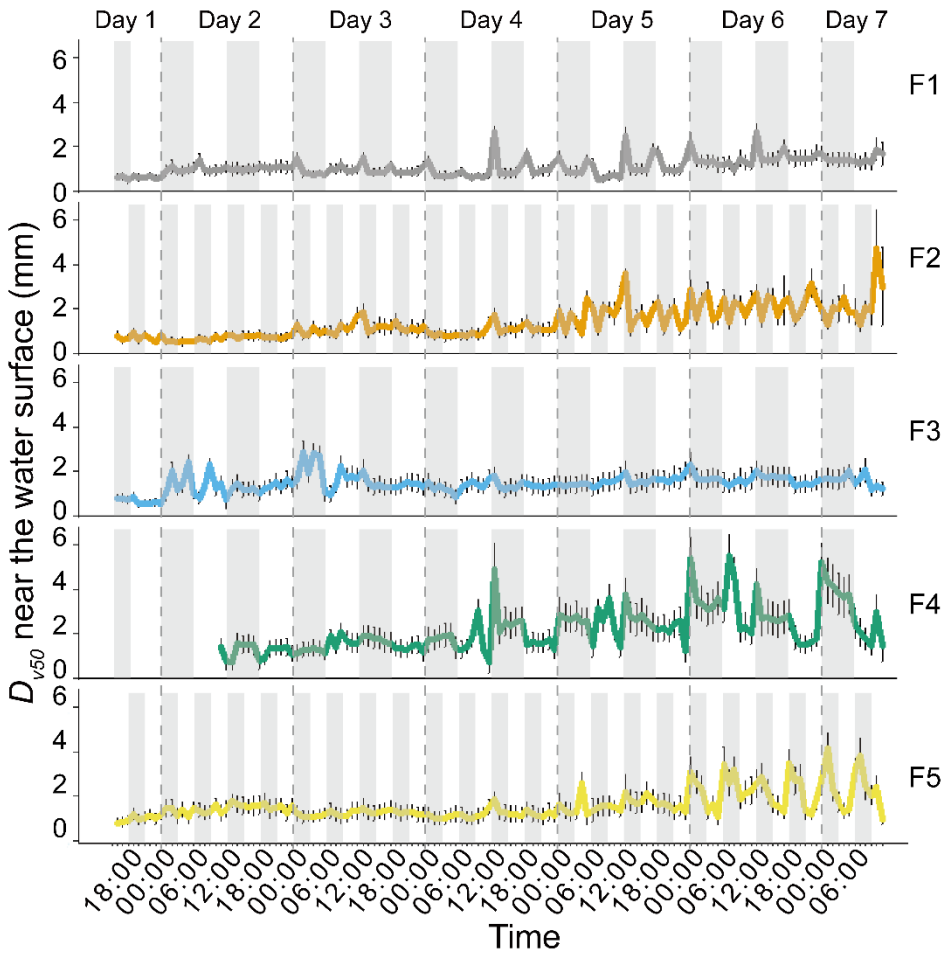

Figure 4. Temporal dynamics of the volume median diameter (D_{v50}) of *Microcystis* colonies near the water surface (0 - 6 cm depth) in different experimental flumes (F1 – F5, see legend for color assignment). Symbols show mean values and error bars are standard deviations. The periods of high wind speed (wind disturbances) were represented with gray shading. The initial lack of data in F4 was due to a technical issue. F1: 6 h of high-magnitude (4.5 m^{-1}) wind disturbance; F2: 3 h of high-magnitude wind disturbance; F3: 6 h of moderate-magnitude (3.8 m^{-1}) wind disturbance; F4: 6 h of low-magnitude (1.5 m^{-1}) wind disturbance; F5: 3 h of low-magnitude wind disturbance.

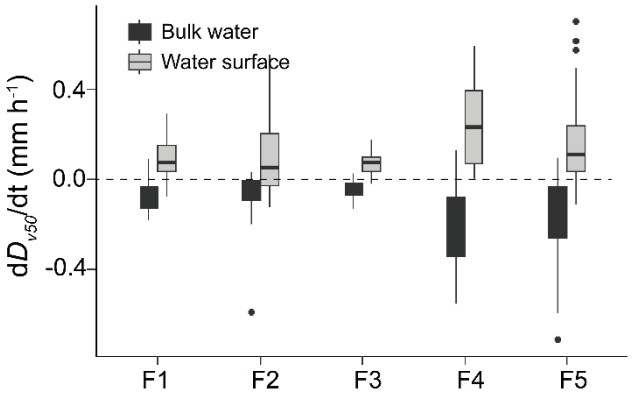

Figure 5. Rates of change in colony size (dD_{v50}/dt) at the water surface (grey-filled box plots) and in the bulk water (black-colored box plots) in different flumes (F1 – F5). The dashed horizontal line indicates the dD_{v50}/dt of 0 mm h^{-1}. Significant differences between dD_{v50}/dt at the water surface and in the bulk water were observedin all flumes (*t*-test, df=21 and 44, $p < 0.001$). F1: 6 h of high-magnitude (4.5 m^{-1}) wind disturbance; F2: 3 h of high-magnitude wind disturbance; F3: 6 h of moderate-magnitude (3.8 m^{-1}) wind disturbance; F4: 6 h of low-magnitude (1.5 m^{-1}) wind disturbance; F5: 3 h of low-magnitude wind disturbance.

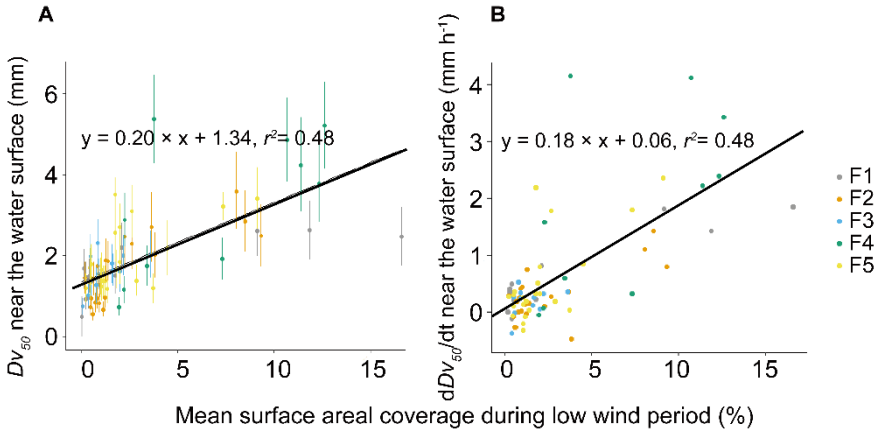

Figure 6. Relationship between the median diameter (D_{v50}) of *Microcystis* colonies near the water surface at the onset of high wind disturbances and mean surface areal coverage during the low wind period before the disturbance (**A**). Relationship between the rate of change in the colony median diameter (dD_{v50}/dt) near the water surface at the onset of wind disturbances and mean surface areal coverage during low wind periods before the disturbance (**B**). Symbols show mean values for different flumes (F1 – F5, see legend) and the error bars shown in (**A**) show the standard deviations. Both solid lines represent linear regressions based on the equations provided in the legend, with a significance level of $p < 0.05$. F1: 6 h of high-magnitude (4.5 m^{-1}) wind disturbance; F2: 3 h of high-magnitude wind disturbance; F3: 6 h of moderate-magnitude (3.8 m^{-1}) wind disturbance; F4: 6 h of low-magnitude (1.5 m^{-1}) wind disturbance; F5: 3 h of low-magnitude wind disturbance.

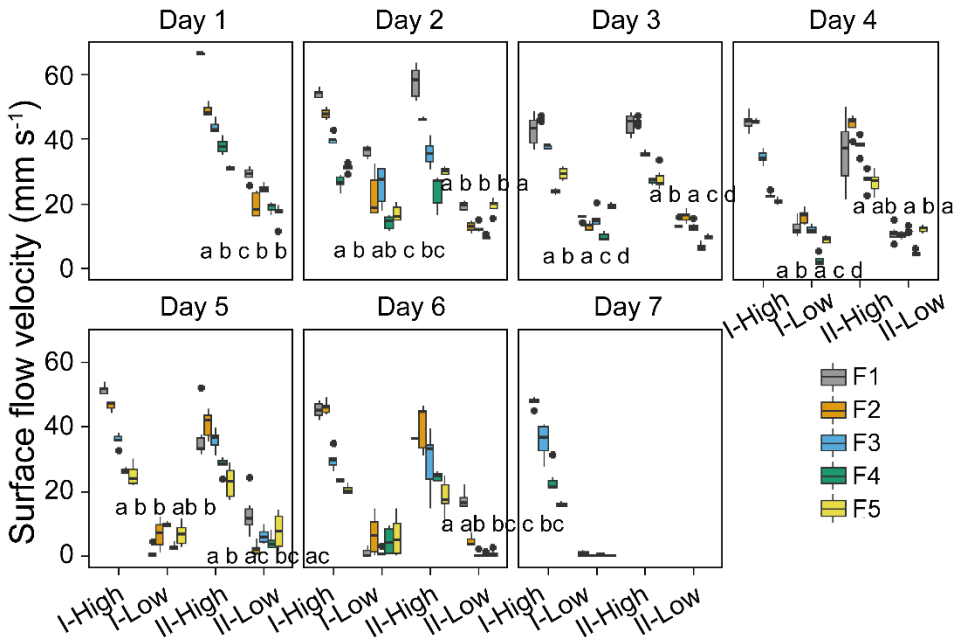

Figure 7. Temporal dynamics of the mean surface flow velocity in different stages (I and II) and experimental flumes (F1 – F5, see legend). High and Low represent periods of high wind speed (wind disturbances, 4.5 m s^{-1} for F1 and F2, 3.8 m s^{-1} for F3, 1.5 m s^{-1} for F4 and F5) and low wind speed (0.5 m s^{-1}), respectively. Different panels denote the time (day) after the start of the experiment. Each box plot shows mean flow velocities observed in hourly video observations in the given stage in different flumes during the 7 days. Different lowercase letters indicate significant differences in flow velocity at different stages during low wind periods among different flumes, while the same letter, or the lack of a letter, indicates no significant differences. F1: 6 h of high-magnitude (4.5 m^{-1}) wind disturbance; F2: 3 h of high-magnitude wind disturbance; F3: 6 h of moderate-magnitude (3.8 m^{-1}) wind disturbance; F4: 6 h of low-magnitude (1.5 m^{-1}) wind disturbance; F5: 3 h of low-magnitude wind disturbance.

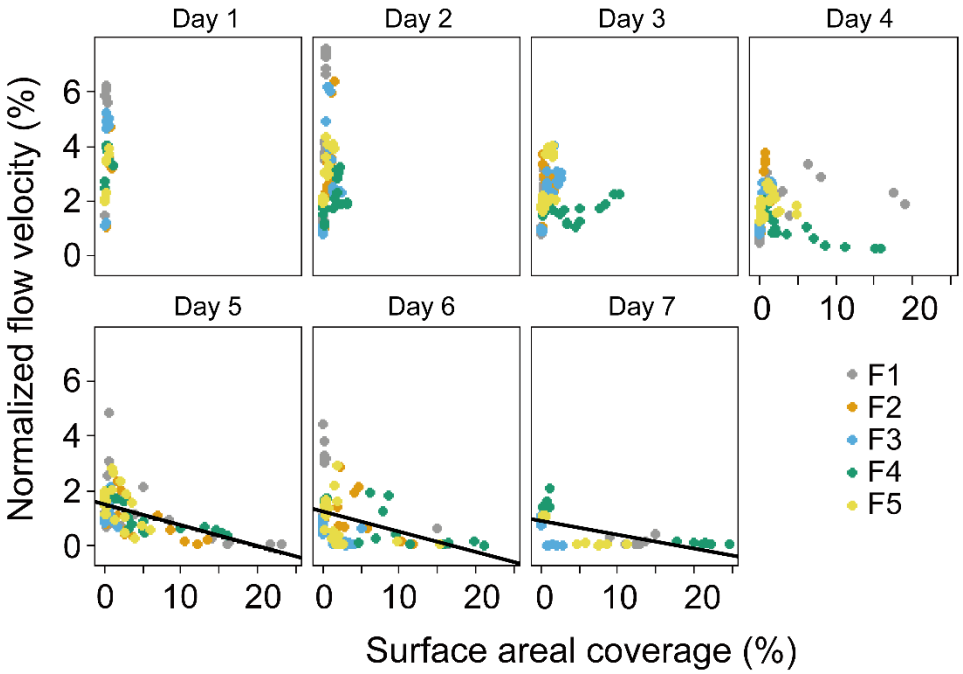

Figure 8. Normalized surface flow velocities (ratio of surface flow speed to wind speed) versus areal coverage of the water surface with algae. Symbols show mean values for different flumes F1 – F5, see legend. Different panels denote the time (day) during the experiment. No significant linear relationship was observed from Day 1 - 4 ($p > 0.05$), while significant linear relationship was observed from Day 5 to Day 7 (solid black lines, $p < 0.05$). F1: 6 h of high-magnitude (4.5 m^{-1}) wind disturbance; F2: 3 h of high-magnitude wind disturbance; F3: 6 h of moderate-magnitude (3.8 m^{-1}) wind disturbance; F4: 6 h of low-magnitude (1.5 m^{-1}) wind disturbance; F5: 3 h of low-magnitude wind disturbance.

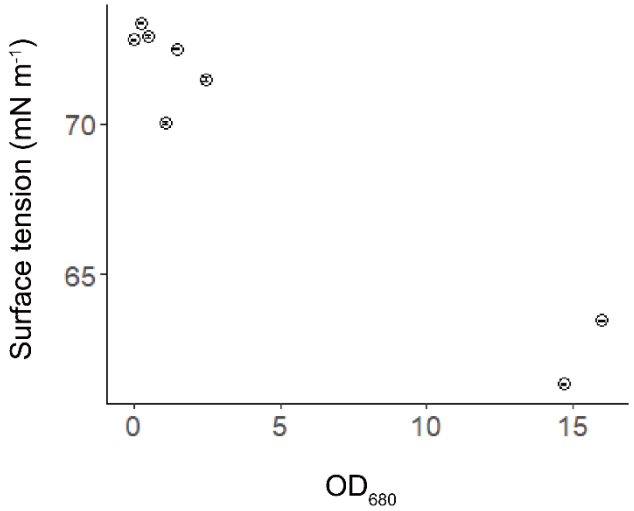

Figure 9. Water surface tension versus optical density of algal samples at 680 nm (OD_{680}). Error bars show the standard deviation of replicated surface tension measurements (*n*=3).

Table 1. Wind speed measured at 2 cm above the water surface in the flumes and the corresponding equivalent wind speed in the atmospheric boundary layer at 10 m height (U_{10}) derived from observed surface velocities at the beginning of the experiment using a wind factor of 0.01 (Wu 1975).

Wind speed measured in the flumes (m s^{-1})	Calculated wind speed at 10 m height (m s^{-1})	Magnitudes of wind disturbance
0.5	2.0 ± 0.5	No wind disturbance
1.5	2.8 ± 0.2	Low-magnitude
3.8	3.9 ± 0.4	Intermediate-magnitude
4.5	5.3 ± 0.4	High-magnitude

Supplementary Material

Supplementary Figures and Tables

1. Supplementary Tables

Supplementary Table 1: The composition of the stock solution containing BG11 medium (100X, Blue-Green Medium).

Compound	Concentration [g L^{-1}]
$NaNO_3$ (sodium nitrate)	150
K_2HPO_4 . $3H_2O$ (dipotassium phosphate)	3.14
$MgSO_4$.$7H_2O$ (magnesium sulfate)	3.60
$CaCl_2$.$2H_2O$ (calcium chloride)	3.67
citric acid	0.56
Ferric ammonium citrate	0.60
EDTA (dinatrium-salt)	0.10
Na_2CO_3 (sodium carbonate)	2.00

Supplementary Table 2: The resolution and size of the field of view of the videos recorded by the cameras in the flume experiments.

Flume	Camera	Resolution (μm pixel^{-1})	Field of view (cm^2)
F1	Down-looking	39.7	7.6 × 4.3
	Upper side-looking	25.5	4.9 × 2.8
	Middle side-looking	22.4	4.3 × 2.4
	Bottom side-looking	24.5	4.7 × 2.6
F2	Down-looking	40.0	7.7 × 4.3
	Upper side-looking	22.4	4.3 × 2.4
	Middle side-looking	26.0	5.7 × 3.2
	Bottom side-looking	29.9	7.6 × 4.3
F3	Down-looking	39.6	4.5 × 2.5
	Upper side-looking	23.5	5.6 × 3.2
	Middle side-looking	29.4	6.0 × 3.7
	Bottom side-looking	31.2	7.6 × 4.3
F4	Down-looking	39.2	7.5 × 4.2
	Upper side-looking	24.8	4.8 × 2.7
	Middle side-looking	30.1	5.8 × 3.3
	Bottom side-looking	28.2	5.4 × 3.0
F5	Down-looking	39.0	7.5 × 4.2
	Upper side-looking	21.7	4.2 × 2.3
	Middle side-looking	26.8	5.1 × 2.9
	Bottom side-looking	29.0	5.6 × 3.1

Supplementary Table 3: Linear regression coefficients for the flow velocity normalized by wind speed (y) versus time during the experiment (x in days) observed at the water surface and in three different layers of the water column in the five experimental flumes (F1-F5). r^2 denotes the coefficient of determination of the regressions. Except for near surface in F3, middle layer in F1 and bottom in F2, the slopes were significantly different from zero (p <0.05).

	Surface	Near surface	Middle layer	Bottom
F1	y=-0.55*x+4.29	y=-0.08*x+1.31	y=-0.04*x+0.94	y=-0.02*x+0.73
	r^2=0.82	r^2=0.70	r^2=0.54	r^2=0.74
F2	y=-0.37*x+3.12	y=-0.06*x+1.34	y=-0.07*x+1.40	y=-0.06*x+1.32
	r^2=0.93	r^2=0.70	r^2=0.67	r^2=0.41
F3	y=-0.48*x+3.62	y=-0.10*x+1.30	y=-0.09*x+1.18	y=-0.09*x+1.01
	r^2=0.90	r^2=0.56	r^2=0.91	r^2=0.82
F4	y=-0.36*x+3.04	y=-0.10*x+1.30	y=-0.09*x+0.94	y=-0.06*x+0.63
	r^2=0.79	r^2=0.72	r^2=0.85	r^2=0.90
F5	y=-0.42*x+3.54	y=-0.10*x+1.08	y=-0.09*x+1.20	y=-0.11*x+1.07
	r^2=0.99	r^2=0.73	r^2=0.65	r^2=0.96

2 Supplementary Figures

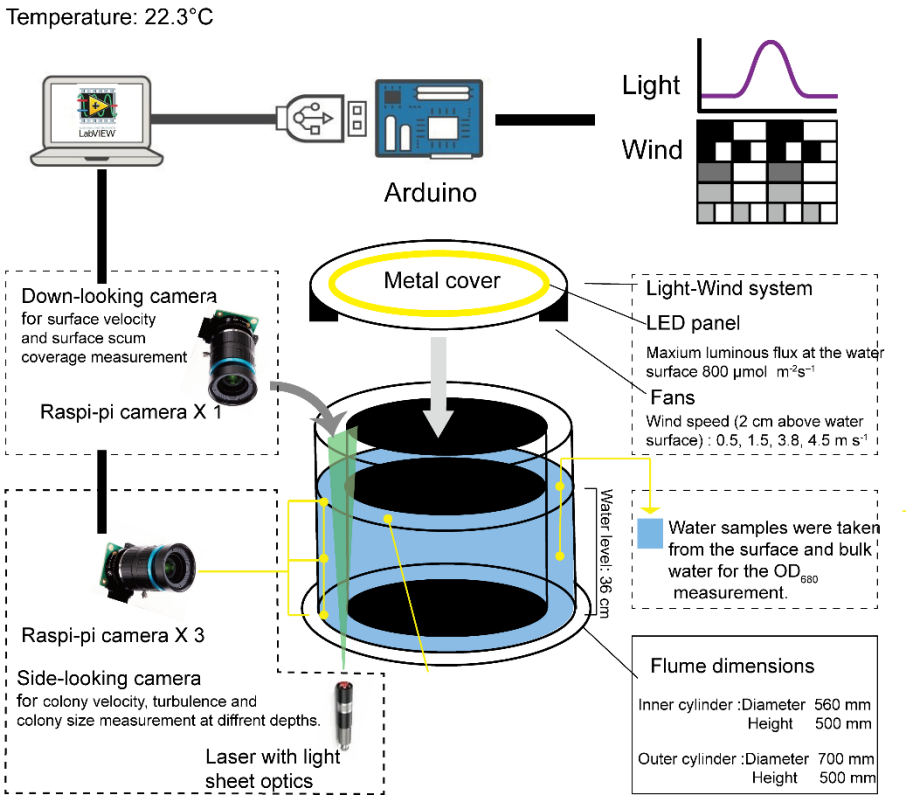

Supplementary Figure 1. Laboratory mesocosms with controlled environmental conditions including wind-generated turbulence and detailed characterization of *Microcystis* colony size and velocity. The water flows between the inner and outer cylinders of the annular flume. The flow is generated by wind, provided by two diagonally arranged fans (5 cm diameter, 12 V maximum supply voltage) above the water surface. Illumination of algae is provided by the five Light-Emitting Diode (LED) panels installed on the lid. Colonies at the air-water interface are observed by a downward-looking camera. In the bulk water, colonies are observed by three side-looking cameras and vertically arranged laser light sheet illumination. The light intensity and wind speed are controlled by an Arduino microcontroller. The microcontroller, all cameras, and the laser illumination for all five flumes are controlled by a central computer using a LabView (community edition, National Instruments, USA) program.

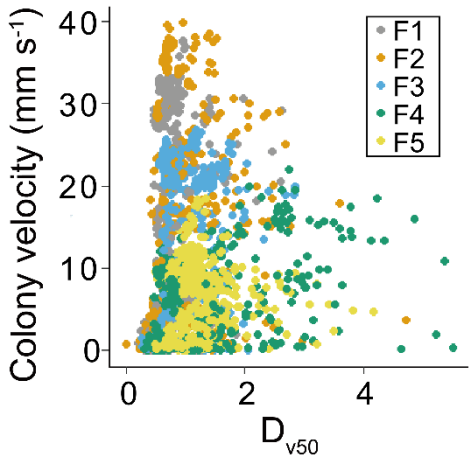

Supplementary Figure 2. The relationship between colony velocity and median volume diameter (D_{v50}) of *Microcystis* colonies.

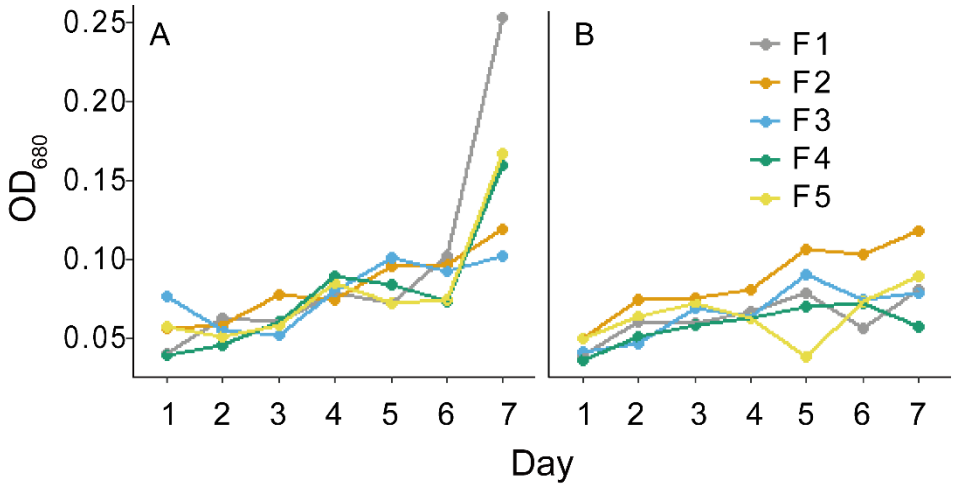

Supplementary Figure 3. The temporal dynamics of optical density at 680 nm (OD_{680}) of *Microcystis* samples in different flumes (see the color assignment) at the water surface (a) and in the middle layer in different flumes (b).

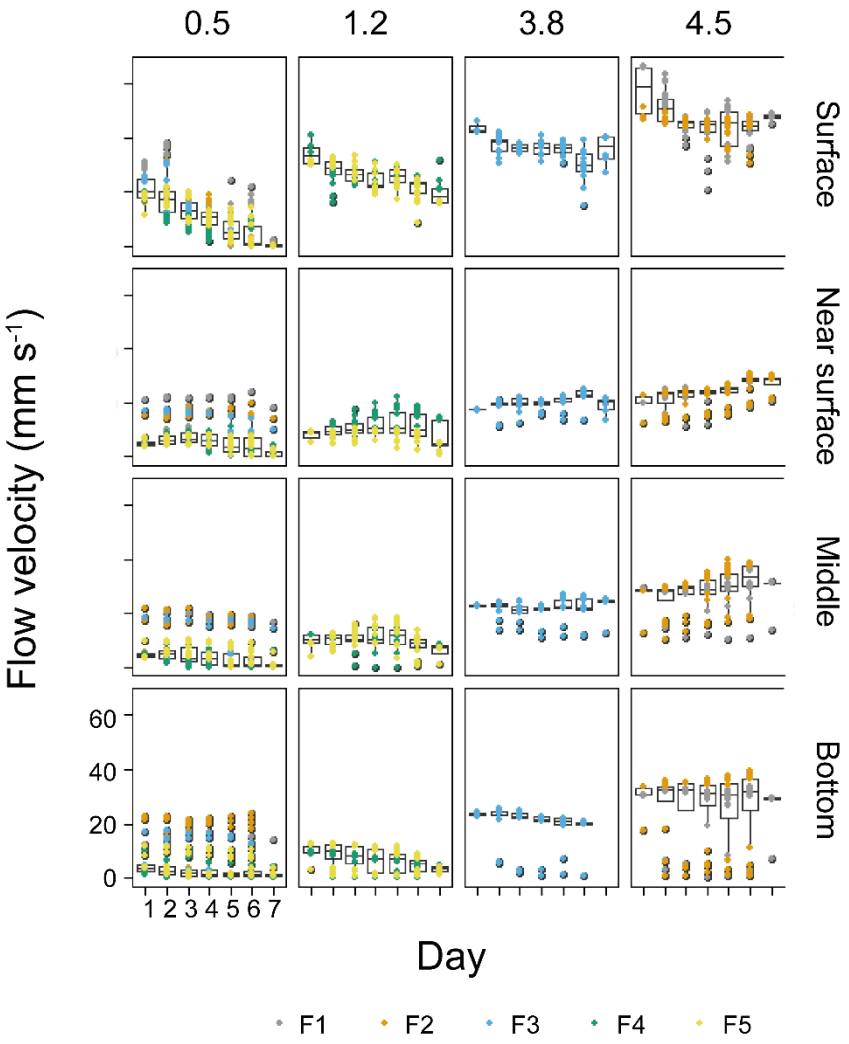

Supplementary Figure 4. Time series of flow velocity at different depths (rows) observed at different wind speed (columns, measured 2 cm above the water surface in the flumes) in different flumes (see legend for color assignment).

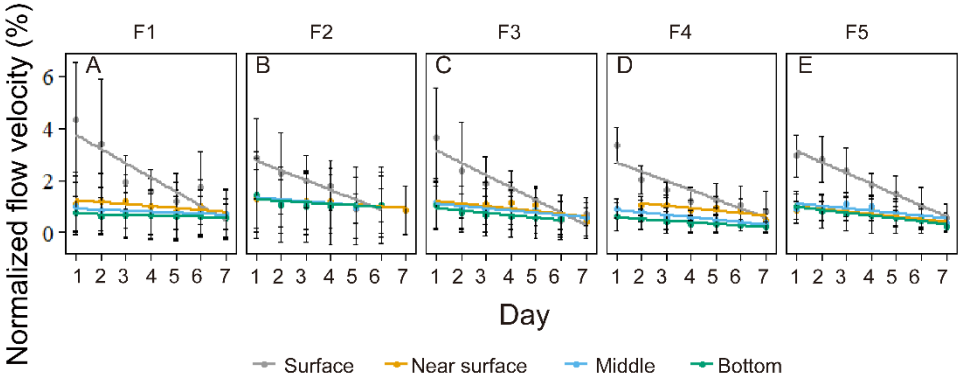

Supplementary Figure 5. Daily mean estimates of the normalized flow velocity (ratio of flow velocity to wind speed) at different depths (see legend for color assignment) to wind speed. Error bars show the standard deviation of the normalized flow velocity. The solid lines show linear regressions according to the equation provided (see Table.S2 for detailed equations and r^2). Except for near surface in F3, middle layer in F1 and bottom in F2, the slopes were significantly different from zero (p <0.05).

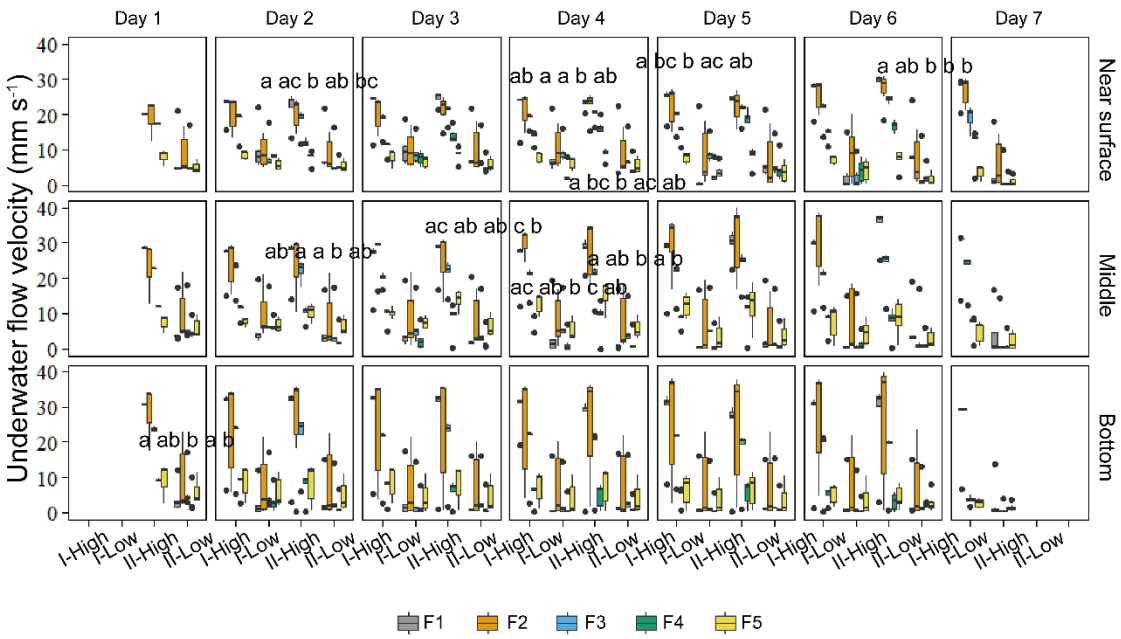

Supplementary Figure 6. Temporal dynamics of the mean underwater flow velocity at different water depth (rows) at different stages (I and II) and in different flumes (F1 – F5, see legend). High and Low represent the period of high wind speed (wind disturbances, 4.5 m s^{-1} for F1 and F2, 3.8 m s^{-1} for F3, 1.5 m s^{-1} for F4 and F5) and low wind speed (0.5 m s^{-1}), respectively. Each box plot shows mean flow velocities observed in hourly video observations at the given stage in different flumes during the 7 days. Different lowercase letters indicate significant differences in surface flow velocity at different stages during low wind periods among different flumes, while the same letter, or the lack of a letter, indicate no significant differences.

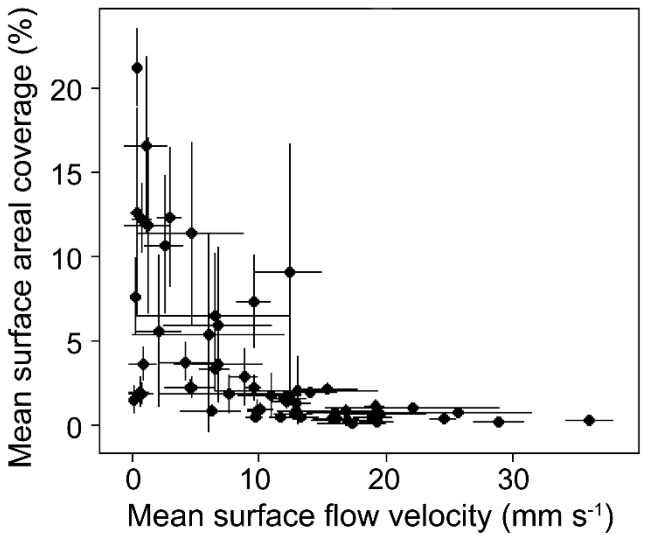

Supplementary Figure 7. Relationship between mean surface areal coverages and mean surface flow speed during low wind periods. Symbols show mean values and error bars indicate standard deviations.

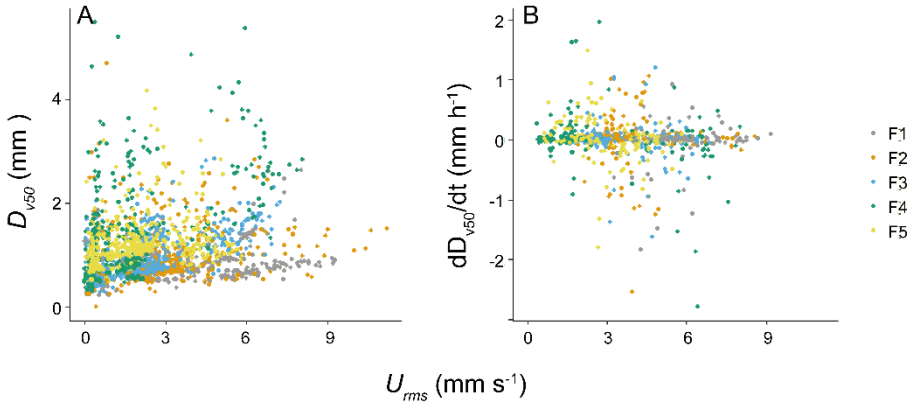

Supplementary Figure 8. The relationship between the median volume diameter (D_{v50}) and the root-mean-square of colony velocity (U_{rms}) (a), and between rate of change of colony size (dD_{v50}/dt) and U_{rms} (b). Different colour represent measurements in different flumes (see legend for color assignment).

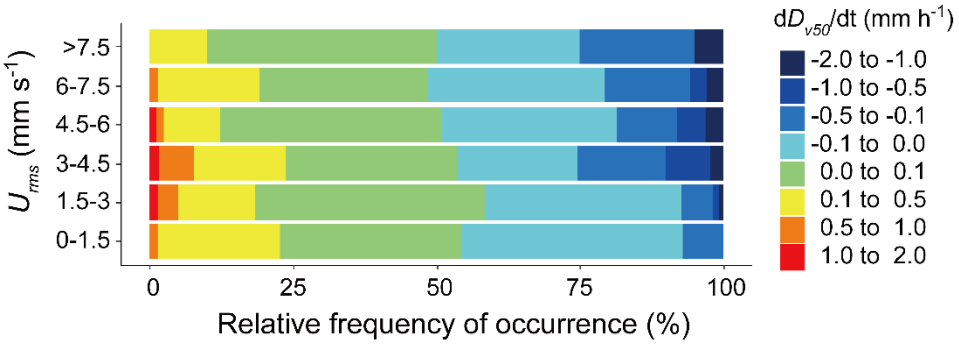

Supplementary Figure 9. Normalized frequency distributions of the mean rate of change of D_{v50} of *Microcystis* colonies (dD_{v50}/dt, see legend for color scaling) for different ranges of root-mean-square colony velocities (U_{rms}).

Appendices II

Selection of photosynthetic traits by turbulent mixing governs formation of cyanobacterial blooms in shallow eutrophic lakes

Huaming Wu[a], Xingqiang Wu[b], Lorenzo Rovelli[a,c], Andreas Lorke[a]

[a]Institute for Environmental Sciences, University of Kaiserslautern-Landau (RPTU), Landau 76829, Germany

[b]Key Laboratory of Algal Biology of Chinese Academy of Sciences, Institute of Hydrobiology, Chinese Academy of Sciences, Wuhan 430072, China

[c]now at the Department of Ecology, Federal Institute of Hydrology (BfG), Koblenz 56068, Germany

Please click the following link to read the publication

https://academic.oup.com/ismej/article/18/1/wrae021/7597770

Selection of photosynthetic traits by turbulent mixing governs formation of cyanobacterial blooms in shallow eutrophic lakes

Huaming Wu[a], Xingqiang Wu[b], Lorenzo Rovelli[a,c], Andreas Lorke[a]

[a]*Institute for Environmental Sciences, University of Kaiserslautern-Landau (RPTU), Landau 76829, Germany*

[b]*Key Laboratory of Algal Biology of Chinese Academy of Sciences, Institute of Hydrobiology, Chinese Academy of Sciences, Wuhan 430072, China*

[C]*now at the Department of Ecology, Federal Institute of Hydrology (BfG), Koblenz 56068, Germany*

Abstract

Prediction of the complex cyanobacteria-environment interactions is vital for understanding harmful bloom formation. Most previous studies on these interactions considered specific properties of cyanobacterial cells as representative for the entire population (e.g., growth rate, mortality, and photosynthetic capacity (P_{max})), and assumed that they remained spatiotemporally unchanged. Although, at the population level, the alteration of such traits can be driven by intraspecific competition, little is known about how traits and their plasticity change in response to environmental conditions and affect the bloom formation. Here we test the hypothesis that intraspecific variations in P_{max} of cyanobacteria (*Microcystis* spp.) play an important role in its population dynamics. We coupled a one-dimensional hydrodynamic model with a trait-based phytoplankton model to simulate the effects of physical drivers (turbulence and turbidity) on the P_{max} of *Microcystis* populations for a range of dynamic conditions typical for shallow eutrophic lakes. Our results revealed that turbulence acts as a directional selective driver for changes in P_{max}. Depending on the intensity of daily-periodic turbulence, representing wind-driven mixing, a shift in population-averaged phenotypes occurred toward either low P_{max}, allowing the population to capture additional light in the upper layers, or high P_{max}, enhancing the efficiency of light utilization. Moreover, we observed that a high intraspecific diversity in P_{max} accelerated the formation of surface scum by up to more than four times compared to a lower diversity. This study offers insights into mechanisms by which cyanobacteria populations respond to turbulence and underscores the significance of intraspecific variations in cyanobacterial bloom formation.

Keywords: Aquatic ecosystems; Cyanobacteria-environment interactions; Surface scum; Intraspecific variation; Population dynamics; Photosynthetic capacity

Highlights:

1. Numerical simulations of *Microcystis* population dynamics including intraspecific variations.
2. Moderate turbulence can induce a stable reduction in the photosynthetic capacity of the population.
3. High diversity in photosynthetic capacity accelerates scum formation.

1.Introduction

Harmful cyanobacterial blooms occur more frequently and more intensely at global scale as the environment is increasingly impacted by anthropogenic eutrophication, pollution, and extreme climate [1, 2]. Although various studies have focused on how abiotic and biotic environmental factors affect cyanobacterial population dynamics [3-6], they implicitly assumed that the variability of observed traits is independent of population dynamics and environmental stressors, such that a set of averaged trait properties adequately represents the population, regardless of the time or location. However, there is growing evidence that this simplified assumption may under-represent the importance of variation between individuals and community structure in population ecology [7-9]. As intraspecific variations have also been observed in cyanobacteria [10-13], their ability for bloom formation under diverse environmental conditions is potentially affected by the coexistence or competition of different traits.

Under the influence of environmental stressors, intraspecific variation is fundamental for driving intraspecific competition and thus shaping the population response. Selection favors traits that enhance individual fitness, leading to their increased prevalence under selective pressures and subsequently reshaping the distribution of traits. This process typically occurs over demographic timescales [14, 15]. Cyanobacteria, renowned for their rapid growth, are capable of doubling their population size within 1-2 days under ideal conditions [16]. This implies that cyanobacteria may have a high potential for selection, by which cyanobacterial populations accumulate favorable traits to cope with contrasting environments.

Photosynthetic capacity is crucial among multiple traits of cyanobacteria that drive the occurrence of surface blooms [17, 18]. Through the process of photosynthesis, cyanobacteria are converting sunlight into energy, which fuels cell division and metabolic processes, including the carbon-reserve metabolism [19]. The carbon-reserve metabolism is associated with buoyancy regulation and affects the vertical position of cyanobacteria in the water [20]. The mass density of cyanobacterial cells is modulated by the rate of carbohydrates produced through photosynthesis or consumed via respiration within the cells. This mechanism enables cyanobacteria to gain access to well-lit surface waters by consuming intracellular ballast, and access to nutrients at larger depths after storing sufficient carbohydrates. This mechanism has been extendedly used in predictive models for bloom dynamics [21, 22].

Given the considerable intraspecific variation in photosynthetic capacity of cyanobacteria, which can range over one order of magnitude [23, 24], it can be expected that traits with differing photosynthetic capacities migrate along different trajectories. This can lead to competition for light among traits and to interactions, e.g., by mutual shading, resulting in distinct life histories. Abiotic factors that regulate cyanobacterial bloom dynamics in lakes, such as turbulence and turbidity, may interact with the intraspecific light competition. High turbidity, for example, can diminish the availability of light in lakes, thereby directly affecting the ambient light prevailing traits, i.e., their light niches. Turbulence, in contrast, can control the vertical distribution of cyanobacteria, potentially either confining or relaxing the boundaries between the light niches utilized by traits with different photosynthetic capacities. A mechanistic understanding of such complex interactions between biotic and abiotic processes and the resulting cyanobacterial population dynamics is still lacking, and so is our understanding of their environmental relevance, e.g., for bloom formation.

In the natural water bodies, these interactions are affected and potentially masked by synoptic and seasonal variations in the physical forcing. Therefore, numerical modeling of the trait dynamics under idealized and simplified environmental conditions (e.g., periodic light and wind forcing) are a more appropriate approach for analyzing such complex interactions.

In this study, we implemented a simplified one-dimensional hydrodynamic model with a trait-based phytoplankton model to examine how turbulence and turbidity affect the photosynthetic capacity of cyanobacterial populations through trait selection and analyze the resulting changes in population composition during bloom formation. The model was used to simulate the growth and vertical distribution of colony-forming *Microcystis* populations with varying ranges of different photosynthetic capacities under commonly occurring turbulence and turbidity levels in lakes. We hypothesize that the photosynthetic capacity of a *Microcystis* population can be substantially altered by turbulence and turbidity and that this selection plays an important role during surface bloom formation. This study is thus expected to be instrumental in advancing our understanding of the cyanobacteria-environment interactions and their role during bloom formation.

2 Materials and methods

2.1 Model description

2.1.1 General description

Our model consists of three components: (1) a one-dimensional hydrodynamic model, (2) an ensemble-averaged transport model for simulating the trait-specific vertical distribution dynamics of cell number concentration, colony size, and cell-tissue density, and (3) an ecological model describing cell and colony photosynthesis and growth. The maximum photosynthetic rate (maximum rate of photosynthesis at optimal light intensity, normalized by carbon content, P_{max} in s^{-1}, [25]) was used to characterize the different photosynthetic capacity of *Microcystis* traits and was assumed to vary within different ranges for different initial population. We discretized the range of P_{max} observed for *Microcystis* populations [26-29] into ten evenly spaced subranges, resulting in ten trait groups (g_1-g_{10}), with increasing P_{max}. The population dynamics was simulated by simultaneously simulating the vertical distribution dynamics of the ten trait groups. The vertical distribution of each trait groups was obtained by solving the extended Langevin–Fokker–Planck equation (see below). While solving this equation for cell density (growth and loss processes), colony size, light-mediated changes in cell tissue density, and vertical colony migration (floating or sinking) velocity, as well as vertical turbulent mixing are considered as dynamic parameters. External environmental conditions include diel variations in turbulent diffusivity and light intensity. The latter interacts with the vertical distribution of the *Microcystis* population through self-shading, which is considered in addition to different background light attenuation coefficients, representing different water turbidity. As such, different trait groups can interact with each other by mutual shading. The models are described in detail below, while the main parameters, their numerical values and reference for parameter selection are summarized in the Supporting Information (Table S1).

The dynamics of *Microcystis* populations were simulated under simplified conditions representing an idealized shallow eutrophic lake, where we disregarded the effects of temporally and vertically varying water temperature and nutrient limitation. We assumed that *Microcystis* growth depends solely on irradiance, which varies with a diel cycle, and that a fixed P_{max} applies to each trait group (see Supporting Information

Text S1 for more details).

2.1.2 Distribution dynamics of *Microcystis* populations

The vertical dynamics of the cell density (C_i) of the trait group i (i = 1…10) was modeled by the extended Langevin–Fokker–Planck equation [30, 31], as follows:

$$\frac{\partial C_i}{\partial t} = -\left(\frac{\partial \rho}{\partial t}\right)\frac{\partial C_i}{\partial \rho} - \left(\frac{\partial d}{\partial t}\right)\frac{\partial C_i}{\partial d} - \left(\frac{\partial z}{\partial t}\right)\frac{\partial C_i}{\partial z} + \frac{\partial}{\partial z}\left(D_z \frac{\partial C_i}{\partial z}\right) + (r - l)C_i \quad (1)$$

Eq. 1 is a one-dimensional advection-diffusion equation commonly used to simulate the vertical migration of cyanobacteria under turbulence [31-33]. C_i (z, ρ, d, t) is the concentration of cells aggregated to colonies of size d (μm), at depth z (m) and time t (s), and with a cell-tissue density ρ (kg m^{-3}). By this definition, the distribution varies along the cell-tissue density coordinate ρ, colony size coordinate d as well as along physical depth coordinate z, and time t. The index i stands for different trait groups (g_1 –g_{10}) of the population. The first three terms on the right-hand side of Eq. 1 are advective terms in the ρ, d, and the vertical coordinate (z), respectively. Herein, $\partial z/\partial t$, $\partial \rho/\partial t$, and $\partial d/\partial t$ denote the rates of change of depth, cell density, and colony size of the respective trait groups. The fourth term describes vertical transport by turbulent diffusion with D_z (m^2 s^{-1}) denoting the turbulent diffusivity at depth z. The last term describes growth and loss processes with r and l being growth and loss (mortality) rates of *Microcystis*. We define the direction of z is positive downward.

2.1.3 Photosynthesis model of *Microcystis*

A classical *P-I* relationship was used to relate the photosynthetic rate (P, s^{-1}) to irradiance (I) as follows [34, 35]:

$$P = \frac{I}{aI^2 + bI + c} \quad (2)$$

where a, b, and c are related to characteristic photosynthesis parameters (i.e., the initial slope (S), the maximum photosynthetic rate (P_{max}) and the optimal light intensity (I_{opt}) can be expressed in terms of the parameters as: S=1/c; I_{opt}=(c/a)$^{1/2}$; P_{max}=1/(b+2*(ac)$^{1/2}$) [34]). In this study, we assumed constant values for I_{opt} (~277.5 μmol photons m^{-2} s^{-1}, [36, 37]) and S (2×10^{-7} (μmol photons)$^{-1}$ m^2, [27]). Especially the latter has been found to be almost constant from March to October (the period of a *Microcystis* bloom) in lake Kasumigaura [27].

2.1.4 Growth, loss, and cell tissue density of *Microcystis*

The rate of carbon fixation by photosynthesis (P in Eq. 2) is allocated to cell growth (gr), the rate of change in ballast (characterized by the rate of change in cell tissue density, $\partial\rho/\partial t$), and the respiration rate (R), following as [36, 38]:

$$gr = \begin{cases} g_{max}, if\ P - R \geq g_{max} \\ P - R, if\ g_{max} > P - R \geq 0 \\ 0, if\ P - R < 0 \end{cases} \quad (3)$$

$$\frac{\partial \rho}{\partial t} = \begin{cases} m_{cell} \cdot (P - R - g_{max}) \cdot \frac{B_g}{V_{cell}}, if\ P - R \geq g_{max} \\ 0, if\ g_{max} > P - R \geq 0 \\ (f_1 \cdot \rho_i + f_2)/60, if\ P - R < 0 \end{cases} \quad (4)$$

where g_{max} is the maximum carbon uptake rate for growth (set to a constant value of 5.5×10^{-6} s^{-1}, corresponding to the growth rate of 0.48 d^{-1}), as it is independent of P_{max} [24]. The respiration rate (R) was assumed to remain constant at 0.55×10^{-6} s^{-1} [25]. B_g represents the mass of carbohydrate (glycogen) ballast produced per gram of assimilated carbon, with a value of 2.38 and V_{cell} is the volume a single *Microcystis* cell (taken to be 67×10^{-18} m^3), and m_{cell} is the amount of carbon contained in each cell (14×10^{-15} kg) [25]. The loss rate of *Microcystis* (l) was assumed to be constant (0.1 d^{-1}, [33]). f_1 (min^{-1}) is the slope of the curve of density change, f_2 is the theoretical rate (kg m^{-3} min^{-1}) of density change with no carbohydrate storage in the cells and ρ_i is the initial density (kg m^{-3}).

2.1.5 Colony size, migration velocity of *Microcystis*, and external environmental conditions

The interactions between environmental conditions and colony size dynamics are complex and involve cell division, cell adhesion, and colony disaggregation. For simplicity, we neglect cell adhesion as colonies formed through adhesion are more readily disaggregated [39]. Hence, colonies consist of cells of a single genotype and identical photosynthetic capacity in this study. The colony size was modulated by the growth and mortality (loss) of *Microcystis* cells and was constrained by an upper limit (420 μm), which corresponds to the largest stable colony size under turbulent conditions [40]. Colonies grow and shrink in size, depending

on whether net grows (r - l) is positive, or negative, respectively. The rate of change of colony diameter ($\partial d/\partial t$) was approximated as a function of net cell growth (r - l) following [22]:

$$\frac{\partial d}{\partial t} \approx d_{t-1}\left(2^{\frac{\triangle t\cdot(r-l)}{\ln(2)}}-1\right)/\triangle t \quad (5)$$

where d_{t-1} is the colony size at the previous time step (t-1) and Δt is the time step in the discretized numerical solution. This equation is derived from the mechanism of colony formation, where the size of the colony increases through cell division [39]. Thus, colony size is indirectly linked to photosynthetic capacity.

The vertical velocity of *Microcystis* follows Stokes' law (Text S2). Due to varying drivers (e.g., wind shear versus convection) and the influence of density stratification, there is no universal profile for the vertical distribution of turbulent diffusivity in lakes. For simplicity, we adopted the empirical vertical turbulent diffusivity (D_z) profile from a previous study [41], wherein the turbulent diffusivity is fixed throughout an upper layer of the lake (approximately 10% of water depth), and declines with depth following a parabolic profile below this layer (see Text S3). In the following, we used the maximum D_z ($D_{z,max}$) within each profile for referring to the corresponding D_z profiles. The irradiance profiles were simulated by Lambert–Beer's law, considering the self-shading of the *Microcystis* population and a constant background turbidity that was varied in our simulations (Text S3).

2.2 Simulation setting

In our simulations, the water depth was fixed to 3 m with a resolution of the vertical discretization of 0.05 m, the cell tissue density ranged from 996 to 1130 kg m^{-3} with a resolution of 3.35 kg m^{-3} [31], and the colony size ranged from 10 to 420 μm with resolution of 10 μm [42]. No-flux conditions are applied at the boundaries of z, ρ, and d axes.

The initial cell density for all trait groups of the *Microcystis* population was uniform throughout the water column, with an initial colony size of 50 μm. The uniform vertical distribution and consistent colony size are widely used initial conditions in former studies [31, 33]. Given the unknown trait distribution in nature, we also used an initially uniform distribution to allow different trait groups to compete equally. The chosen initial colony size and cell density (2×10^4 cells mL^{-1}) correspond to conditions observed in the early phase (~April) of *Microcystis* blooms in lake Taihu [43]. The initial density of colonies was set to 998 kg

m^{-3} (neutrally buoyant).

All simulations started at 6:00 and were performed for 180 consecutive days. Depending on the turbulent eddy diffusion coefficient, the temporal resolution of the simulations was varied from 1.2 to 120 s to ensure that the time step met the stability condition for Eq. 1 [44].

We used an iterative algorithm at each time step (time-stepping solver) to solve the above equations and to obtain the dynamic distributions of all trait groups of *Microcystis* colonies throughout the water column. The solver was implemented through a self-written computer program in MATLAB 2022b, where the first and second derivatives were approximated using a combination of forward and central differences.

We used six *Microcystis* populations with initially varying ranges of P_{max} (population I – VI, Fig. 1). The arithmetic mean P_{max} of each population was 28.9 $\times 10^{-6}$ s^{-1}. Each population is composed of ten trait groups (g_1-g_{10}), which differ among different populations. We simulated the dynamics of the populations under seven different turbulence conditions and with three different background extinction coefficients, resulting in a total of 126 simulations (6 × 7 × 3, Fig. 1). Except for the complete mixing condition, the turbulent conditions used in this study followed a diel pattern, with a constant diffusivity of $D_{z,max}$=10^{-6} m^2 s^{-1} applied during nighttime (18:00 – 6:00), while higher constant diffusivities during daytime (6:00 18:00) were varied between $D_{z,max}$=5×10^{-6}, 1×10^{-5}, 5×10^{-5}, 1×10^{-4}, 5×10^{-4}, and 1×10^{-3} m^2 s^{-1} (turbulent diffusivity change suddenly in the morning and evening). Under complete mixing conditions, we assumed uniform vertical distribution of *Microcystis* cell density throughout the water column and excluded diel patterns, thus focusing solely on the growth and loss of *Microcystis*. The range of turbulent diffusivities used in this study correspond to the observed range in natural lakes and the complete mixing represent strong turbulence such as storm conditions [45]. The respective ranges of P_{max} for different populations, turbulence conditions ($D_{z,max}$), and light extinction coefficients (K_{bg}) used in the simulations are summarized in Fig. 1.

2.3 Data processing

The mean vertical positions of trait groups were described by the centroids (z_c) of their vertical distributions:

$$z_c = \frac{\sum_{j=1}^{m} c_j \cdot z_j}{\sum_{j=1}^{m} c_j} \quad (6)$$

where z_c is the centroid of the population/trait group, m is the number of vertical layers (m =60), C_j is the cell density in the j^{th} layer, and z_j is the depth of the j^{th} layer.

The population-averaged photosynthetic capacity of *Microcystis* ($\overline{P}_{max}$) was characterized by the average value of all trait groups:

$$\overline{P_{max}} = \frac{\sum_{i=1}^{n} \bar{C}_i \cdot P_{\max,i}}{\sum_{i=1}^{n} \bar{C}_i} \quad (7)$$

where n is the number of trait groups in each population (n=10), $\bar{C}_i$ and $P_{max,i}$ are the mean (vertically averaged) cell density and the maximum photosynthetic rate of each trait group (g_i).

The distribution of irradiance in the water column was characterized by the euphotic depth, which was calculated as the depth at which the light intensity decreased to 1% of its maximum value at the water surface.

The relative cell density of trait groups (*RC*) was used as a proxy for the distribution of traits with different photosynthetic capacity within the populations. This was determined by calculating the ratios of trait group cell density to total population cell density.

We established specific thresholds to differentiate different levels of blooms and surface scum for the *Microcystis* population (see Supporting Information Text S4 for more details).

3 Results

3.1 Effect of turbulence on population composition and photosynthetic capacity

We observed an exponential growth of the population during the initial phase, which levelled off after 90 –180 days when the cell densities reached constant maximal values for all simulated turbulence and turbidity conditions (Fig. S1). Similarly, the mean population depth (i.e., the depth of its centroid) showed an initial decrease followed by an increase and eventual stabilization in the upper part of the water column under all turbulence conditions, except for the complete mixing (Fig. S2). The hourly time series of the centroid depth of the population exhibits a diel pattern, with the centroid increasing during daytime and decreasing during nighttime (Fig. S3). However, the population composition and the population-averaged P_{max} ($\overline{P}_{max}$) responded differently to turbulence and turbidity conditions (Fig. S4 & Fig. S5). We identified

four representative turbulence-dependent patterns in population composition dynamics, which we exemplarily describe for the lowest turbidity (0.6 m^{-1}, Fig. 2).

Under weak turbulence ($D_{z,max}$ =5×10^{-6} m^2 s^{-1}), the relative cell density (*RC*) of the trait groups was similar during the initial 30-day period, with a nearly constant $\overline{P}_{max}$ (Fig. 2). The centroid of the *Microcystis* trait group with the lowest photosynthetic rate (g_1) moved rapidly to the water surface (Fig. S6). This is primarily due to its higher floating velocity (Fig. S7a), which results from a rapid decrease in mass-density (Fig. S7c), compared to the other groups. Consequently, its cell density increased rapidly between 30 and 60 days (Fig. S6a), leading to an increase in the *RC* of g_1, while the $\overline{P}_{max}$ decreased (Fig. 2). In contrast to g_1, trait groups g_2 –g_{10} showed opposing migration behavior during the first 30 days, with increasing depths of the centroids of their distributions (Fig. S6b) due to high mass-densities (Fig. S7c). However, during 30-180 days, their centroid depths decreased and gradually approached the water surface (Fig. S6) and their cell densities increased (Fig. S6a). This change is a consequence of their decreasing mass-densities (Fig. S7c), likely due to increasing self-shading (decreasing euphotic depth, Fig. S6b). At day 60, the cell density of the group g_1 started to decrease, while its centroid remained at the water surface for a period of around 40 days before continuously increased to larger depths after day 100 (Fig. S6a). The decline of g_1 is likely attributed to the competitive advantage of g_2 –g_{10} (with higher P_{max}) over g_1 at the water surface. Additionally, there was an increase in the *RC* of the trait groups g_2 –g_{10} after 60 days, leading to a reversal of the decline and a continuous increase of the $\overline{P}_{max}$ (Fig. 2). At day 180, the population was dominated by the trait groups g_2 –g_6.

Under moderate turbulence (e.g., $D_{z,max}$ =1×10^{-4} m^2 s^{-1}), the centroid of trait group g_1 initially decreased and stabilized at the water surface after 20 days (Fig. S6b). As time progressed, the cell density of g_1 increased continuously, while that of the remaining trait groups (g_2 –g_{10}) initially increased, followed by a subsequent decrease (Fig. S6a). Simultaneously, an increasing *RC* of g_1 within the *Microcystis* population and a reduction of the $\overline{P}_{max}$ was observed (Fig, 2). The trait groups g_2 –g_{10}, unlike under weak turbulence, did not accumulate at the water surface, which can be explained by the higher turbulent dispersion as well

as their low floating velocities (~ 0 μm s^{-1}, Fig. S7a). The latter is the results of their decreasing colony size (Fig. S7b), likely caused by their declining growth (cf. eq. 5). Consequently, the decrease in the $\overline{P}_{max}$ did not reverse under moderate turbulence. After 90 days, the trait group g_1 had become the dominant trait group the *Microcystis* population, with a *RC* exceeding 99.9% (Fig. 2). This indicates that moderate turbulence could result in a stable population dominated by almost a single trait of low P_{max}.

Under strong turbulence (e.g., $D_{z,max}$ =1×10^{-3} m^2 s^{-1}), the centroid of trait group g_1 did not reach the water surface, but it still remained at shallower depths than those of trait groups g_2 –g_{10} (Fig. S6b). After 60 days, there was a significant increase in the cell density and *RC* of trait group g_1 (Fig. S6a & Fig. 2). This resulted in a continued decrease in the $\overline{P}_{max}$, similar to what was observed for moderate turbulence (Fig. 2). However, unlike the population composition observed under moderate turbulence, the *RC* of trait groups g_2 –g_{10} still exceeded approximate 8% under high turbulent conditions at the end of the simulation (Fig. 2).

Complete mixing homogenized the population throughout the water column, leading to a location of the centroid of all trait groups at mid depth (Fig. S6b). The cell density of each trait group was positively correlated with its corresponding P_{max}: Over the entire simulation period of 180 days, *Microcystis* trait groups with high P_{max} gradually developed higher cell densities and *RC* (Fig. S6a and Fig. 2), suggesting that trait groups with higher photosynthetic rates were more competitive and had slightly higher growth rates under completely mixed conditions. This was associated with a simultaneous increase in the $\overline{P}_{max}$ of the entire *Microcystis* populations (Fig. 2).

3.2 Effect of turbidity on population composition and photosynthetic capacity

The population composition dynamics of *Microcystis* generally followed the typical pattern for different turbulence regimes (as we present in section 3.1) across the range of tested turbidity (Fig. S4). Although the pattern of the $\overline{P}_{max}$ was primarily influenced by turbulence, we observed that turbidity affected time when the $\overline{P}_{max}$ began to decline and reverse under low turbulence conditions. Here we exemplarily presented these results for the lowest turbulence ($D_{z,max}$=5×10^{-6} m^2 s^{-1}, Fig. 3).

Under different turbidities, the $\overline{P}_{max}$ consistently exhibited a pattern of initial stability, followed by a

decline, and eventual increase (Fig. 3). All trait groups initially exhibited a similar growth trend (Fig. S8a), during which $\overline{P}_{max}$ remained relatively constant. However, higher turbidity accelerated the decline of $\overline{P}_{max}$ compared to lower turbidity (Fig. 3). In addition. as turbidity increased, the time at which $\overline{P}_{max}$ started to change (defined as a change from the initial $\overline{P}_{max}$ of more than 5%) decreased from 40 days to 12 days and 7 days for background extinction coefficients (K_{bg}) of 0.6 m^{-1}, 1.2 m^{-1}, and 1.8 m^{-1} (Fig. S9).

Turbidity also affected the reversal of the declining $\overline{P}_{max}$ under low turbulence. High turbidity (1.8 m^{-1}) delayed the occurrence of the reversal (the time at which $\overline{P}_{max}$ undergoes a change in direction from decreasing to increasing) compared to low turbidity (0.6 m^{-1}) by a factor of 2.5 (Fig. 3). This can be explained by the observation that low turbidity led to larger colony size of g_2-g_{10} and therefore their higher floatation velocity (Fig. S10), facilitating their faster upward migrations than under high turbidity (Fig. S8b). As a result, the trait distribution of the population at the end of the simulation (180 days) differed for different turbidities (Fig. 3). Under low turbidites, the population was dominated by traits with higher photosynthetic capacity (g_3 –g_{10}), while under high turbidity, the population was dominated by traits with low photosynthetic capacity (g_1 and g_2).

3.3 Effect of intraspecific variation on bloom and scum formation

We simulated the processes of bloom and scum formation of *Microcystis* population with varying initial ranges of photosynthetic capacity (Population I - Population VI) under different turbulence and turbidity. The simulated cell densities showed good consistency with those in the supplementary simulations performed with different initial conditions for the vertical distribution of the colonies and for initial colony size (Fig. S11).

We found that low turbulence promoted the growth of population with wide ranges of P_{max}, while high turbulence promoted the growth of population with more narrow ranges of P_{max} (Fig. 4). This resulted in differences of total cell density between different populations with different ranges of P_{max} decreased with increasing turbulence. Under complete mixing conditions, the total biomass of populations with different ranges of P_{max} showed similar levels (Fig. 4). Under moderate and low turbulence conditions, the initially

more diverse population (with initially wider range of P_{max}) exhibited profoundly higher cell densities compared to the populations with a narrower range. The cell density of population I was found to be up to 2.5 times higher than that of population VI under such conditions (Fig. 4). In contrast, high turbidity tended to increase the difference of total cell density among different populations and decreased the maximum cell density. Similarly, our results showed that *Microcystis* populations with a wider initial range of P_{max} can form denser scum layers. We observed higher cell density in the surface scum layer for populations with a wide range of in P_{max} over the period of 180 days, particularly in populations I, II, and III (Fig. 5).

The timescale for moderate and severe bloom formation ranged from 26 to more than 180 days. Similarly, we observed that the duration for the *Microcystis* population to develop blooms generally decreased as the range of intraspecific variations in P_{max} expanded (Fig. 6). However, under K_{bg} = 0.6 m^{-1}, the time required for all the tested populations to form a moderate bloom was similar, ranging from 26 to 27 days (Fig. 6a). This suggests that the influence of turbulence and intraspecific variation in photosynthetic capacity on the occurrence of moderate blooms is not apparent at low turbidity, likely due to the comparable growth rates among the different populations in well-illuminated environments. Generally, a wide range of P_{max}, low turbidity and low turbulence were accelerating bloom formation (Fig. 6a). The effect of turbidity on the formation of blooms and scum depended on the intensity of turbulence. Under low turbulence (diffusivities below 1×10^{-4} m^2 s^{-1}), the total cell density was marginally affected by turbidity, while under higher turbulence (diffusivities exceed 1×10^{-4} m^2 s^{-1}), the total cell density under K_{bg} of 1.8 m^{-1} decreased by up to 55%, compared to that under K_{bg} of 0.6 m^{-1} (Fig. 4). This result is likely because *Microcystis* tended to float to the water surface under conditions of low turbulence, which minimizes the impact of turbidity.

The formation time of surface scum was negatively correlated to the range of P_{max} within the tested population (Fig.6c and d). Population I showed a significant reduction in the timescale required to form moderate surface scum, up to more than four times faster than population VI (Fig. 6c). By contrast, populations with an initially narrow range of P_{max} (e.g., Population IV, V, and VI) were unable to develop severe blooms or scum during the simulation period (Fig. 6). Surface scum was also less likely to occur under high turbidities (1.8 m^{-1}) and high turbulences (diffusivity of 5×10^{-4} and $1\times10^{-3}m^2$ s^{-1}, and mixing

conditions, Fig. 6c-d).

4 Discussion

4.1 Benefits of diversification of photosynthetic capacity for *Microcystis* populations

In this study, we investigated the selective process for the photosynthetic capacity of *Microcystis* traits under various simplified mixing dynamics and turbidity conditions typical for eutrophic and shallow lakes. Our findings demonstrate that both turbulence and turbidity play important roles in reshaping the population composition and the population-averaged photosynthetic capacity. Turbulence can selectively shift the population-averaged photosynthetic capacity towards either a high or low photosynthetic rate, primarily depending on the intensity of turbulence (Fig. 2). High turbidity, in contrast, accelerates the change in population-averaged photosynthetic capacity, likely by increasing light limitation and the competition for light. It also affects the trait composition and population dynamics of *Microcystis* (Fig. 3).

The underlying basis of the plasticity in population-averaged photosynthetic capacity lies in the contrary role of photosynthetic capacities in the migration and growth of *Microcystis*. *Microcystis* with high photosynthetic capacity have a greater growth potential but readily accumulate excessive ballast, which hinders access to light in the upper layers. Conversely, *Microcystis* with low photosynthetic capacity exhibit higher flotation velocities (Fig. S7), and consequently tend to position at shallower depths to capture additional light. Our results show that fast-floating *Microcystis* (e.g., trait group g_1) can stratify, if the turbulent diffusivity is smaller than 10^{-3} m^2 s^{-1} (Fig. S6b), similar to findings in previous studies [33, 42]. By the intraspecific diversification of the photosynthetic capacity, the *Microcystis* population can accumulate traits with the fittest photosynthetic capacity (accompanied by changes in population composition) across variable environmental conditions, optimizing the utilization of light resources for growth. The flexibility observed in the photosynthetic capacity of cyanobacterial populations, brought to light by our simulations, offers insights into how turbulence and turbidity might affect the population dynamics and primary production.

We also simulated the development of bloom and scum by *Microcystis* population with different initial diversities (range) of photosynthetic capacity. The simulated maximum depth-averaged cell density of

Microcystis (approximate 3.2 $\times 10^6$ cells mL^{-1}), and cell density of surface scum (approximate 1.8 $\times 10^8$ cells mL^{-1}) under ideal conditions exceed those observed during bloom periods in lake Taihu and lake Dianchi, China [46, 47], but are comparable to the values observed in Nakdong River (South Keara), Central Park Lake, and Prospect Park Lake (USA) [48, 49]. Depending on the diversity of photosynthetic capacity and environmental conditions, the timescale for surface bloom formation varied from 26 to 180 days, which is consistent with observations in natural systems during cyanobacterial bloom periods [48-51]. Our results reproduce the diel migration pattern of *Microcystis* (Fig. S3) that is commonly observed in lakes [20], supporting the validity of the model. The main simulation results also showed good consistency with the supplementary simulations applying different initial conditions, indicating that the model is not very sensitive to changes in the initial vertical distribution and colony size.

Our results further demonstrate that high diversity of photosynthetic traits within the seed population promotes bloom formation of *Microcystis* populations across a broad range of physical environmental conditions, particularly under conditions of high turbidity and low turbulence (Fig. 4). This finding can be attributed to the fact that high diversity provides a larger pool of traits for selection to act upon and ensures a more efficient use of available light. Because of the adaptations, the diversity of photosynthetic capacity also plays an important role in the formation of scum layers. The diversity of photosynthetic capacity largely determines whether scum can occur within a 180-day period in shallow eutrophic lakes (Fig. 6). A wide range of photosynthetic capacity accelerate the formation of dense scum layer by decreasing the timescale for its development by up to more than 4-fold, compared to more narrow ranges (Fig. 6).

The general paradigm suggesting that higher intraspecific trait diversity facilitates faster population growth has been proposed in prior studies [8, 52, 53], but its specific effects on cyanobacteria and surface scum has not been explored. The findings presented here indicate that this paradigm is applicable to cyanobacteria. As such, our study introduces a new perspective for investigating and predicting cyanobacterial blooms.

4.2 Environmental relevance and limitations

Although the model is limited to a narrow range of environmental conditions, i.e., period of relatively

stable water condition with no significant nutrients limitation, our results have clearly highlighted the importance of the photosynthetic trait in shaping the *Microcystis* population dynamics and could offer an alternative explanation for some field observations. For example, in Lake Kasumigaura, despite a relatively stable mean water temperature during the two periods in July to August and September to October, there was a significant decrease in P_{max} of *Microcystis* during the first period, followed by an increase during the second period [27].

We expect that the interactions observed between cyanobacteria with diverse traits, turbulence, and light in our study would similarly apply to more dynamic conditions and exert varying degrees of influence on the photosynthetic capacity and population dynamics within dynamically changing real-world environments. To enhance the understanding of *Microcystis* dynamics under more dynamic environmental conditions, it would be advantageous to incorporate intraspecific trait variations into more complex models, such as integrating additional ecological factors (e.g., nutrient limitation) and utilizing more sophisticated hydrodynamic models such as including variable atmospheric forcing [21]. It is worth noting that obtaining the initial conditions of trait composition, which are necessary and essential for the trait-based model, could be achieved by collecting a substantial number of samples from lakes.

Our model did not account for all the processes that may directly or indirectly influence the dynamics of cyanobacterial populations due to the partially unclear mechanisms involved. For example, the plastic photosynthetic capacity response of traits to the environment (e.g., temperature and nutrient); the additional interactions among *Microcystis* colonies; and the intricate interplay between colony size and the environment, which also involves colony disaggregation and cell adhesion [39, 40, 54]. Particularly, cell adhesion may facilitate the formation of multi-trait colonies. Furthermore, our study only considered variations in one key trait, whereas additional traits, such as toxigenicity and the optimal light intensity of the P-I curve, may also influence population dynamics. The latter may allow certain groups to reach different P_{max} at lower or higher irradiance than other groups within each population. With such differentiation, populations that might more effectively exploit a wider range of available irradiance, i.e., population with less niche overlap, are expected to outperform the type of population currently utilized in our study, at least

under some of our modelled environmental conditions. A more accurate depiction of the intricate population dynamics would include these processes and more traits variations.

Our finding of a consistently dominant population characterized by low photosynthetic capacity (Fig. 2) under periodic moderate turbulence presents an intriguing possibility to employ artificial mixing techniques for manipulating traits and their diversity within the *Microcystis* population. For example, implementing controlled, moderate artificial mixing during bloom events could potentially reduce the diversity of photosynthetic capacity, lower the resilience of the population, and mitigate future blooms. This concept offers a new theoretical foundation for using artificial mixing as a means to mitigate blooms [55].

Recently, increasing underwater light attenuation due to ongoing anthropogenic pollution has been observed [56]. The increased turbidity is expected to enhance buoyancy [36] but concurrently reduces the growth of *Microcystis*. Although our model predicts an overall negative impact of turbidity on scum formation (Fig. 4 & Fig. 5), our results also revealed an intensification of differences in bloom formation among populations with varying diversities due to elevated turbidity (Fig. 4). Hence, we call for the inclusion of intraspecific variation to better predict how physical environmental variables affect ecosystem productivity and shape the fate of cyanobacteria in present-day and future environmental conditions.

Acknowledgements

This study was financially supported by the German Research Foundation (grant no. LO 1150/18) and the National Natural Science Foundation of China (grant nos. 42061134013).

Competing Interests statement

The authors declare no competing financial interests.

Data Availability statements

The scripts and datasets in the current study are available at the Knowledge Network for Biocomplexity (KNB) repository (doi:10.5063/F1V986J0).

Reference:

1. Ho JC, Michalak AM, Pahlevan N. Widespread global increase in intense lake phytoplankton blooms since the 1980s. Nature 2019;574:667-670.
2. Paerl HW, Huisman J. Blooms like it hot. Science 2008;320:57-8.

3. Harke MJ, Steffen MM, Gobler CJ, Otten TG, Wilhelm SW, Wood SA, et al. A review of the global ecology, genomics, and biogeography of the toxic cyanobacterium, *Microcystis* spp. Harmful Algae 2016;54:4-20.
4. Hellweger FL, Martin RM, Eigemann F, Smith DJ, Dick GJ, Wilhelm SW. Models predict planned phosphorus load reduction will make Lake Erie more toxic. Science 2022;376:1001-1005.
5. Huo D, Gan N, Geng R, Cao Q, Song L, Yu G, et al. Cyanobacterial blooms in China: diversity, distribution, and cyanotoxins. Harmful Algae 2021;109:102106.
6. Tromas N, Fortin N, Bedrani L, Terrat Y, Cardoso P, Bird D, et al. Characterising and predicting cyanobacterial blooms in an 8-year amplicon sequencing time course. ISME J. 2017;11:1746-1763.
7. Fox GA, Kendall BE. Demographic stochasticity and the variance reduction effect. Ecology 2002;83:1928-1934.
8. Violle C, Enquist BJ, McGill BJ, Jiang L, Albert CH, Hulshof C, et al. The return of the variance: intraspecific variability in community ecology. Trends Ecol Evol. 2012;27:244-252.
9. Brass DP, Cobbold CA, Ewing DA, Purse BV, Callaghan A, White SM. Phenotypic plasticity as a cause and consequence of population dynamics. Ecol Lett. 2021;24:2406-2417.
10. Wilson AE, Wilson WA, Hay ME. Intraspecific variation in growth and morphology of the bloom-forming cyanobacterium *Microcystis aeruginosa*. Appl Environ Microbiol. 2006;72:7386-7389.
11. Guedes IA, Pacheco ABF, Vilar MCP, Mello MM, Marinho MM, Lurling M, et al. Intraspecific variability in response to phosphorus depleted conditions in the cyanobacteria *Microcystis aeruginosa* and *Raphidiopsis raciborskii*. Harmful Algae 2019;86:96-105.
12. Sandrini G, Matthijs HCP, Verspagen JMH, Muyzer G, Huisman J. Genetic diversity of inorganic carbon uptake systems causes variation in CO2 response of the cyanobacterium *Microcystis*. ISME J. 2014;8:589-600.
13. Briand E, Escoffier N, Straub C, Sabart M, Quiblier C, Humbert JF. Spatiotemporal changes in the genetic diversity of a bloom-forming *Microcystis aeruginosa* (cyanobacteria) population. ISME J. 2009;3:419-429.
14. Collins S, Bel G. Phenotypic consequences of 1,000 generations of selection at elevated CO2 in a

green alga. Nature 2004;431:566–569.

15. Hutchins DA, Walworth NG, Webb EA, Saito MA, Moran D, McIlvin MR, et al. Irreversibly increased nitrogen fixation in *Trichodesmium* experimentally adapted to elevated carbon dioxide. Nat Commun. 2015;6:8155.

16. Lochte K, Turley CM. Bacteria and cyanobacteria associated with phytodetritus in the deep sea. Nature 1988;333:67–69.

17. Wang Z, Li G, Huang H, Zhang W, Wang J, Huang S, et al. Effects of solar radiation on the cyanobacteria: diversity, molecular phylogeny, and metabolic activity. Front Ecol Evol. 2022;10:928816.

18. Litchman E, de Tezanos Pinto P, Edwards KF, Klausmeier CA, Kremer CT, Thomas MK, et al. Global biogeochemical impacts of phytoplankton: a trait-based perspective. J Ecol. 2015;103:1384-1396.

19. Kromkamp JC, Mur LR. Buoyant density changes in the cyanobacterium *Microcystis aeruginosa* due to changes in the cellular carbohydrate content. FEMS Microbiol Lett. 1984;25:105-109.

20. Ibelings BW, Mur LR, Walsby AE. Diurnal changes in buoyancy and vertical distribution in populations of *Microcystis* in two shallow lakes. J Plankton Res. 1991;13:419–436.

21. Aparicio Medrano E, van de Wiel BJH, Uittenbogaard RE, Dionisio Pires LM, Clercx HJH. Simulations of the diurnal migration of *Microcystis aeruginosa* based on a scaling model for physical-biological interactions. Ecol Model. 2016;337:200-210.

22. Ranjbar MH, Hamilton DP, Etemad-Shahidi A, Helfer F. Impacts of atmospheric stilling and climate warming on cyanobacterial blooms: An individual-based modelling approach. Water Res. 2022;221:118814.

23. Harding WR. Phytoplankton primary production in a shallow, well- mixed, hypertrophic South African lake. Hydrobiologia. 1997;344:87–102.

24. López-Rodas V, Costas E, Bañares E, García-Villada L, Altamirano M, Rico M, et al. Analysis of polygenic traits of *Microcystis aeruginosa* (Cyanobacteria) strains by Restricted Maximum Likelihood (REML) procedures: 2. Microcystin net production, photosynthesis and respiration. Phycologia 2019;45:243-248.

25. Reynolds CS. Temporal scales of variability in pelagic environments and the response of

phytoplankton. Freshw. Biol. 1990;23:25-53.

26. Robarts RD, Zohary T. Temperature effects on photosynthetic capacity, respiration, and growth rates of bloom-forming cyanobacteria. N Z J Mar Freshwater Res. 1987;21:391-399.

27. Takamura N, Iwakuma T, Yasuno M. Photosynthesis and primary production of *Microcystis aeruginosa* Kütz. in Lake Kasumigaura. J Plankton Res. 1985;7:303-312.

28. Takamura N, Yasuno M, Sugahara K. Overwintering of *Microcystis aeruginosa* Kütz. in a shallow lake. J Plankton Res. 1984;6:1019-1029.

29. Lehman PW, Boyer G, Satchwell M, Waller S. The influence of environmental conditions on the seasonal variation of *Microcystis* cell density and microcystins concentration in San Francisco Estuary. Hydrobiologia 2007;600:187-204.

30. Risken H. The Fokker-Planck Equation. Springer-Verlag, New York, USA. 1996.

31. Aparicio Medrano E, Uittenbogaard RE, Dionisio Pires LM, van de Wiel BJH, Clercx HJH. Coupling hydrodynamics and buoyancy regulation in *Microcystis aeruginosa* for its vertical distribution in lakes. Ecol Model. 2013;248:41-56.

32. Peeters F, Straile D, Lorke A, Ollinger D. Turbulent mixing and phytoplankton spring bloom development in a deep lake. Limnol Oceanogr. 2007;52:286-298.

33. Huisman J, Sharples J, Stroom JM, Visser PM, Kardinaal WEA, Verspagen JMH, et al. Changes in turbulent mixing shift competition for light between phytoplankton species. Ecology 2004;85:2960-2970.

34. Han BP. A mechanistic model of algal photoinhibition induced by photodamage to photosystem-II. J Theor Biol. 2002;214:519-527.

35. Bechet Q, Shilton A, Guieysse B. Modeling the effects of light and temperature on algae growth: state of the art and critical assessment for productivity prediction during outdoor cultivation. Biotechnol Adv. 2013;31:1648-1663.

36. Visser PM, Passarge J, Mur LR. Modelling vertical migration of the cyanobacterium *Microcystis*. Hydrobiologia 1997;349:99–109.

37. Wu Z, Song L. Physiological comparison between colonial and unicellular forms of *Microcystis*

aeruginosa Kütz.(Cyanobacteria). Phycologia 2008;47:98-104.

38. Howard A, Irish AE, Reynolds CS. A new simulation of cyanobacterial underwater movement (SCUM'96). J Plankton Res. 1996;18:1375-1385.

39. Xiao M, Li M, Reynolds CS. Colony formation in the cyanobacterium *Microcystis*. Biol Rev Camb Philos Soc. 2018;93:1399-1420.

40. O'Brien KR, Meyer DL, Waite AM, Ivey GN, Hamilton DP. Disaggregation of *Microcystis aeruginosa* colonies under turbulent mixing: laboratory experiments in a grid-stirred tank. Hydrobiologia 2004; 519:143–152.

41. Webster IT, Hutchinson PA. Effect of wind on the distribution of phytoplankton cells in lakes revisited. Limnol Oceanogr. 1994;39:365-373.

42. Taylor J, Calderer MC, Hondzo M, Voller VR. A theoretical modeling framework for motile and colonial harmful algae. Ecol Evol. 2022;12:e9042.

43. Zhu W, Li M, Luo Y, Dai X, Guo L, Xiao M, et al. Vertical distribution of *Microcystis* colony size in Lake Taihu: Its role in algal blooms. J Gt Lakes Res. 2014;40:949-955.

44. Biringen S. A note on the numerical stability of the convection-diffusion equation. J Comput Appl Math. 1981;7:17-20.

45. Wüest A, Lorke A. Small-scale hydrodynamics in lakes. Annu Rev Fluid Mech. 2003;35:373-412.

46. Zhu W, Zhou X, Chen H, Gao L, Xiao M, Li M. High nutrient concentration and temperature alleviated formation of large colonies of *Microcystis*: Evidence from field investigations and laboratory experiments. Water Res. 2016;101:167-175.

47. Feng B, Wang C, Wu X, Tian C, Zhang M, Tian Y, et al. Spatiotemporal dynamics of cell abundance, colony size and intracellular toxin concentrations of pelagic and benthic *Microcystis* in Lake Caohai, China. J Environ Sci. 2019;84:184-196.

48. Saraf SR, Frenkel A, Harke MJ, Jankowiak JG, Gobler CJ, McElroy AE. Effects of *Microcystis* on development of early life stage Japanese medaka (Oryzias latipes): Comparative toxicity of natural blooms, cultured *Microcystis* and microcystin-LR. Aquat Toxicol. 2018;194:18-26.

49. Ha K, Cho EA, Kim HW, Joo GJ. *Microcystis* bloom formation in the lower Nakdong River, South Korea: importance of hydrodynamics and nutrient loading. Mar Freshwater Res. 1999;50:89-94.

50. Huisman J, Codd GA, Paerl HW, Ibelings BW, Verspagen JMH, Visser PM. Cyanobacterial blooms. Nat Rev Microbiol. 2018;16:471-483.

51. Duan H, Ma R, Xu X, Kong F, Zhang S, Kong W, et al. Two-decade reconstruction of algal blooms in China's Lake Taihu. Environ Sci Technol. 2009;43:3522-3528.

52. Brandenburg KM, Wohlrab S, John U, Kremp A, Jerney J, Krock B, et al. Intraspecific trait variation and trade-offs within and across populations of a toxic dinoflagellate. Ecol Lett. 2018;21:1561-1571.

53. Barrett RD, Schluter D. Adaptation from standing genetic variation. Trends Ecol Evol. 2008;23:38-44.

54. Durham WM, Climent E, Barry M, De Lillo F, Boffetta G, Cencini M, et al. Turbulence drives microscale patches of motile phytoplankton. Nat Commun. 2013;4:2148.

55. Visser PM, Ibelings BW, Bormans M, Huisman J. Artificial mixing to control cyanobacterial blooms: a review. Aquat. Ecol. 2015;50:423-441.

56. Huang X, Ke F, Lu J, Xie H, Zhao Y, Yin C, et al. Underwater light attenuation inhibits native submerged plants and facilitates the invasive co-occurring plant *Cabomba caroliniana*. Divers Distrib. 2023;29:543-555.

Figure legend

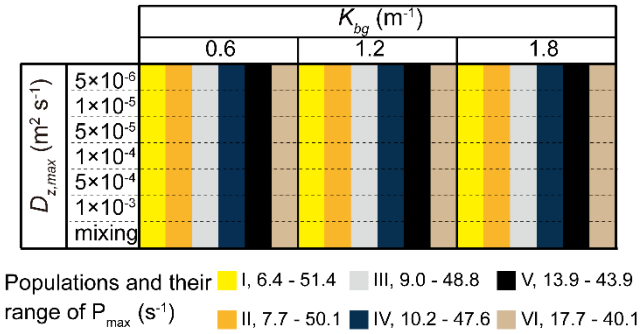

Fig. 1: Experimental design of the numerical simulations, which were conducted for all combinations of different initial *Microcystis* populations (I-VI with varying ranges of photosynthetic capacity, P_{max}, marked by different color), different turbulent diffusivities ($D_{z,max}$) and different turbidity (K_{bg}) conditions.

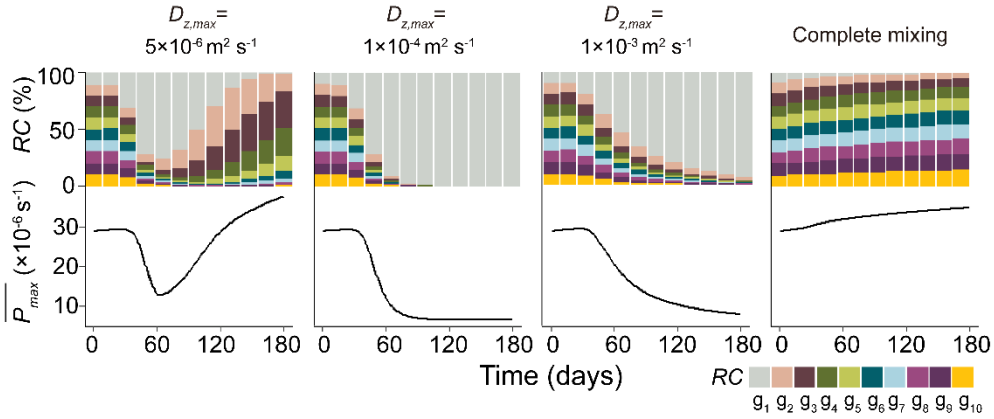

Fig. 2: Population dynamics of *Microcystis* (population I) for four different turbulence conditions (different columns: $D_{z,max}$=5×10^{-6} m^2 s^{-1}; $D_{z,max}$ =1×10^{-4} m^2 s^{-1}; $D_{z,max}$ =1×10^{-3} m^2 s^{-1}; complete mixing). The upper panels show the relative cell density (*RC*) of the 10 different trait groups (g_1 – g_{10}), while the lower panels show the population-averaged photosynthetic capacity of the *Microcystis* population ($\overline{P}_{max}$, solid lines). The cell densities (RC) are shown as staggered area charts. Group g_1 has the minimum P_{max}, while g_{10} has maximum P_{max}. The turbidity conditions were K_{bg}=0.6 m^{-1}.

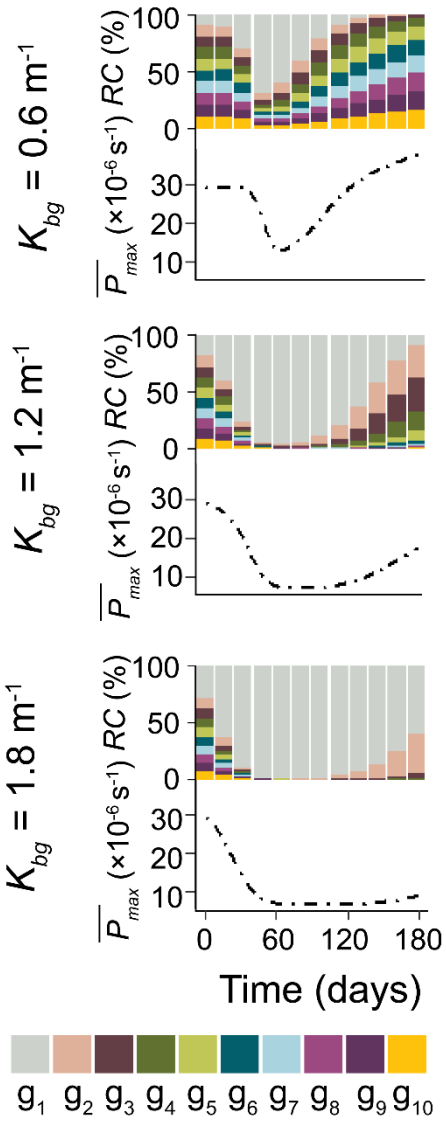

Fig. 3: The effect of turbidity on the population dynamics of *Microcystis* (Population I) under weak turbulence ($D_{z,max}$ = **5×10^{-6} m^2 s^{-1}**) (see different rows: K_{bg}=0.6 m^{-1}; K_{bg} =1.2 m^{-1}; K_{bg} =1.8 m^{-1}): The upper panels in each row show the relative cell density (*RC*) of the 10 different trait groups (g_1 – g_{10}) as staggered area charts, while the lower panels in each row show the population-averaged photosynthetic capacity of the *Microcystis* ($\overline{P}_{max}$, solid ,). Group g_1 has the minimum P_{max}, while g_{10} has maximum P_{max}.

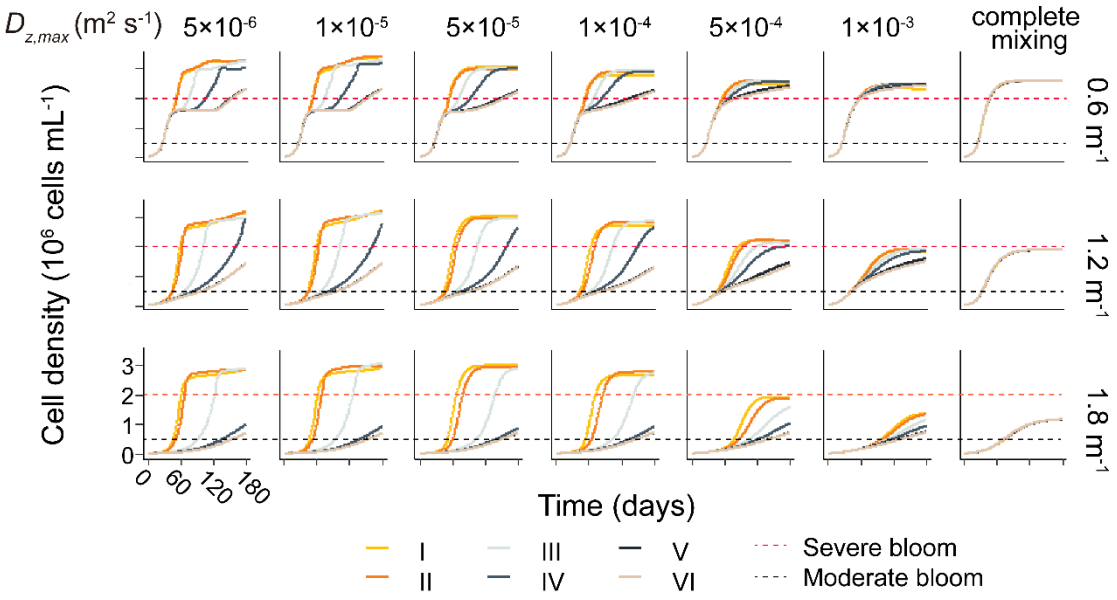

Fig. 4: Time series of mean cell density of *Microcystis* populations with different spectra of P_{max} (Population I to IV, see color assignment) under different turbulence (columns) and turbidity (characterized by K_{bg} in m^{-1} for the different rows).

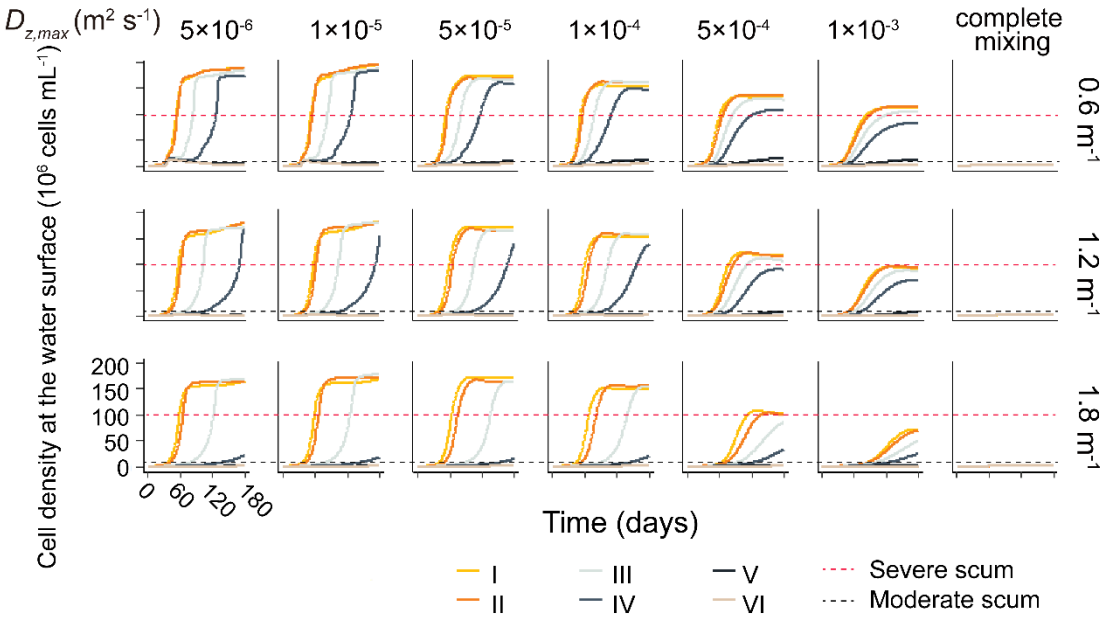

Fig. 5: Time series of the cell density in the uppermost depth layer of *Microcystis* populations with different spectra of P_{max} (Population I to IV, see color assignment) under different turbulence (columns) and turbidity (characterized by K_{bg} in m^{-1}). The red dashed horizontal lines show the threshold for surface scum.

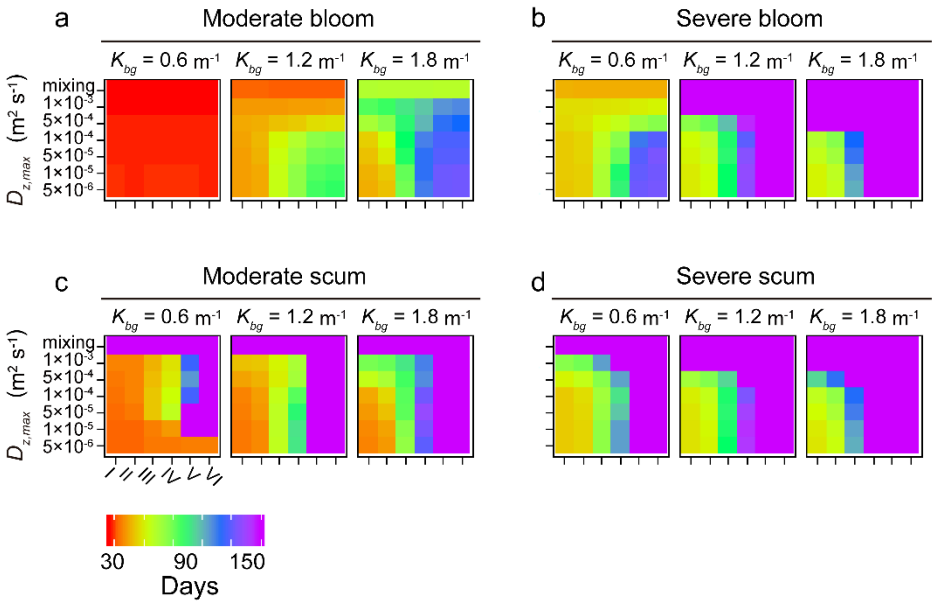

Fig. 6: Time required for *Microcystis* populations with varying initial ranges of P_{max} (population I-VI) to form blooms (moderate bloom, panel **a** and severe blooms **b**) and surface scum (moderate scum, panel **c** and severe scum, **d**) under different turbulence (rows) and turbidity (columns) conditions. Time is indicated by color, according to the color bar below the graphs; purple indicates a timescale of 180 days or more.

Supporting Information for:

Selection of photosynthetic traits by turbulent mixing governs formation of cyanobacterial blooms in shallow eutrophic lakes

Huaming Wu[a], Xingqiang Wu[b], Lorenzo Rovelli[a,c], Andreas Lorke[a]

[a]*Institute for Environmental Sciences, University of Kaiserslautern-Landau (RPTU), Landau 76829, Germany*

[b]*Key Laboratory of Algal Biology of Chinese Academy of Sciences, Institute of Hydrobiology, Chinese Academy of Sciences, Wuhan 430072, China*

[C]*now at the Department of Ecology, Federal Institute of Hydrology (BfG), Koblenz 56068, Germany*

Text: Methods

Text S1

The photosynthetic capacity of phytoplankton can be influenced by other environmental conditions, including temperature, nutrients, and pollutants [1-3], however, there is currently no universally established relationship between photosynthetic capacity and these factors. Moreover, the alteration of population-averaged P_{max} is driven by intraspecific variations and competition, both of which are factors not expected to be eliminated. To isolate and investigate the specific effects of turbulence and turbidity on the population-average P_{max}, we excluded the impacts of other environmental conditions in this study and assumed a fixed P_{max} for each trait group.

Text S2: Colony size and migration velocity

The rising/sinking velocity of colonies was derived as a function of colony size d and cell tissue density ρ using Stokes' law:

$$\frac{\partial z}{\partial t} \approx \frac{g d^2 (\rho_{col} - \rho_w)}{18 \mu \varphi} \quad \text{(S1)}$$

where g (m s^{-2}) is gravitational acceleration, ρ_w (kg m^{-3}) is the density of water, ρ_{col} (kg m^{-3}) is the mass-density of colonies, which is estimated from the cell tissue density (see below), φ is a shape coefficient and μ is the dynamic viscosity of water (kg s m^{-2}). According to Stokes's law, colonies with larger size have higher floating velocities.

We estimated the mass-density of the colony (ρ_{col}) as follows:

$$\rho_{col} = \rho \cdot (1 - n_{gas}) \cdot n_{cell} + \rho_{mul} \cdot (1 - n_{cell}) \quad \text{(S2)}$$

Where ρ is the cell tissue density (cf. Eq. 4 in the main text), n_{gas} is the volumetric ratio of gas vesicles to the total cell, n_{cell} is the volumetric ratio of cells to the colony. ρ_{mul} is the mass-density of mucilage. The values used here are shown in Table S1.

Text S3: External environmental conditions

We assumed that the vertical dispersion of colonies can be described by the turbulent diffusivity D_z, given that their size was smaller than the Kolmogorov micro scale of turbulence by over one order of magnitude, and assuming that vertical mixing was independent of cell-tissue density and colony size, i.e., we neglected

the diffusion term in the ρ and d dimensions in Eq. 1 [4].

The turbulent diffusivities at depth z (D_z) were estimated following [5]:

$$D_z = \begin{cases} a\left[z - \frac{z^2}{H}\right], & z \geq \frac{H}{10} \\ a\frac{H}{10}, & z < \frac{H}{10} \end{cases} \quad \text{(S3)}$$

Where a (m s^{-1}) is a constant, and H is the maximum water depth. The maximum turbulent diffusivity ($D_{z,max}$) derived from eq. S2 is $a \times H/4$. Here we varied the value of a (6.67×10^{-6} – 1.33×10^{-3} m s^{-1}) to calculate the turbulent diffusivity profiles with different $D_{z,max}$.

The irradiance profiles were simulated by Lambert–Beer's law, taking into account the self-shading of the *Microcystis* population and a constant background turbidity that was varied in our simulations:

$$I(z,t) = I_{surf} e^{\{-\int_0^z [K_m \sum_i C_i(\delta,t)] d\delta - K_{bg} z\}} \quad \text{(S4)}$$

Where $I(z,t)$ is the light intensity at depth z and time t, I_{surf} is the light intensity at the water surface, which was simulated by a sinusoidal pattern during daytime ($I_{surf} = I_{max} \times \sin(\pi t/L)$ from 6:00 – 18:00 and set to zero at night (18:00 – 06:00). I_{max} is the maximum daily light intensity and is set to 1000 µmol photon m^{-2} s^{-1}. L is the duration of daytime and is set to 12 h. K_m (0.0084 cm^2 10^{-6} cells^{-1}) [6] and K_{bg} (0.6 – 1.8 m^{-1}, [6, 7]) are the extinction coefficients of *Microcystis* and algae-free water (background), respectively. $\Sigma C_i(\delta,t)$ is the total cell density of all trait groups at time t and depth δ.

Text S4: Cell density threshold for moderate and severe bloom and scum

The depth-averaged cell density at 6:00 was used as a measure for bloom formation, while the cell density in the uppermost layer (~5 cm) served as an indicator for surface scum. A mean cell density of 0.5×10^6 cells mL^{-1} was designated as the threshold for moderate blooms, while a threshold of 2×10^6 cells mL^{-1} was used as a threshold for severe blooms. In the case of surface scum, a cell density of 1×10^7 cells mL^{-1} at the uppermost layer indicated middle scum, suggesting a moderate accumulation of *Microcystis* at the water surface. Conversely, a cell density of 1×10^8 cells mL^{-1} at the uppermost layer was considered severe scum, indicating a substantial and pronounced accumulation of *Microcystis* at the water surface.

Table S1: Definition, description, values, and references of the parameters used in the model.

Symbol	Description (unit)	Value	Reference
I_{opt}	Optimal light intensity (μmol photons m^{-2} s^{-1})	277.50	[7]
S	Initial slope of P-I curve (h μmol photons m^{-2} $s^{-1})^{-1}$)	2.00×10^{-7}	[8]
g_{max}	Maximum carbon requirement for growth (s^{-1})	5.50×10^{-6}	[9]
R	Respiration rate (s^{-1})	0.55×10^{-6}	[9]
V_{cell}	Volume a single *Microcystis* cell (m^3)	67.00×10^{-18}	[9]
l	Loss rate of *Microcystis* (d^{-1})	0.10	[10]
g	Gravitational acceleration (m s^{-2})	9.80	[4]
ρ_w	Density of water (kg m^{-3})	998.00	[4]
ρ_{mul}	Density of mucilage (kg m^{-3})	998.70	[11]
φ	Shape coefficient of colonies	1.00	[4]
μ	dynamic viscosity of water (kg m^{-1} s^{-1})	1.00×10^{-3}	[4]
I_{max}	Maximum daily light intensity (μmol photons m^{-2} s^{-1})	1000.00	[6]
L	Duration of daytime (h)	12.00	[6]
K_m	Extinction coefficient of *Microcystis* (cm^2 10^{-6} cells m)	0.84×10^{-2}	[6]
f_1	Slope of the curve of density change (min^{-1})	-9.49×10^{-4}	[7]
f_2	Theoretical rate of density change with no carbohydrate storage in the cells (kg m^{-3} min^{-1})	9.84×10^{-1}	[7]
m_{cell}	Amount of carbon contained in each cell (kg)	14.00×10^{-15}	[9]
n_{gas}	volumetric ratio of gas vesicles to the total cell	0.07	[6]
n_{cell}	Volumetric ratio of cells to the colony	0.20	[6]
B_g	The mass of carbohydrate (glycogen) ballast	2.38	[9]

	produced per gram of assimilated carbon (g)		
H	The maximum water depth (m)	3.00	This study

Figure legend:

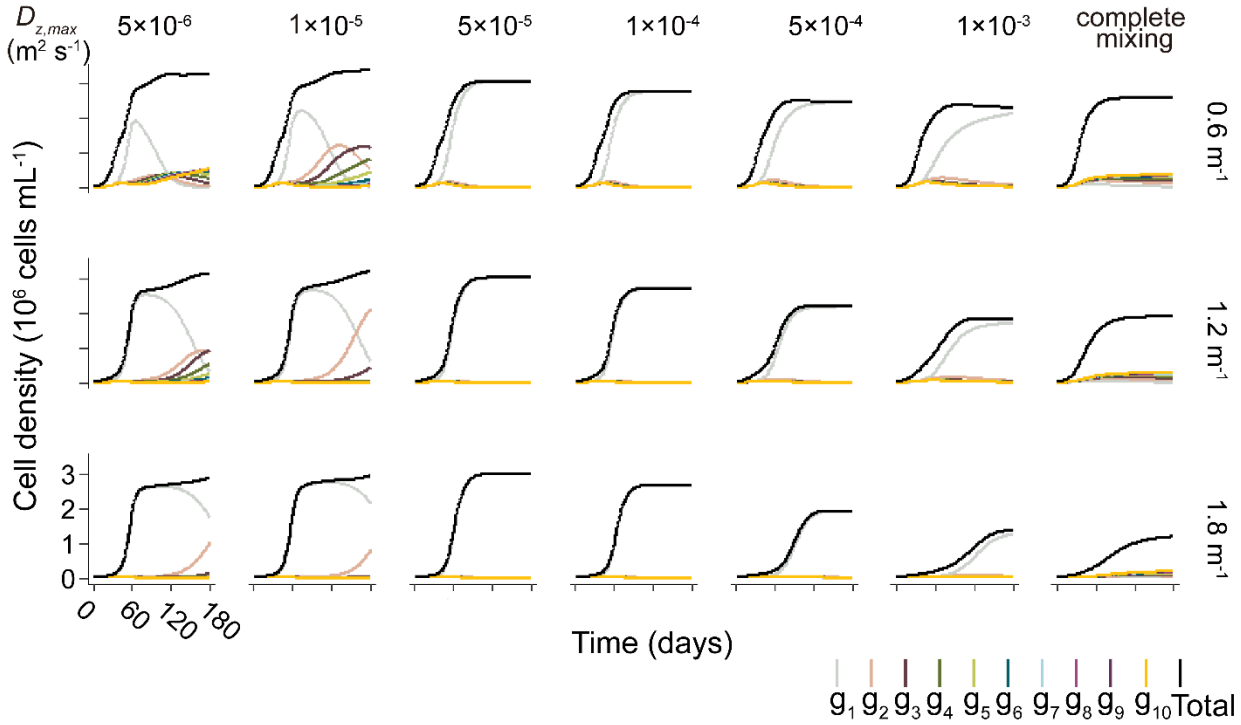

Fig. S1: Time series of cell density of the population (population I) and its trait groups (see color assignment) under different turbulent diffusivities ($D_{z,max}$, see the columns) and turbidity (rows) conditions. Axis scaling is identical in all panels.

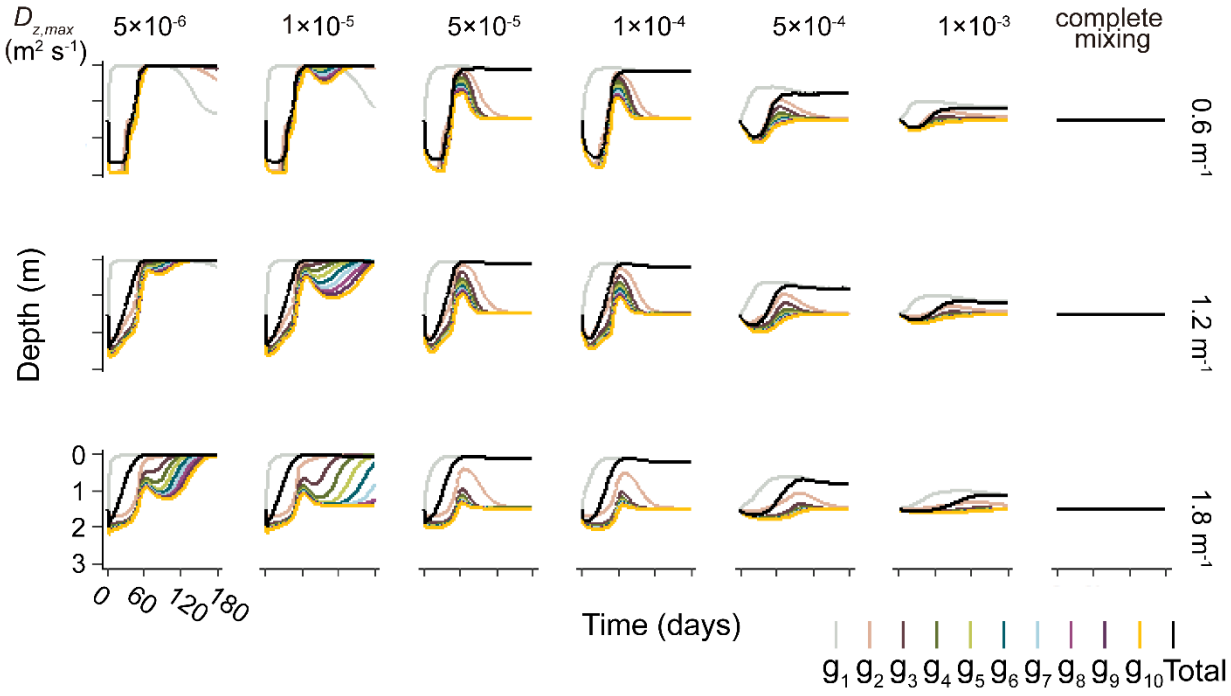

Fig. S2: Time series of the depth of the centroid of the population (population I) and traits groups (see color assignment) under different turbulence (columns) and turbidity (rows) conditions.

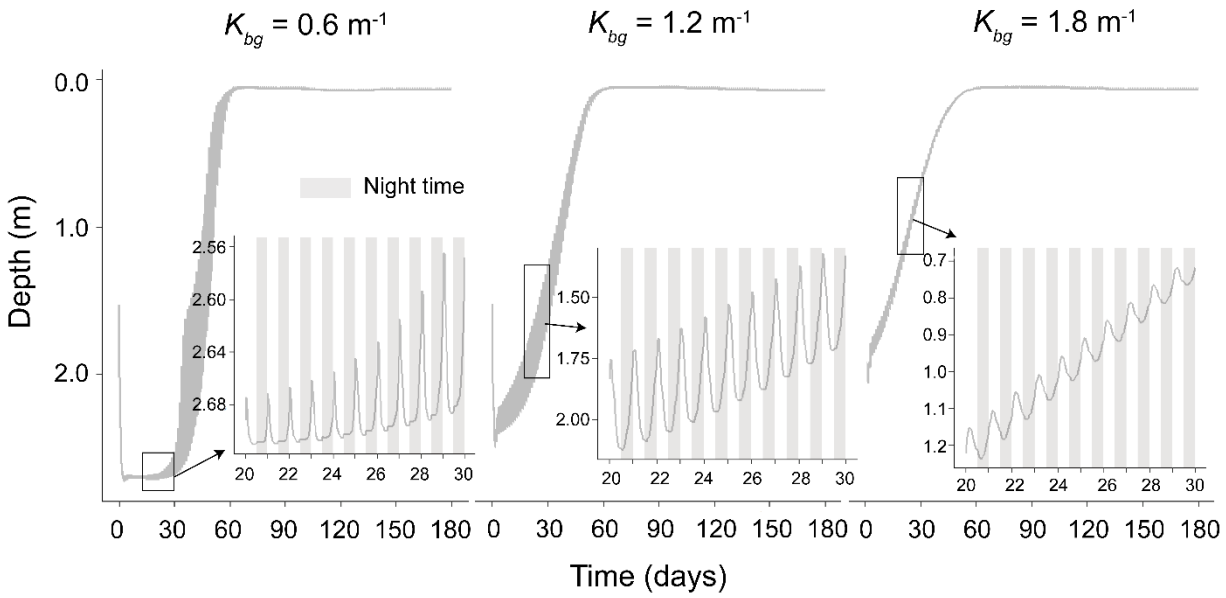

Fig. S3: Hourly time series of the centroid depth of Population I under different turbidity conditions (columns), exemplified for weak turbulence ($D_{z,max}$ = 5×10^{-6} m^2 s^{-1}). The inset graphs highlight the diel vertical migration by showing the data marked by the black rectangle at higher resolution. In these graphs, the grey-shaded area mark night time conditions (no light).

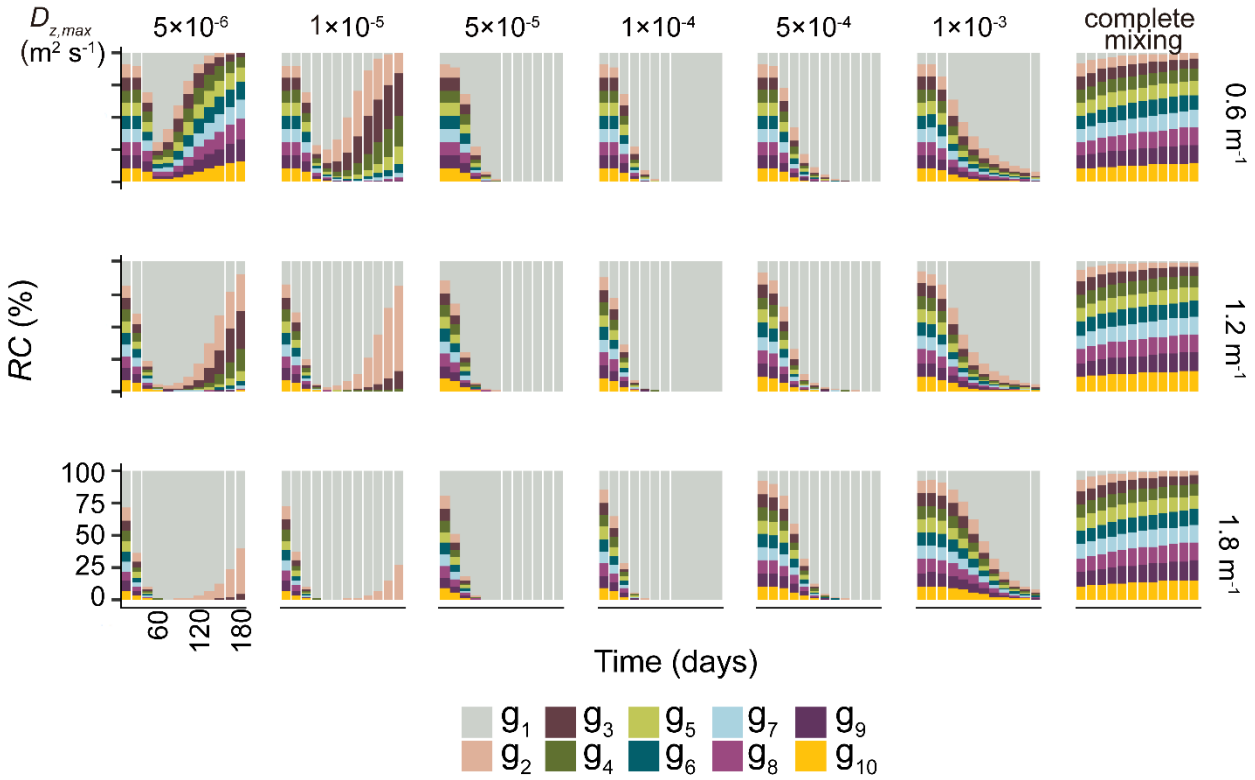

Fig. S4: Staggered bar charts showing time series of the relative cell density (*RC*) of the different trait groups (see color assignment, Population I) under different turbulence columns) and turbidity (rows) conditions.

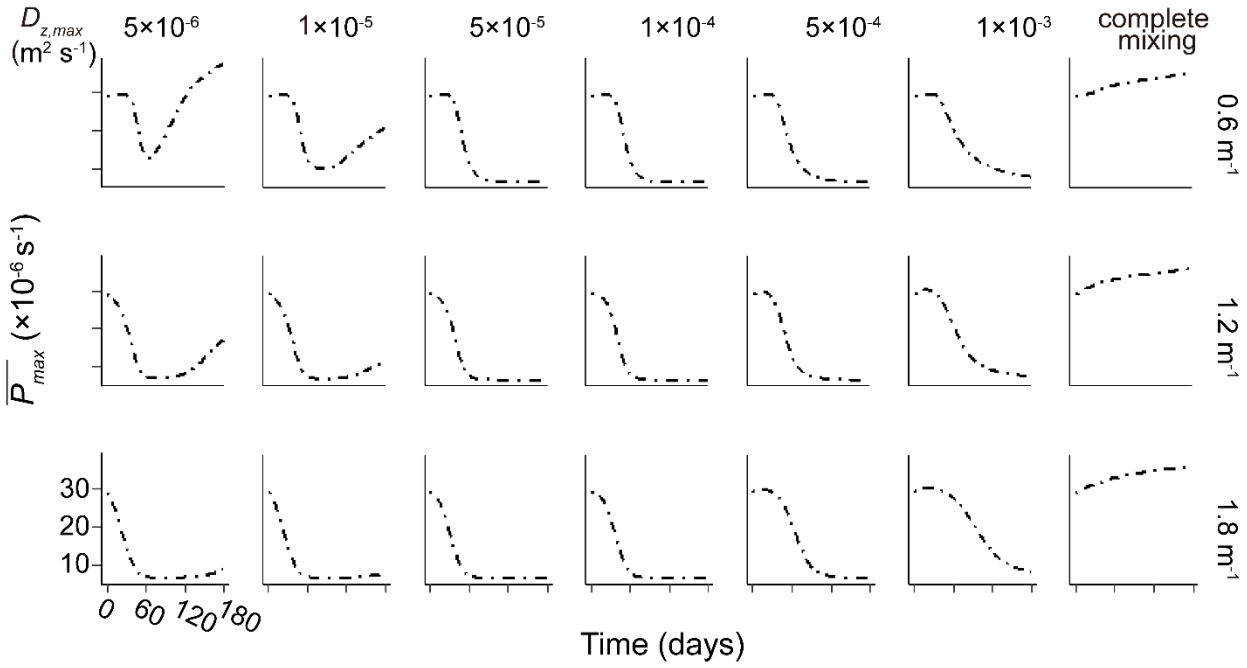

Fig. S5: Time series of population-averaged photosynthetic capacity (P_{max}) of population I under different turbulence (columns) and turbidity (rows) conditions.

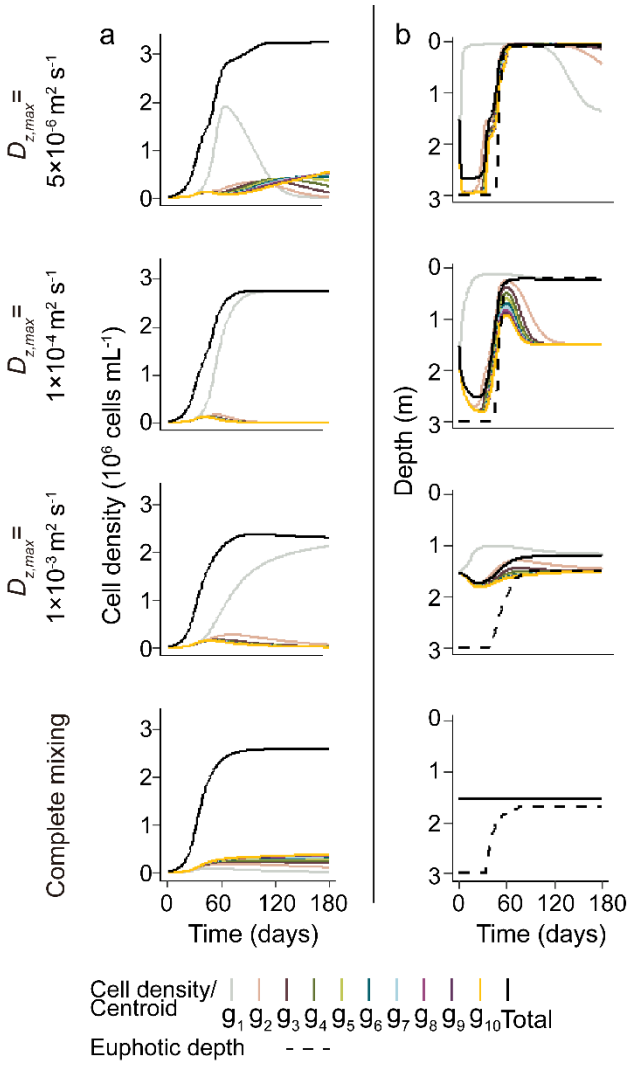

Fig. S6: **Population dynamics of *Microcystis* (population I) for four different turbulence conditions** (different rows: $D_{z,max}$=5×10^{-6} m^2 s^{-1}; $D_{z,max}$ =1×10^{-4} m^2 s^{-1}; $D_{z,max}$ =1×10^{-3} m^2 s^{-1}; complete mixing). Different columns show time series of cell density (**a**) and depth of the centroid (**b**) of the 10 different trait groups (g_1 – g_{10}, see the color assignments). Group g_1 has the minimum P_{max}, while g_{10} has the maximum P_{max}. The black solid lines in the panel **a** and **b** represent the cell density and the centroid of the overall *Microcystis* population, respectively. The black dashed line represents the euphotic depth. The turbidity conditions were K_{bg}=0.6 m^{-1}.

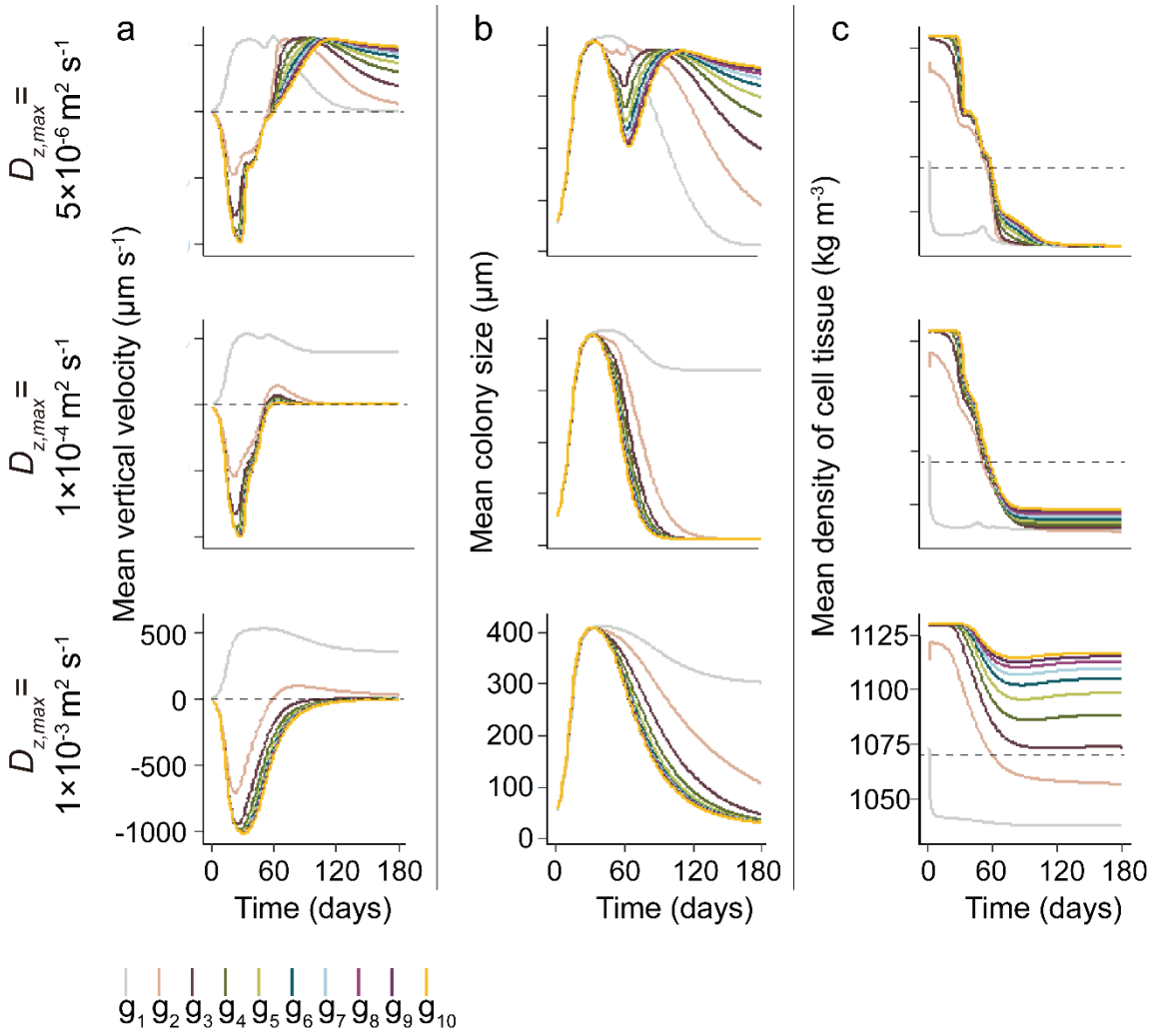

Fig. S7: Time series of vertical velocity (a), colony size (b) and density of cell tissue (c) of different trait groups (see color assignment) of population I under different turbulence conditions (different rows) and a background extinction coefficient (turbidity) of 0.6 m^{-1}. The horizontal dashed lines in panel a indicate a vertical velocity of zero and the dashed lines in panel c represent neutral buoyancy of colonies.

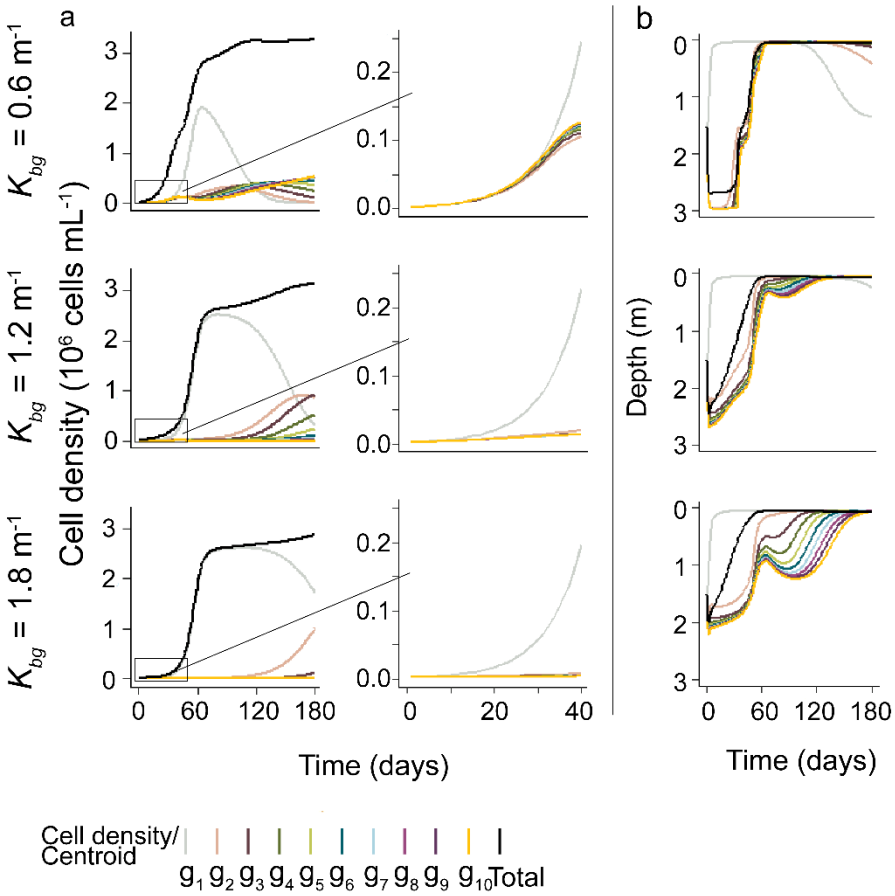

Fig. S8: The effect of turbidity on the population dynamics of *Microcystis* (Population I) under weak turbulence ($D_{z,max}$ = 5×10^{-6} m^2 s^{-1}) (see different rows: K_{bg}=0.6 m^{-1}; K_{bg} =1.2 m^{-1}; K_{bg} =1.8 m^{-1}): Different columns show time series of cell density (**a**) and depth of the centroid (**b**) of the 10 different trait groups ($g_1 - g_{10}$, see the color assignments). Group g_1 has the minimum P_{max}, while g_{10} has maximum P_{max}. The black solid lines in the panel **a** and **b** represent the cell density and the centroid of the overall *Microcystis* population, respectively.

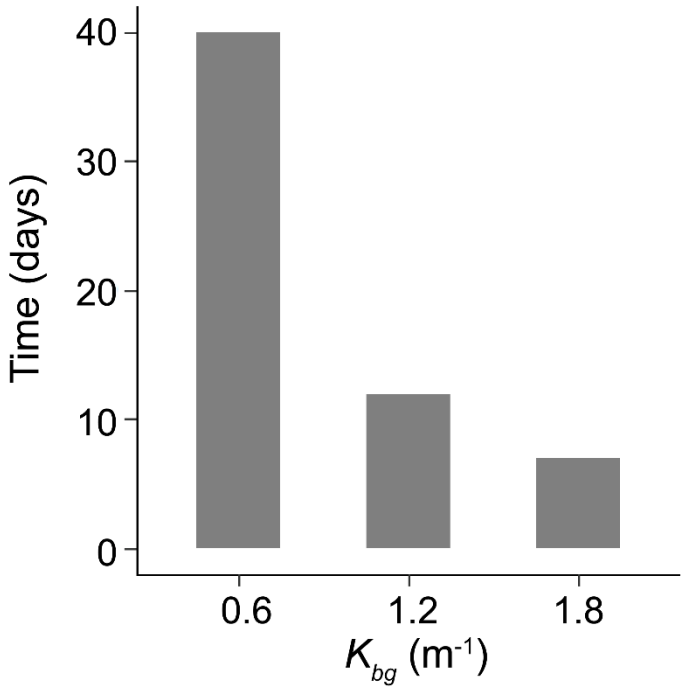

Fig. S9: The time at which the population-averaged photosynthetic capacity (P_{max}) deviated more than 5% of its initial value for different turbidity conditions (background extinction coefficients K_{bg}).

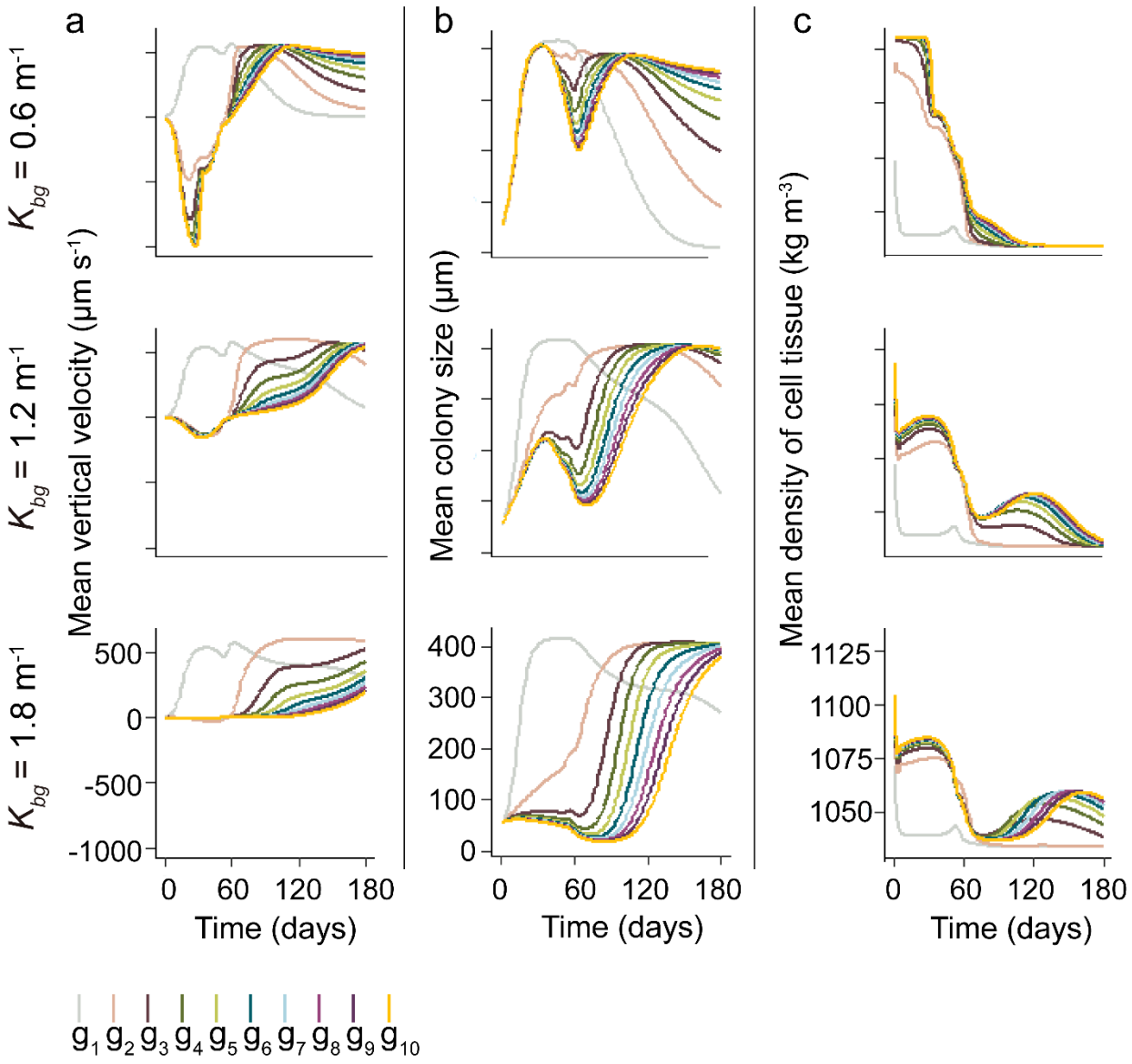

Fig. S10: Time series of vertical velocity (a), mean colony size (b) and density of cell tissue (c) of different trait groups (see color assignment below the graphs) of population I under different turbidity conditions (different rows). All results were obtained for a turbulent diffusivity of $D_{z,max} = 5 \times 10^{-6}$ m^2 s^{-1}.

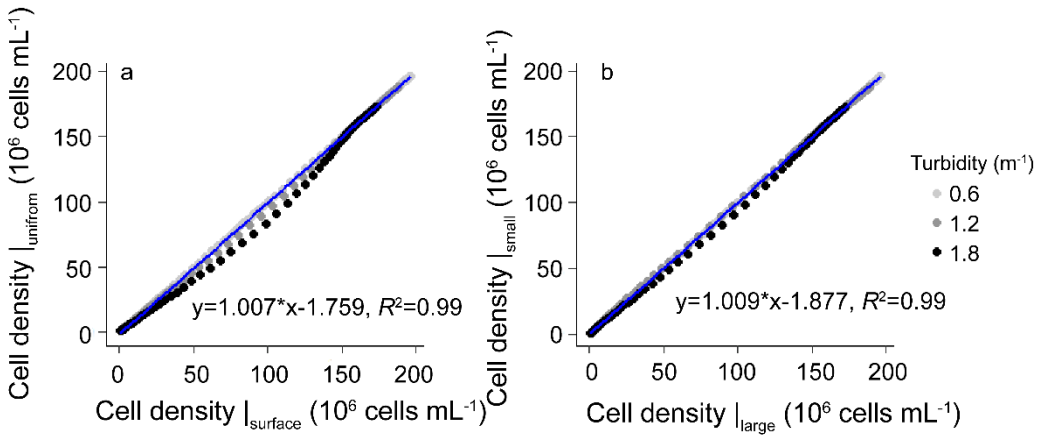

Fig. S11: Comparison of cell density simulated for different initial conditions: **a**) Initially uniform distribution (Cell density$|_{unifrom}$) vs. an initial distribution where colonies were concentrated at the water surface (Cell density$|_{surface}$), and **b**) initially large colony size (95 µm, Cell density$|_{large}$) vs. initially small colony size (50 µm, Cell density$|_{small}$). The simulations were performed under different turbidity conditions (see the color assignments) and under weak turbulence ($D_{z,max}$ = 5×10^{-6} m^2 s^{-1}).

Reference

1. Wang Z, Li D, Li G, Liu Y. Mechanism of photosynthetic response in *Microcystis aeruginosa* PCC7806 to low inorganic phosphorus. Harmful Algae 2010;9:613-619.

2. Zhou S, Shao Y, Gao N, Deng Y, Qiao J, Ou H, et al. Effects of different algaecides on the photosynthetic capacity, cell integrity and microcystin-LR release of *Microcystis aeruginosa*. Sci Total Environ. 2013;463-464:111-119.

3. Davison IR. Environmental effects on algal photosynthesis: temperature. J Phycol. 1991;27:2-8.

4. Aparicio Medrano E, Uittenbogaard RE, Dionisio Pires LM, van de Wiel BJH, Clercx HJH. Coupling hydrodynamics and buoyancy regulation in *Microcystis* aeruginosa for its vertical distribution in lakes. Ecol Model. 2013;248:41-56.

5. Webster. IT, Hutchinson PA. Effect of wind on the distribution of phytoplankton cells in lakes revisited. Limnol Oceanogr. 1994;39,:365-373.

6. Wu H, Wu X, Yang T, Wang C, Tian C, Xiao B, et al. Feedback regulation of surface scum formation and persistence by self-shading of *Microcystis* colonies: Numerical simulations and laboratory experiments. Water Res. 2021;194:116908.

7. Visser PM, Passarge J, Mur LR. Modelling vertical migration of the cyanobacterium *Microcystis*. Hydrobiologia 1997;349:99–109.

8. Takamura N, Iwakuma T, Yasuno M. Photosynthesis and primary production of *Microcystis aeruginosa* Kütz. in Lake Kasumigaura. J Plankton Res. 1985;7:303-312.

9. Reynolds CS. Temporal scales of variability in pelagic environments and the response of phytoplankton. Freshw Biol. 1990;23:25-53.

10. Huisman J, Sharples J, Stroom JM, Visser PM, Kardinaal WEA, Verspagen JMH, et al. Changes in turbulent mixing shift competition for light between phytoplankton species. Ecology 2004;85:2960-2970.

11. Reynolds C, Jaworski G, Cmiech HL, G. On the annual cycle of the blue-green alga *Microcystis*

aeruginosa K¨utz. emend. Elenkin. Philos. Trans. R. Soc. Lond., B, Biol. Sci. 1981;293, 419–477.

Appendices III

Intraspecific competition can promote cold-water cyanobacterial blooms: Revisiting cyanobacteria-temperature relationships based on traits

Yanxue Zhang[a,c,e,1], Huaming Wu[b,1*], Xingqiang Wu[a*], Hans-Peter Grossart[c, d] , Andreas Lorke[b]

[a]Key Laboratory of Algal Biology of Chinese Academy of Sciences, Institute of Hydrobiology, Chinese Academy of Sciences, Wuhan 430072, China

[b]Institute for Environmental Sciences, University of Kaiserslautern-Landau (RPTU), Landau 76829, Germany

[c]Department of Plankton and Microbial Ecology, Leibniz Institute of Freshwater Ecology and Inland Fisheries, Stechlin 16775, Germany

[d]Institute of Bicochemistry and Biology, Potsdam University, Potsdam 14469, Germany

[e]University of Chinese Academy of Sciences, Beijing 100049, China

Intraspecific competition can promote cold-water cyanobacterial blooms: Revisiting cyanobacteria-temperature relationships based on traits

Yanxue Zhang[a,c,e,1], Huaming Wu[b,1], Xingqiang Wu[a], Hans-Peter Grossart[c,d] , Andreas Lorke[b]

[a]*Key Laboratory of Algal Biology of Chinese Academy of Sciences, Institute of Hydrobiology, Chinese Academy of Sciences, Wuhan 430072, China*

[b]*Institute for Environmental Sciences, University of Kaiserslautern-Landau (RPTU), Landau 76829, Germany*

[c]*Department of Plankton and Microbial Ecology, Leibniz Institute of Freshwater Ecology and Inland Fisheries, Stechlin 16775, Germany*

[d]*Institute of Bicochemistry and Biology, Potsdam University, Potsdam 14469, Germany*

[e]*University of Chinese Academy of Sciences, Beijing 100049, China*

[1] These authors contributed equally to this work.

Running title: Cold-water cyanobacterial blooms

Key words: Climate change; Harmful algal blooms (HABs); Cyanobacteria-environment interactions; Intraspecific variations; Thermal effect; Phytoplankton community; Population dynamics

Type of article: Letter

Number of words in the abstract: 148

Number of words in the main text: 5066

Number of references: 56

Number of figures: 4

Number of tables: 0

Number of text boxes: 0

Correspondence:

Author contributions

Yanxue and X.W. designed the experiment. Y.Z. carried out the sampling and experimentation. H.W. and A.L. conceived the study and contributed to the modeling simulation, and data analysis. Y.Z., H.W., X.W., A.L., and H.P.G. contributed to the writing of the manuscript.

Data accessibility statement

The code of the 1D lake model SIMSTRAT is available on Github (https://github.com/Eawag-AppliedSystemAnalysis/Simstrat/). The MATLAB code to reproduce the simulations, along with the original and modeled data is archived on The Knowledge Network for Biocomplexity (KNB) repository (doi:10.5063/F1S180ZH).

Abstract

Climate change is disrupting regular phytoplankton succession in lakes, leading to cold-water cyanobacterial blooms (CWCBs) and increasing ecological uncertainty. The role of trait distributions in this process remains unexplored. Here, we tested the hypothesis that thermal history of cyanobacteria affects their thermal adaptations by altering the distribution of optimum growth temperature (T_{opt}). Using a one-dimensional trait-based phytoplankton-hydrodynamics model, we simulated cyanobacteria dynamics in Lake Dianchi over 364 days. The model demonstrated that T_{opt} diversification promotes psychrophilic strains, leading to CWCBs while mitigating summer blooms as T_{opt} distribution retains the memory of past cold temperatures. This memory produced an inverse relationship between T_{opt}-diverse populations and temperatures, challenging the current cyanobacteria-temperature paradigm. Our findings suggest that predictions derived from fixed-trait populations with a single T_{opt} may not apply to populations with flexible traits, i.e. multiple T_{opt}, highlighting that forecasts without trait-based analysis may misinterpret climate change effects on harmful cyanobacteria.

Highlights:

1. Diversification of thermal traits promotes cold-water cyanobacterial blooms.
2. Cyanobacterial populations can exhibit an inverse relationship with temperature.
3. Cold-water blooms foreshadow a shift toward prolonged but less intense cyanobacterial blooms throughout the year.
4. Thermal trait diversity affects direction and magnitude of cyanobacterial population responses to temperature changes.
5. High intraspecific trait diversity enhances population success across various environmental gradients.

Introduction

Phytoplankton are dynamic microbial primary producers that comprise less than 1% of the total global biomass(Bar-On *et al.* 2018) but are responsible for nearly 50% of global primary productivity (Field *et al.* 1998), fueling aquatic food webs and playing a fundamental role in biogeochemical cycles (Field *et al.* 1998; Falkowski *et al.* 2008). In freshwater ecosystems, seasonally varying climatic forcing typically drives quasi-periodical turnover of phytoplankton communities. This is often evidenced by a shift from diatoms and green algae during winter/spring to cyanobacteria during summer/autumn (Hrycik *et al.* 2022). This regular seasonal turnover contributes to predictable ecosystem functions and enhances ecosystem stability. However, this pattern is deviating in many lakes of the world, with cyanobacteria dominating and outcompeting other phytoplankton species also in winter, leading to frequently observed cold-water cyanobacterial blooms (CWCBs) (Babanazarova *et al.* 2013; Bizic-Ionescu *et al.* 2014; Ma *et al.* 2016; Reinl *et al.* 2023). CWCBs profoundly impact freshwater ecosystems through complex bottom-up effects, exacerbating biodiversity loss, disrupting ecosystem functionality, and prolonging cyanotoxins production by toxic cyanobacterial strains (e.g., *Microcystis* sp.). This may magnify the detrimental effects of cyanobacterial harmful algal blooms (CyanHABs) on human and environmental health (Ma *et al.* 2016; Reinl *et al.* 2023).

Ecological hypotheses suggests that intraspecific trait distributions and flexibility can change in response to environmental fluctuations (Violle *et al.* 2012; Lajoie & Vellend 2015; Moran *et al.* 2016). These changes may affect competitive relationships among species by repartitioning niches, and potentially disrupting seasonal species succession within biological communities when exceeding certain thresholds. This is particularly true for cyanobacteria with generally short generation times (Lochte & Turley 1988), wide ranges of intraspecific traits (Rossi *et al.* 2023; Wu *et al.* 2024), and the ability to rapidly adapt to changing environmental conditions through intraspecific competition. These features offer a significant potential for alterations in trait flexibility, distribution and adaptive responses, which presumably contribute to deviations in seasonal phytoplankton succession and the formation of CWCBs.

In freshwater ecosystems, cyanobacteria inhabit a dynamic environment where spatiotemporally heterogeneous temperatures interact with the coupling between diel vertical migration of cyanobacteria and turbulence. This interaction continuously shapes the fitness of traits with differing optimum growth temperature (T_{opt}). Thus, in cyanobacterial populations, traits with different T_{opt} coexist and T_{opt} distribution patterns may vary in response to temperature fluctuations. For instance, seasonal temperature changes may reshape the distribution of T_{opt} and drive selection within cyanobacterial population, where individuals with different T_{opt} interact through intraspecific competition. Such complex processes directly impact thermal adaptations of cyanobacterial populations, as well as their resulting ecological ramifications, e.g., formation of CyanHABs. Consequently, the composition of a cyanobacterial population, consisting of strains with varying thermal traits, and its response to changing temperatures depend on the thermal conditions the population has previously experienced. However, the connection between CyanHABs formation, intraspecific trait diversity, and thermal history has been largely overlooked in previous studies.

The thermal conditions in lakes are governed by climatic and weather conditions and can exhibit high inter-annual variabilities, with average temperatures fluctuating by 1-2°C, particularly during summer(Scheffer *et al.* 2001; Quayle *et al.* 2002; Doubek *et al.* 2021). Current and future temperature fluctuations and the frequency of extreme events are predicated to increase, e.g., due to more frequent and severe heatwaves (Perkins *et al.* 2012; Fischer & Knutti 2015). Additionally, changing temperatures alter lake hydrodynamics, affecting vertical mixing patterns (Wüest & Lorke 2003) and the spatial distribution of cyanobacterial blooms in the water column (Stockwell *et al.* 2020). These processes collectively modulate the thermal regime experienced by cyanobacterial populations, altering their thermal adaptations and growth patterns, potentially contributing to the formation of CWCBs. Currently, a mechanistic understanding of these complex interactions is limited, as is our comprehension of CyanHABs development under climate change.

Here, we hypothesize that the thermal history of cyanobacterial populations alters their response to seasonal temperature variations by selecting for different T_{opt}, enhancing the prevalence of CWCB-forming psychrophilic cyanobacterial strains. To test this hypothesis, we use a one-dimensional hydrodynamic model

coupled with a trait-based phytoplankton model to investigate the indirect effect of thermal history on the development of trait-diverse cyanobacterial populations. Simulations were conducted exemplarily for Lake Dianchi in Kunming city, China (Fig. 1), where cyanobacterial blooms have occurred annually since the 21st century and CWCBs have occurred in recent years during winter, and for which our model was calibrated. We then contrast the cyanobacteria dynamics of three populations, each with different T_{opt} compositions, under three temperature sequences with varied summer temperatures. Our study reveals the memory of past temperature in the population that modifies the thermal response via changes in T_{opt} distribution, leading to following interesting phenomena, some of which were unexpected: i) Diversification in T_{opt} promotes CWCBs; ii) The thermal response trajectory of cyanobacterial populations can be determined by the temporal sequence of temperature; iii) Depending on the diversity of T_{opt}, cyanobacterial population size can exhibit an inverse relationship with temperature. This work indicates that predictions based on fixed traits appear to be insufficient to accurately describe dynamics of CyanHABs, highlighting the utmost importance of the so far underappreciated trait-based analysis in predicting CyanHABs, especially in the light of an increasingly variable future climate.

Materials and methods

Study site

Lake Dianchi is a shallow, eutrophic lake located in Kunming, China (24°40'-25°01'N, 102°36'-102°47'E). It has a mean water depth of 5.3 m and a surface area of approximately 309 km² (Fig. 1). The lake has suffered from severe cyanobacterial blooms (mostly *Microcystis* sp., Fig. S1) every year since the 21st century.

Field measurements were conducted from Jan 2023 to Jan 2024. Meteorological data, including air temperature, wind speed, wind direction, solar radiation, shortwave radiation, longwave radiation, relative humidity, and surface water temperature were recorded at hourly intervals by a meteorological station (WXT520, HM Scientific Ltd.) installed on a buoy in the northern part of the lake (MS, Fig. 1). Monthly water sampling and measurements were conducted at four sites (S1-S4, Fig. 1). These included measurements of algal chlorophyll-a concentrations (Chl*a*), cell density, phytoplankton community

composition, Secchi disk depth, temperature in the water column and chemical properties of water samples, such as total nitrogen, total phosphorus, and pH at ca. 1 m water depth (see Text S1 for further details). Due to constant turbulent mixing of the lake, we considered these samples to be representative of the entire water column.

Model description

A one-dimensional (1D) hydrodynamic model coupled with a trait-based phytoplankton model was used to simulate the lake's mixing and thermal dynamics, and the related cyanobacteria dynamics. The hydrodynamic model operated under atmospheric forcing, with its outputs (including vertical profiles of turbulent diffusivity and water temperature) serving as inputs for the trait-based phytoplankton model. The phytoplankton model was employed to simulate the dynamics of a cyanobacterial population with varying thermal traits (optimum growth temperature, T_{opt}). The phytoplankton model comprised two components: trait-specific growth influenced by light, nutrients, pH, and water temperature; as well as buoyancy-driven vertical migration and turbulent mixing. The models are elaborated upon in the subsequent sections, while the primary parameters, their numerical values, and references for parameter selection are summarized in Table S2.

Hydrodynamic model

For simulating the vertical distributions of temperature and turbulent mixing, we used the one-dimensional hydrodynamic model SIMSTRAT, which employs an implicit Euler numerical scheme (Goudsmit *et al.* 2002; Peeters *et al.* 2002). Turbulent mixing is described through a k-ε closure model, where turbulent kinetic energy (k) and its dissipation rate (ε) are explicitly represented as state variables. The primary sources of turbulent kinetic energy include direct wind forcing and convectively-driven flows. Previous research has validated the capability of this model to accurately simulate the hydrodynamic and thermal structure of lakes in response to atmospheric forcing (Peeters *et al.* 2007; Schwefel *et al.* 2016; Råman Vinnå *et al.* 2017).

For the hydrodynamic simulations, we used a fixed lake bathymetry (Fig. 1) and hourly measurements of meteorological variables. For the latter, we used meteorological data from Lake Dianchi measured at station MS (Fig. 1) during the period from Jan 2023 to Jan 2024.

Using these inputs, SIMSTRAT calculated vertical profiles of turbulent kinetic energy (k), energy dissipation rates (ε), and thermal stratification, based on heat exchange at the lake surface and the vertical transport of heat by turbulent diffusion. Surface heat fluxes are estimated from the meteorological measurements using empirical relationships that account for long and short-wave radiation, evaporation, and heat conduction (Goudsmit *et al.* 2002).

Vertical profiles of turbulent diffusivity (K_z) are derived from the simulated values of k and ε according to the following equation:

$$K_z = C_k \cdot k^2 / \varepsilon \quad (1)$$

where C_k is the Kolmogorov constant for which we used a value of 0.076 (Umlauf & Burchard 2003).

In the hydrodynamic model, the water depth was fixed to 4.4 m, which is the average depth sampling sites S1-S4. The resolution of the vertical discretization was set to 0.14 m and the temporal resolution was 1 min. The light extinction coefficient was set to a fixed value of 3.3 m^{-1}, which corresponds to the average light extinction coefficient in Lake Dianchi in 2023 (Fig. S2). Hence, interaction between the hydrodynamic model and the phytoplankton model through light extinction was neglected in this study.

Phytoplankton model

Cyanobacterial population dynamics was assessed by simulating n different strains, with each having a different T_{opt}, using a series of n coupled 1D reaction– advection–diffusion equations, as follows:

$$\frac{\partial C_i}{\partial t} = -\left(\frac{\partial z}{\partial t}\right)\frac{\partial C_i}{\partial z} + \frac{\partial}{\partial z}\left(D_z \frac{\partial C_i}{\partial z}\right) + \mu_{net} C_i \quad (2)$$

where i= 1, …, n. C_i (z, t) is the concentration of cyanobacterial cells with thermal trait i (or strain i) at depth z (m) and time t (s). The first term on the right-hand side of Eq. 2 describes buoyancy-driven (advective) transport along the vertical coordinate (z, defined as positive downward), with $\partial z/\partial t$ denoting

the vertical velocity of the cells. The second term describes vertical transport by turbulent diffusion with D_z (m^2 s^{-1}) denoting the turbulent diffusivity at depth z, which is the output of the hydrodynamic model. The last term describes growth and loss processes with μ_{net}, which depicts the cyanobacteria net growth rates. The equations describing cell densities for n different traits (Eq. 2) are coupled through the light-dependent growth rates, where the vertical light distribution is affected by cell density distribution of the cyanobacterial population. Hence, different traits interact through the competition for light and self-shading.

Net growth of cyanobacterial strain i ($\mu_{net,i}$) was calculated as a function of temperature, nutrient concentration, light, pH, and a loss term using the following equation:

$$\mu_{net,i} = \mu_{max} f_i(T) f(I) f(pH) \min[f(N), f(P)] - l \quad (3)$$

μ_{max} is the maximum growth rate of cyanobacterial strain i under non-limiting conditions. $f_i(T)$, f(pH), $f(N)$, and $f(P)$ are functions applied to regulate growth dependence on temperature (T), light intensity (I), pH, nitrogen (N), and phosphorus (P) concentrations, respectively. l is the term that represents the combined effect of respiration and mortality (loss) and it is assumed to be constant (l=0.1, (Huisman *et al.* 2004)). The temperature response function was applied to the growth rate, which allows inhibition above an optimum growth temperature(Lehman *et al.* 1975), as follows:

$$f_i(T) = \exp\left(-2.3 \cdot \left(\frac{T_{opt,i} - T}{T_{tr}}\right)^2\right) \quad (4)$$

where $T_{opt,i}$ (℃) is the optimum growth temperature of strain i, T_{tr} (℃) denotes the thermal tolerance range of the strain, which is calculated as the difference between T_{opt} and the minimum temperature for growth (T_{min}). Here we used a constant value for T_{tr} of 16 ℃, which is supported by previous observations(Rossi *et al.* 2023).

PH-dependence of growth rate was considered because the pH in Lake Dianchi exhibited large variations during 2023 (varying from 7.8 - 9.4, Fig. S3) and cyanobacteria are sensitive to such pH fluctuations (Mangan *et al.* 2016; Wei *et al.* 2022). Similar to temperature, cyanobacterial growth is maximal for an optimum pH (pH_{opt}):

$$f(pH) = \exp\left(-2.3 \cdot \left(\frac{pH_{opt} - pH}{pH_{tr}}\right)^2\right) \quad (5)$$

where pH_{tr} denotes the pH tolerance range, which was calculated as the difference between pH_{opt} and the minimum pH for growth (pH_{min}). Here we use a pH_{opt} of 9.5 (Wei *et al.* 2022) and a pH_{min} of 4 (Pham *et al.* 2023).

Nutrient limitation was described using a Michaelis–Menten function for both nutrients:

$$f(N) = \frac{N}{K_N + N} \tag{6}$$

$$f(P) = \frac{P}{K_P + P} \tag{7}$$

where K_N and K_P are the half-saturation constants for N and P limitation, respectively. These constants were set to 0.2 mg N L^{-1} (Baker *et al.* 2023) and 0.02 mg P L^{-1} (Baldia *et al.* 2007), respectively. The minimum value of the two rate limiting terms was used in Eq. 2. The concentration of total phosphate (P mg L^{-1}) and total nitrogen (N, mg L^{-1}) were determined from monthly field data measured in Lake Dianchi.

Irradiance was calculated from hourly measurements of solar radiation (W m^{-2}). About 45% of the solar radiation was assumed to be photosynthetically active (Pinker & Laszlo 1992), and a value of 4.6 was used to convert W m^{-2} to irradiance at the water surface ($I_{surf}(t)$ in µmol m^{-2} s^{-1})(Langhans & Tibbitts, 1998). The irradiance that cells were exposed to at depth ($I(z,t)$) was then estimated by Lambert-Beer‘s law of exponential light extinction. The extinction coefficient was assumed to consist of a background value that is constant with depth (K_{bg} (m^{-1})), and depth-dependent light extinction by cyanobacterial cells (K_m (0.034 m^2 10^{-10} $cells^{-1}$)) (Huisman *et al.* 2004):

$$I(z,t) = I_{surf} exp\left(-\int_0^z [K_m \sum_i C_i(\delta,t)]\, d\delta - K_{bg} z\right) \tag{8}$$

K_{bg} was calculated from the Secchi disk depth (SD, in m) using an empirical equation:

$$K_{bg} = \frac{K_s}{SD} - K_{chla} \cdot Chla \tag{9}$$

where K_s is the factor to convert SD to light extinction for which we used a value of 1.7 (Liu *et al.* 2010; Zhang *et al.* 2012). K_{chla} (0.15 m^2 mg^{-1} Chl*a* (Ganf *et al.* 1989)) is the conversion factor from Chl*a* to light extinction coefficient, Chl*a* was determined by monthly measurements in Lake Dianchi.

The light limiting term in Eq. 2 was described by a Michaelis–Menten function as:

$$f(I) = \frac{I}{K_I + I} \tag{10}$$

where K_I is the half-saturation constant for light limitation that was set to 25 μmol m^{-2} s^{-1} (Kromkamp & E.Walsby 1990).

Cyanobacteria, such as *Microcystis* sp., *Planktothrix* sp. and *Aphanizomenon* sp, often have light-dependent buoyancy regulation, where buoyancy is enhanced under low irradiance and reduced under high irradiance(Petra Visser 1997). Since Lake Dianchi was dominated by *Microcystis* sp., we exemplarily use the empirical relationship between irradiance (μmol photons $m^{-2}s^{-1}$) and vertical migration velocity (v, μm s^{-1}) as follows(Bernhardt *et al.* 2008):

$$v = \begin{cases} 7.0, & if \quad I > 100 \\ 2.3, & if \quad 100 \geq I > 30 \\ -2.3, & if \quad 30 \geq I > 5 \\ -34.7, & if \quad I \leq 5 \end{cases} \tag{11}$$

where positive vertical velocities indicate sinking of cyanobacteria, while negative vertical velocities indicate a rise.

The simulations started on 31 Jan 2023 and were performed for 364 consecutive days. The initial cell density was set to a value of 3.3×10^4 cells mL^{-1}, which was measured on 31 Jan 2023 in Lake Dianchi. Given the unknown trait distribution in nature, we used a uniform initial cell density for all trait groups throughout the water column and performed a sensitivity test to examine the effect of varying initial trait distribution on cyanobacteria dynamics (Fig. S4) The range of T_{opt} and T_{min} we used was 18-30 ℃ and 2-14℃, respectively, which is within the range of literature values for *Microcystis* (Rossi *et al.* 2023).

We used an iterative algorithm at each time step (time-stepping solver) to solve the above equations and to obtain the dynamic distributions of all trait groups of cyanobacteria throughout the water column. The solver was implemented through a code in MATLAB 2022b, where the first and second derivatives were approximated using a combination of forward and central differences.

Model setting of the phytoplankton model

In the phytoplankton model, water depth and resolution of the vertical discretization were the same as those used in the hydrodynamic model. The temporal resolution was 1 s and no-flux conditions were applied at the boundaries.

To test the effects of the thermal trait range on the formation of cyanobacterial blooms and evaluate their predictive performance for the formation of cold-water blooms, we compared a population with a single fixed T_{opt} (24°C) against populations with a narrow T_{opt} range (21-27°C) and a wider T_{opt} range (18-30°C). These two ranges of T_{opt} were centered around 24°C. Accordingly, the cyanobacterial population was divided into strains based on their specific optimum growth temperature, with each strain representing a 1°C increment within the observed T_{opt} range.

To test for indirect effects of historic temperature on the dynamics of populations with varying range of T_{opt} and the resulting cold-water blooms, we varied the thermal conditions by increasing and decreasing the air temperature by 2 ℃ during summertime (from 1 May 2023 to 30 Sep 2023). Such changes in air temperature are within the magnitude of inter-annual temperature variations, which can change by 1-2℃ (Quayle *et al.* 2002). We ran the hydrodynamic model while keeping the other conditions and parameters constant, obtaining the simulated water temperatures and turbulent diffusivities under such conditions. The phytoplankton models, including single-trait and narrow range of T_{opt} were then ran with the output from the respective hydrodynamic models. Furthermore, we conducted extended simulations over four years by repeating annual environmental conditions to investigate the trend of bloom development in populations with wide range of T_{opt}.

To better compare the obtained bloom dynamics in different simulations, we chose cell densities of cyanobacteria from September 17 to October 7, 2023 (when the simulated cell densities reached maximum values in all simulations), to represent the peak amplitude of blooms (C_{peak}). We focused on the cell densities at the end of the simulations (from January 10 to January 30, 2024, when water temperatures were the lowest) as representative of the cell density in cold water (C_{CW}). We defined psychrophilic strains as cyanobacteria traits with $T_{opt} \leq 21$ ℃, and thermophilic strains as those with $T_{opt} > 21$ ℃.

Model evaluation

SIMSTRAT was calibrated for Lake Dianchi conditions by adjusting three constant parameters, including scaling factors for heat flux by shortwave radiation, transfer of momentum from the atmosphere to lake water, and the transfer of wind energy to seiche energy(Peeters *et al.* 2002). The performance of the hydrodynamic model was assessed by comparison with hourly observations of surface water temperature as well as the monthly measured water temperature at depths of 1.5 and 3 m.

The trait-based phytoplankton model was calibrated by adjusting three lake-specific parameters including U_{max}, K_{chla}, and K_s. The performance of the trait-based phytoplankton model using a cyanobacterial population with a T_{opt} range of 18-30℃ was evaluated by comparing the total simulated cell densities with measured cyanobacterial cell densities. The best-matching parameters for the phytoplankton model are given in Supporting Information Table S2.

Statistical analysis

The Shapiro-Wilk test was used to assess the normality of data. A post hoc LSD (least significant difference) test with one-way ANOVA was used to compare the C_{peak} and C_{CW} if the data were normally distributed with homogeneous variance. Otherwise, Kruskal-Wallis tests with post-Hoc pairwise comparisons using the Mann-Whitney U test were used. The relationships between C_{peak} and C_{CW}, as well as changes in summer temperatures were fitted by linear regressions. All statistical analyses were performed using the software package SPSS 27.0 (IBM Corp, USA). Data were tested for statistical significance at a significance level (p) of 0.05.

Results

Model calibration against water temperature

After calibration of the hydrodynamic model, the simulated water temperature exhibited excellent agreement with measurements throughout the simulation period (Fig. 2). The correlation coefficient between simulated and measured water temperature was 0.99 and the root mean square errors (RMSE) were ≤1°C at all three depth with available measurements (0, 1.5, and 3 m). The final calibration parameters for the hydrodynamic model are presented in Table S1.

No significant thermal stratification was observed, with the temperature difference throughout the water column (defined as the difference between the highest and lowest temperatures in the water column) remaining below 1°C for 90% of the simulation period (Fig. S5).

Role of diverse thermal traits in cyanobacteria dynamics

The cyanobacterial cell density in Lake Dianchi exhibited a general decline from January to April, followed by a steady increase until September, where it peaked at 4×10^5 cells mL^{-1}. After reaching this maximum in September 2023, the cell density decreased to approximately 1.2×10^5 cells mL^{-1} by January 2024 (Fig. 3a). Simulated cell densities for a population with a wide range of optimum growth temperature (T_{opt} between 18 and 30°C) showed better agreement with observed cell densities than the simulations with a narrower range or a single trait, with RMSE of 6.4×10^4 cells mL^{-1}, compared to RMSEs of 7.8×10^4 cells mL^{-1} and 9.0×10^4 cells mL^{-1}, respectively (Fig. 3a). Specifically, during the peak bloom period and at the end of the simulation period, the simulated cell density of the population with the wide range was closer to the observed cell density, than the simulation results for the other two populations. Similar to the observed cell density, the simulated cell density peaked in September 2023, which was associated with an increase in the light-limitation function, followed by a subsequent decline as the light-limitation function decreased (Fig. S6). The light-limitation function also exhibited high values in Jan 2023 and Jan 2024, corresponding to periods when Secchi disk depth was high (Fig. S2a). From May to September, the simulated cell density increased as the temperature-limitation function remained generally high, despite fluctuations in the light-limiting function. Throughout the simulation, the nutrient and pH limitation functions were similar, ranging

from 0.75 to 0.95 (Fig. S6; note that the limiting functions vary between zero and one, with one indicating no limitation).

The range of intraspecific variations in T_{opt} significantly affected the seasonal dynamics of cyanobacterial cell density. Populations with a wide range of T_{opt} formed blooms 1-2 months earlier compared to those with a narrower range and a single thermal trait (Fig. 3a), similar to the trend of temperature-limitation functions, which also showed an earlier increase for the population with a wide range. Only the blooms formed by the population with a wide range persisted throughout the winter period. The cell density during the representative cold-water periods (C_{CW}, 10 Jan to 30 Jan, 2024) of population with a wide range is significantly higher than those with a narrow range, and the narrow range was significantly higher than that the single-trait population (Fig. 3c). At the end of the simulation (31 Jan 2024), the cell densities of population with the wide range exceeded those of single-trait populations and of the population with a narrower range by up to approximate 16-fold and 3-fold, respectively (Fig. 3a). The temperature-limitation functions followed the order of wide range> narrow range> single trait at this time. However, during peak bloom periods, the cell density of the population with a wide range of T_{opt} was approximately 10% lower than those of the other populations (Fig. 3b), which is similar to the results showing that the temperature-limitation function of the population with a wide range of T_{opt} was also lower than those of the other populations during this period (Fig. S6).

Analysis of the population composition shows that a wide range of optimum growth temperature facilitated the dominance of psychrophilic strains, with cell densities exceeding those of thermophilic strains throughout the simulation period (Fig. 3d). For more narrow ranges of optimum growth temperatures, thermophilic strains became increasingly prevalent.

Sensitivity analysis showed a marginal effect of the initial trait distribution on cyanobacteria dynamics, wherein a lower initial population-averaged T_{opt} led to a slight increase in cell density from May to July (Fig. S4). The extended simulations showed that population with wide range of T_{opt} led to decreasing cell density during the periods of peak blooms (C_{peak}, 17 Sep to 7 Oct) but increasing cell density during the presentative cold-water periods (C_{CW}) in the following three years (Fig. S7).

Diversity-dependent response of cyanobacteria to temperature history

We compared the responses of populations with varying ranges of T_{opt} to changes in summer air temperatures (Fig. 4). The single-trait population resulted in higher cell density during the periods of peak blooms under increasing summer temperatures ($p < 0.05$), while no significant difference was observed for C_{CW}. Compared to single-trait population, multi-trait populations displayed contrasting responses to changes in summer temperatures. The cell densities during both the peak bloom and the winter period significantly decreased with increasing summer temperatures ($p < 0.01$). For populations with a wide range of T_{opt}, a reduction by 2°C led to an approximately 10% increase in cell densities during the maximum bloom period, and an up to twofold increase in C_{CW}, compared to the increased summer temperature.

Discussion

We demonstrated that a wide range of intraspecific variations of optimum growth temperature (T_{opt}) enhances the predictive performance of an ecological model describing the dynamics of cyanobacteria populations in Lake Dianchi, particularly bloom formation during cold-water periods (Fig. 3). In contrast to a narrow range or a single T_{opt}, a wide range promotes the formation of CyanHABs by up to threefold or even one order of magnitude, respectively, at the end of the simulation under unfavorable temperatures (Fig. 3c). This is because the population with a wide range of T_{opt} supports the persistence of psychrophilic cyanobacteria (Fig. 3d). This finding indicates that diversification of thermal traits, achievable through shifting selection pressures under environmental fluctuations (Driscoll *et al.* 2016), can play an important role in CWCBs. This remarkably rapid adaptation to temperature variations through intraspecific competition and change in trait distribution parallels previous studies (Sandrini *et al.* 2016; Wu *et al.* 2024), where cyanobacteria demonstrated adaptive genotypic and phenotypic shifts over several months in response to elevated CO_2 and mixing conditions. Our findings, however, also indicate a marginal effect of initial trait distribution on cyanobacterial dynamics (Fig. S4). This is likely attributed to initial light limitation (Fig. S6), which suppresses the growth of the entire population, thereby obscuring the influence of intraspecific trait distribution on population dynamics. This implies that the impact of thermal trait distribution unfolds only under conditions where other environmental factors are favorable.

Unexpectedly, a wider range of T_{opt} led to a 10% reduction in summer bloom amplitudes compared to a narrower range or single-trait population (Fig. 3b). This is attributed to the dominance of psychrophilic strains prior to temperature elevation (Fig. 3d), which subsequently hinder the growth of thermophilic strains through intraspecific competition for light. This finding suggests that the composition of T_{opt} acts as an information legacy that retains a memory of past thermal conditions, constituting an ecological memory (defined as 'the capacity of past experiences to influence present or future responses of a community (Padisak 1992; Canarini *et al.* 2021; Letourneau *et al.* 2022)). Such memory resists temperature fluctuations, leading to a lag in the response to seasonally changing temperatures, consequently reducing bloom amplitudes and tending to homogenize seasonal variations in cyanobacterial cell density. Our extended simulations indicated that CWCBs foreshadow a shift towards prolonged, albeit less intense, CyanHABs (Fig. S7).

This ecological memory may also cause the observed unexpected responses of cyanobacterial populations with varying T_{opt} ranges to changes in summer temperatures. The 'memory' of previous low temperatures in a trait-diverse cyanobacterial population causes it to favor cooler summers over hotter ones, during which this population can maintain more psychrophilic strains that promote CWCBs during winter. Our results show that the cell density of the population with a wide T_{opt} range exhibited an inverse correlation with temperature. A reduction of 2°C facilitated summer CyanHABs and CWCBs (by up to twofold for CWCBs), compared to a 2°C increase (Fig. 4). This effect, however, not only depends on trait diversity, but may also be counteracted and masked by other blooms drivers like eutrophication, potentially leading to increasing intensity of blooms in the light of global warming, as observed in former studies (Paerl & Huisman 2008; Beaulieu *et al.* 2013; Ho & Michalak 2019). Nevertheless, it aligns with a study that found that heat waves during summertime inhibit rather than promote cyanobacterial blooms (Anneville *et al.* 2015), and a global study showing that global warming has variable effects (both positive and negative) on phytoplankton blooms across 71 lakes worldwide (Ho *et al.* 2019). This counterintuitive finding, although it may not be universal, provides a mechanistic understanding of how increasing temperatures can affect blooms in an opposite direction, and a warning that neglecting trait variations may lead to erroneous

conclusions. It also demonstrates that the present thermal response of cyanobacteria populations can be determined by the temporal sequence of temperature that shaped their trait distribution.

The simulated CWCBs were still lower than the observed one (Fig. 3a), implying the existence of additional mechanisms such as adaptations to other winter stressors including low light availability, nutrient levels, and limited mixing conditions (Reinl *et al.* 2023). Particularly, light served as an important driver limiting cyanobacteria dynamics in our study (Fig. S6). Such adaptations may also play a role in the development of CWCBs, which should be investigated by incorporating more different traits (e.g., optimum irradiance, nutrient uptake rates, and vertical velocity, etc.). Furthermore, in deep lakes with stronger stratification, cyanobacteria may experience more dynamic temperature variations. For example, internal waves can entrain cyanobacteria within the thermocline (Cuypers *et al.* 2011), where strong temperature and light gradients may enhance trait diversity including simultaneous low-light thermal adaptation. Interactions between thermal stratification, and vertical migration also open an intriguing possibility that cyanobacteria with varying optimum growth temperature, light and nutrient requirements and vertical velocities occupy different preferred depths, effectively differentiating their thermal niches throughout the water column, linking several independent traits. For simplicity, the present model neglected the fact that cyanobacteria can interact with the thermal regime by enhancing light extinction, which affects heat absorption and consequently thermal stratification. This interaction could potentially influence the dynamics of thermal traits through positive or negative feedback. A more complete depiction of the intricate adaption of cyanobacteria population would include these processes, as well as deep lake and nutrient-limited scenarios. It should be noted that while our model simulated CWCBs in Lake Dianchi using the literature-documented ranges of T_{opt} (18-30°C) and T_{min} (2-14°C) (Rossi *et al.* 2023), it would be advantageous to obtain the actual range of these thermal traits through extensive sampling and measurements to support the suggested trait-based approach.

Our results support the general notion that high intraspecific trait diversity enhances population success across various environmental gradients (Barrett & Schluter 2008; Violle *et al.* 2012; Brandenburg *et al.* 2018). Moreover, we showed that intraspecific competition in populations with specific thermal traits can

alter their responses to changing temperatures, further highlighting the important role of these variations in population ecology (Des Roches *et al.* 2018). Specifically, by examining the link between intraspecific variations and CyanHABs, our study revealed two previously unknown findings: i) the diversification in thermal traits can promote CWCBs, and ii) the responses of the cyanobacterial populations to temperature depend on their thermal trait diversity. Our findings suggest that integrating intraspecific variations into current predictive models is a key step towards comprehending how increasingly variable climatic drivers and their legacy effects shape species succession at the bottom of aquatic food webs.

Acknowledgements

This study was financially supported by the German Research Foundation (grant no. LO 1150/18), the National Key R&D Program of China (2022YFC3203601), the Yunnan Province-Kunming City Major Science and Technology Project (202202AH210006), and the Key R&D Program of Hubei Province (2022BCA068).

Competing Interests statement

The authors declare no competing financial interests.

Reference

Anneville, O., Domaizon, I., Kerimoglu, O., Rimet, F. & Jacquet, S. (2015). Blue-Green Algae in a "Greenhouse Century"? New Insights from Field Data on Climate Change Impacts on Cyanobacteria Abundance. *Ecosystems*, 18, 441-458. Available from: https://doi.org/10.1007/s10021-014-9837-6

Babanazarova, O., Sidelev, S. & Schischeleva, S. (2013). The structure of winter phytoplankton in Lake Nero, Russia, a hypertrophic lake dominated by Planktothrix-like Cyanobacteria. *Aquatic Biosystems*, 9. Available from: https://doi.org/10.1186/2046-9063-9-18

Baker, D., Godwin, C.M., Khanam, M., Burtner, A.M., Dick, G.J. & Denef, V.J. (2023). Variation in resource competition traits among Microcystis strains is affected by their microbiomes. *mLife*, 2, 401-415. Available from: https:// doi.org/10.1002/mlf2.12094

Baldia, S.F., Evangelista, A.D., Aralar, E.V. & Santiago, A.E. (2007). Nitrogen and phosphorus utilization in the cyanobacterium Microcystis aeruginosa isolated from Laguna de Bay, Philippines. *Journal of Applied Phycology*, 19, 607-613. Available from: https:// doi.org/10.1007/s10811-007-9209-0

Bar-On, Y.M., Phillips, R. & Milo, R. (2018). The biomass distribution on Earth. *Proceedings of the National Academy of Sciences of the United States of America*, 115, 6506-6511. Available from: https://doi.org/10.1073/pnas.1711842115

Barrett, R.D. & Schluter, D. (2008). Adaptation from standing genetic variation. *Trends in Ecology & Evolution*, 23, 38-44. Available from: https://doi.org/10.1016/j.tree.2007.09.008

Beaulieu, M., Pick, F. & Gregory-Eaves, I. (2013). Nutrients and water temperature are significant predictors of cyanobacterial biomass in a 1147 lakes data set. *Limnology and Oceanography*, 58, 1736-1746. Available from: https://doi.org/10.4319/lo.2013.58.5.1736

Bernhardt, J., Elliott, J.A. & Jones, I.D. (2008). Modelling the effects on phytoplankton communities of changing mixed depth and background extinction coefficient on three contrasting lakes in the English Lake District. *Freshwater Biology*, 53, 2573-2586. Available from: https:// doi.org/10.1111/j.1365-2427.2008.02083.x

Bizic-Ionescu, M., Amann, R. & Grossart, H.P. (2014). Massive regime shifts and high activity of heterotrophic bacteria in an ice-covered lake. *PLoS One*, 9, e113611. Available from: https://doi.org/10.1371/journal.pone.0113611

Brandenburg, K.M., Wohlrab, S., John, U., Kremp, A., Jerney, J., Krock, B. *et al.* (2018). Intraspecific trait variation and trade-offs within and across populations of a toxic dinoflagellate. *Ecology Letters*, 21, 1561-1571. Available from: https://doi.org/10.1111/ele.13138

Canarini, A., Schmidt, H., Fuchslueger, L., Martin, V., Herbold, C.W., Zezula, D. *et al.* (2021). Ecological memory of recurrent drought modifies soil processes via changes in soil microbial community. *Nature Communications*, 12, 5308. Available from: https://doi.org/10.1038/s41467-021-25675-4

Cuypers, Y., Vincon-Leite, B., Groleau, A., Tassin, B. & Humbert, J.F. (2011). Impact of internal waves on the spatial distribution of Planktothrix rubescens (cyanobacteria) in an alpine lake.The *ISME Journal*, 5, 580-589. Available from: https://doi.org/10.1038/ismej.2010.154

Des Roches, S., Post, D.M., Turley, N.E., Bailey, J.K., Hendry, A.P., Kinnison, M.T. *et al.* (2018). The ecological importance of intraspecific variation. *Nature Ecology & Evolution*, 2, 57-64. Available from: https://doi.org/10.1038/s41559-017-0402-5

Doubek, J.P., Anneville, O., Dur, G., Lewandowska, A.M., Patil, V.P., Rusak, J.A. *et al.* (2021). The extent and variability of storm-induced temperature changes in lakes measured with long-term and high-frequency data. *Limnology and Oceanography*, 66, 1979-1992. Available from: https://doi.org/10.1002/lno.11739

Driscoll, W.W., Hackett, J.D. & Ferriere, R. (2016). Eco-evolutionary feedbacks between private and public goods: evidence from toxic algal blooms. *Ecology Letters*, 19, 81-97. Available from: https://doi.org/10.1111/ele.12533

Falkowski, P.G., Fenchel, T. & Delong, E.F. (2008). The Microbial Engines That Drive Earth's Biogeochemical Cycles. *Science*, 320, 1034-1039. Available from: https://doi.org/10.1126/science.1153213

Field, C.B., Behrenfeld, M.J., Randerson, J.T. & Falkowski, P. (1998). *Science*, 281, 237-240. Available from: https:// doi.org/10.1126/science.281.5374.237

Fischer, E.M. & Knutti, R. (2015). Anthropogenic contribution to global occurrence of heavy-precipitation and high-temperature extremes. *Nature Climate Change*, 5, 560-564. Available from: https://doi.org/10.1038/nclimate2617

Ganf, G.G., Oliver, R.L. & Walsby, A.E. (1989). Optical Properties of Gas-vacuolate Cells and Colonies of Microcystis in Relation to Light Attenuation in a Turbid, Stratified Reservoir (Mount Bold Reservoir, South Australia). Australian Journal of Marine and Freshwater Research., 40, 595-611. Available from: https://doi.org/10.1071/MF9890595

Goudsmit, G.H., Burchard, H., Peeters, F. & Wüest, A. (2002). Application of k-ϵ turbulence models to enclosed basins: The role of internal seiches. *Journal of Geophysical Research: Oceans*, 107, 3230. Available from: https://doi.org/10.1029/2001JC000954

Ho, J.C. & Michalak, A.M. (2019). Exploring temperature and precipitation impacts on harmful algal blooms across continental U.S. lakes. *Limnology and Oceanography*, 65, 992-1009. Available from: https://doi.org/10.1002/lno.11365

Ho, J.C., Michalak, A.M. & Pahlevan, N. (2019). Widespread global increase in intense lake phytoplankton blooms since the 1980s. *Nature*, 574, 667-670. Available from: https://doi:10.1038/s41586-019-1648-7

Hrycik, A.R., McFarland, S., Morales-Williams, A. & Stockwell, J.D. (2022). Winter severity shapes spring plankton succession in a small, eutrophic lake. *Hydrobiologia*, 849, 2127-2144. Available from: https://doi.org/10.1007/s10750-022-04854-4

Huisman, J., Sharples, J., Stroom, J.M., Visser, P.M., Kardinaal, W.E.A., Verspagen, J.M.H. *et al.* (2004). Changes in Turbulent Mixing Shift Competition for Light between Phytoplankton Species. *Ecology*, 85, 2960-2970. Available from: https://doi.org/10.1890/03-0763

Kromkamp, J. & E.Walsby, A. (1990). A computer model of buoyancy and vertical migration in cyanobacteria. *Journal of Plankton Research*, 12, 161-183. Available from: https://doi.org/10.1093/plankt/12.1.161

Lajoie, G. & Vellend, M. (2015). Understanding context dependence in the contribution of intraspecific variation to community trait-environment matching. *Ecology*, 96, 2912-2922. Available from: https://doi.org/10.1890/15-0156.1

Lehman, J.T., Botkin, D.B. & Likens, G.E. (1975). The assumptions and rationales of a computer model of phytoplankton population dynamics1. *Limnology and Oceanography*, 20, 343-364. Available from: https://doi.org/10.4319/lo.1975.20.3.0343

Letourneau, J., Holmes, Z.C., Dallow, E.P., Durand, H.K., Jiang, S., Carrion, V.M. *et al.* (2022). Ecological memory of prior nutrient exposure in the human gut microbiome. The *ISME Journal*, 16, 2479-2490. Available from: https://doi.org/10.1038/s41396-022-01292-x

Liu, W.-C., Wu, R.-S., Wu, E.M.-Y., Chang, Y.-P. & Chen, W.-B. (2010). Using water quality variables to predict light attenuation coefficient: case study in Shihmen Reservoir. *Paddy and Water Environment*, 8, 267-275. Available from: https://doi.org/10.1007/s10333-010-0207-5

Lochte, K. & Turley, C.M. (1988). Bacteria and cyanobacteria associated with phytodetritus in the deep sea. *Nature*, 333, 67–69. Available from: https://doi.org/10.1038/333067a0

Ma, J., Qin, B., Paerl, H.W., Brookes, J.D., Hall, N.S., Shi, K. *et al.* (2016). The persistence of cyanobacterial (Microcystis spp.) blooms throughout winter in Lake Taihu, China. *Limnology and Oceanography*, 61, 711-722. Available from: https://doi.org/10.1002/lno.10246

Mangan, N.M., Flamholz, A., Hood, R.D., Milo, R. & Savage, D.F. (2016). pH determines the energetic efficiency of the cyanobacterial CO_2 concentrating mechanism. *Proceedings of the National Academy of Sciences of the United States of America*, 113, E5354-5362. Available from: https://doi.org/10.1073/pnas.1525145113

Moran, E.V., Hartig, F. & Bell, D.M. (2016). Intraspecific trait variation across scales: implications for understanding global change responses. *Global Change Biology*, 22, 137-150. Available from: https://doi.org/10.1111/gcb.13000

Padisak, J. (1992). Seasonal succession of phytoplankton in a large shallow lake (Balaton, Hungary) - a dynamic approach to ecological memory, its possible role and mechanisms. *Journal of Ecology*, 80, 217-230. Available from: https://doi.org/10.2307/2261008

Paerl, H.W. & Huisman, J. (2008). Blooms Like It Hot. *Science*, 320, 57-58. Available from: https://

Peeters, F., Livingstone, D.M., Goudsmit, G.-H., Kipfer, R. & Forster, R. (2002). Modeling 50 years of historical temperature profiles in a large central European lake. *Limnology and Oceanography*, 47, 186-197. Available from: https://doi.org/10.4319/lo.2002.47.1.0186

Peeters, F., Straile, D., Lorke, A. & Ollinger, D. (2007). Turbulent mixing and phytoplankton spring bloom development in a deep lake. *Limnology and Oceanography*, 52, 286-298. Available from: https://doi.org/10.4319/lo.2007.52.1.0286

Perkins, S.E., Alexander, L.V. & Nairn, J.R. (2012). Increasing frequency, intensity and duration of observed global heatwaves and warm spells. *Geophysical Research Letters*, 39, L20714. Available from: https://doi.org/10.1029/2012GL053361

Pham, M.L., Askarzadmohassel, E. & Brandl, M. (2023). Growth of freshwater cyanobacterium Aphanizomenon sp. ULC602 in different growing and nutrient conditions. *Frontiers in Microbiology*, 14, 1220818. Available from: https://doi.org/10.3389/fmicb.2023.1220818

Pinker, R.T. & Laszlo, I. (1992). Global Distribution of Photosynthetically Active Radiation as Observed from Satellites. *Journal of Climate*, 5, 56-65. Available from: http://www.jstor.org/stable/26197041

Quayle, W.C., Peck, L.S., Peat, H., Ellis-Evans, J.C. & Harrigan, P.R. (2002). Extreme Responses to Climate Change in Antarctic Lakes. *Science*, 295. Available from: https://doi.org/10.1126/science.1064074

Langhans, R.W., Tibbitts, T.W. (1998). Plant Growth Chamber Handbook. *Photosynthetica*, 35, 232. Available from: https://doi.org/10.1023/A:1006995714717

Råman Vinnå, L., Wüest, A. & Bouffard, D. (2017). Physical effects of thermal pollution in lakes. *Water Resources Research*, 53, 3968-3987. Available from: doi.org/10.1002/2016wr019686

Reinl, K.L., Harris, T.D., North, R.L., Almela, P., Berger, S.A., Bizic, M. *et al.* (2023). Blooms also like it cold. *Limnology and Oceanography Letters*, 8, 546-564. Available from: https://doi.org/10.1002/lol2.10316

Rossi, S., Carecci, D. & Ficara, E. (2023). Thermal response analysis and compilation of cardinal temperatures for 424 strains of microalgae, cyanobacteria, diatoms and other species. *Science of The Total Environment*, 873, 162275. Available from: https://doi.org/10.1016/j.scitotenv.2023.162275

Sandrini, G., Ji, X., Verspagen, J.M., Tann, R.P., Slot, P.C., Luimstra, V.M. *et al.* (2016). Rapid adaptation of harmful cyanobacteria to rising CO2. *Proceedings of the National Academy of Sciences of the United States of America*, 113, 9315-9320. Available from: https://doi.org/10.1073/pnas.1602435113

Scheffer, M., Straile, D., van Nes, E.H. & Hosper, H. (2001). Climatic warming causes regime shifts in lake food webs. *Limnology and Oceanography*, 46, 1780-1783. Available from: https://doi.org/10.4319/lo.2001.46.7.1780

Schwefel, R., Gaudard, A., Wüest, A. & Bouffard, D. (2016). Effects of climate change on deepwater oxygen and winter mixing in a deep lake (Lake Geneva): Comparing observational findings and modeling. *Water Resources Research*, 52, 8811-8826. Available from: https://doi.org/10.1002/2016wr019194

Stockwell, J.D., Doubek, J.P., Adrian, R., Anneville, O., Carey, C.C., Carvalho, L. *et al.* (2020). Storm impacts on phytoplankton community dynamics in lakes. *Global Change Biology*, 26, 2756-2784. Available from: https://doi.org/10.1111/gcb.15033

Umlauf, L. & Burchard, H. (2003). A generic length-scale equation for geophysical turbulence models. *Journal of Marine Research*, 61, 235–265. Available from: https://elischolar.library.yale.edu/journal_of_marine_research/9

Violle, C., Enquist, B.J., McGill, B.J., Jiang, L., Albert, C.H., Hulshof, C. *et al.* (2012). The return of the variance: intraspecific variability in community ecology. *Trends in Ecology & Evolution*, 27, 244-252. Available from: https://doi.org/10.1016/j.tree.2011.11.014

Visser, P. M., Passarge, J., & Mur, L. R. (1997). Modelling vertical migration of the cyanobacterium Microcystis. *Hydrobiologia*, 349, 99–109. Available from: https://doi.org/10.1023/A:1003001713560

Wei, S., Zhuang, G., Cheng, L. & Wang, S. (2022). The proliferation rule of Microcystis aeruginosa under different initial pH conditions and its influence on the pH value of the environment. *Environmental Science and Pollution Research International*, 29, 13835-13844. Available from: https:// doi.org/10.1007/s11356-021-16719-9

Wu, H., Wu, X., Rovelli, L. & Lorke, A. (2024). Selection of photosynthetic traits by turbulent mixing governs formation of cyanobacterial blooms in shallow eutrophic lakes. The *ISME Journal*, 18, wrae021. Available from: https://doi.org/10.1093/ismejo/wrae021

Wüest, A. & Lorke, A. (2003). Small-Scale Hydrodynamics in Lakes. *Annual Review of Fluid Mechanics*, 35, 373-412. Available from: https://doi.org/10.1146/annurev.fluid.35.101101.161220

Zhang, Y., Liu, X., Yin, Y., Wang, M. & Qin, B. (2012). Predicting the light attenuation coefficient through Secchi disk depth and beam attenuation coefficient in a large, shallow, freshwater lake. *Hydrobiologia*, 693, 29-37. Available from: https://doi.org/10.1007/s10750-012-1084-2

Figures:

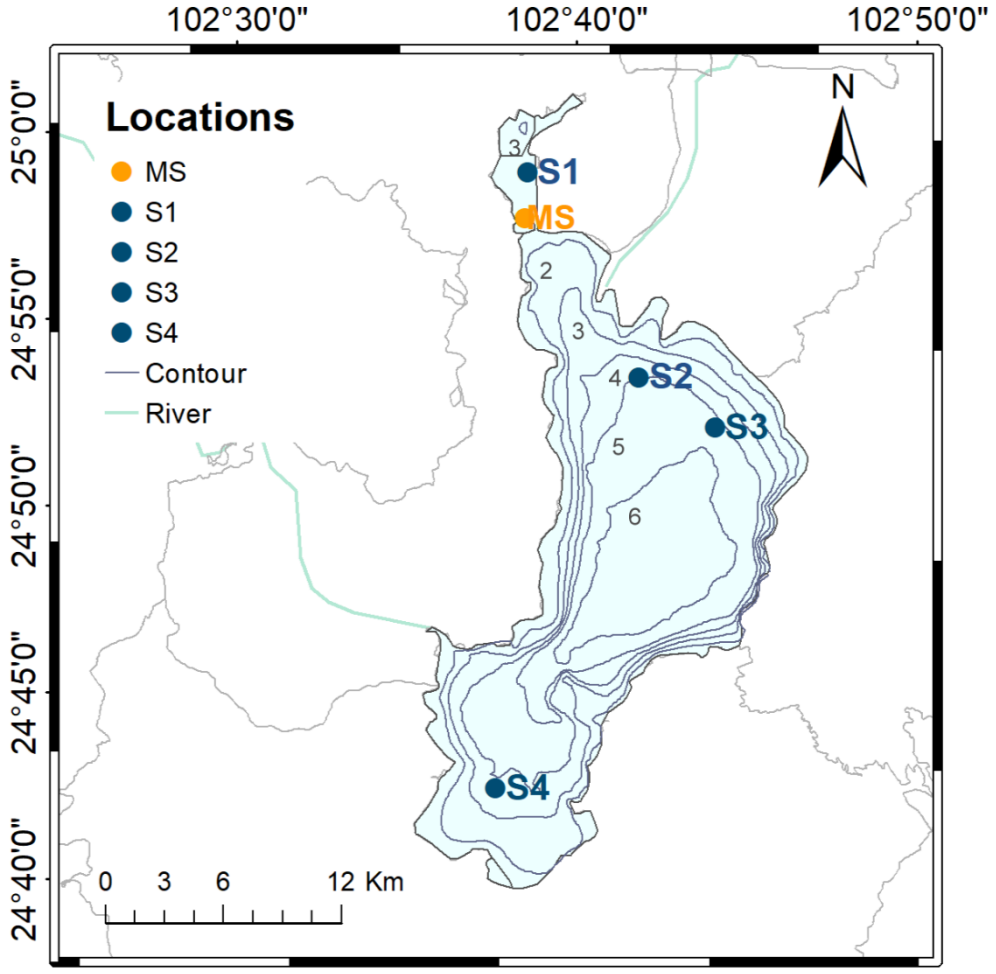

Fig. 1. Bathymetry of Lake Dianchi (light blue area) with the locations of sampling stations (S1-S4) and the meteorological station (MS). Green solid lines denote the river course and light grey lines denote district boundaries in the Lake Dianchi basin.

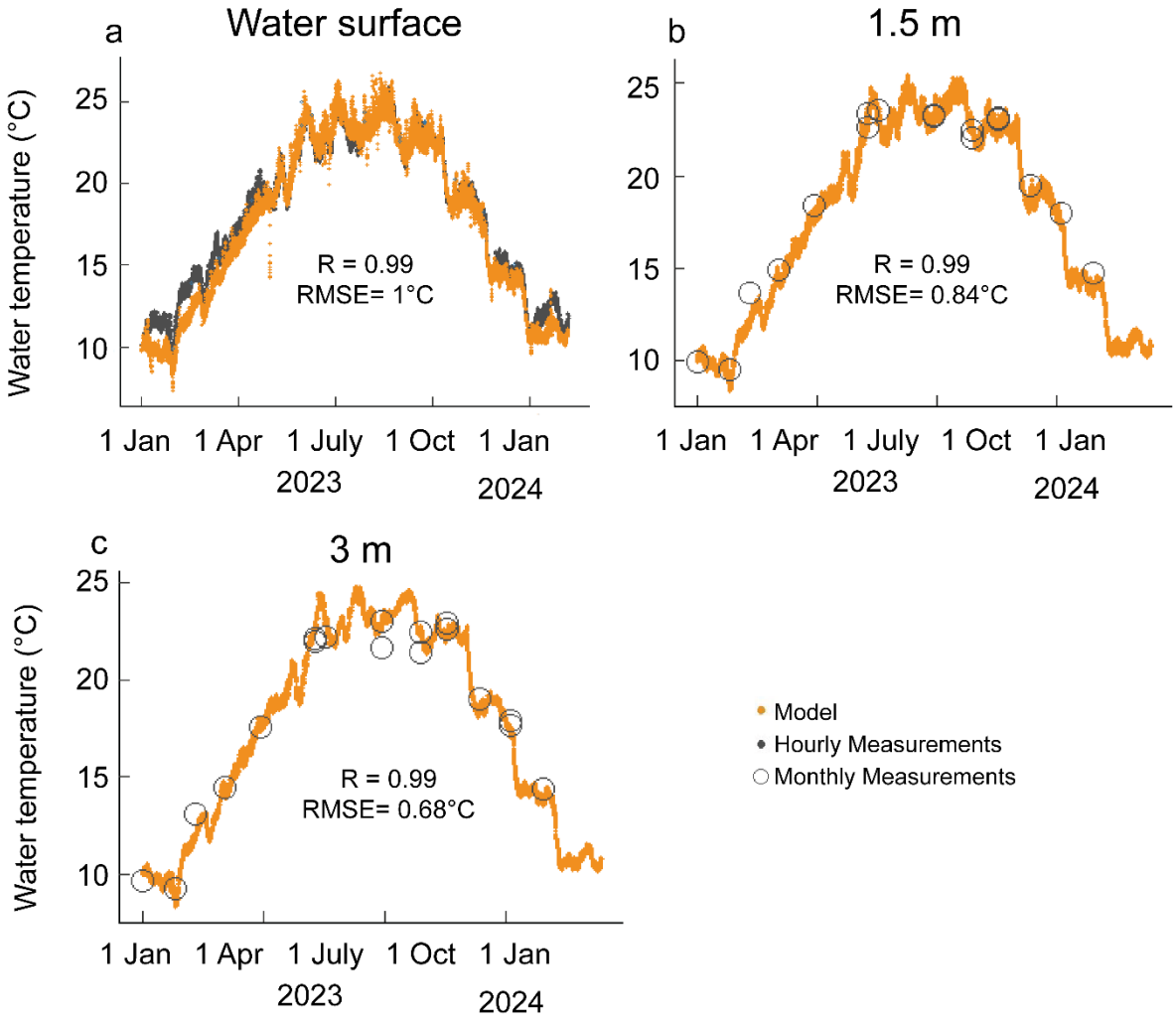

Fig. 2. Comparison between measured (black dots) and modeled (orange dots) water temperature in Lake Dianchi from 1 Jan, 2023, to 31 Jan, 2024, at the water surface (a), 1.5 m depth (b), and 3 m depth (c). *R* denotes the correlation coefficient, and RMSE denotes the root mean square error between predicted and observed temperatures. Surface water temperatures were recorded by a meteorological station at hourly intervals, while water temperatures at depths of 1.5 m and 3 m were measured during monthly in field investigations.

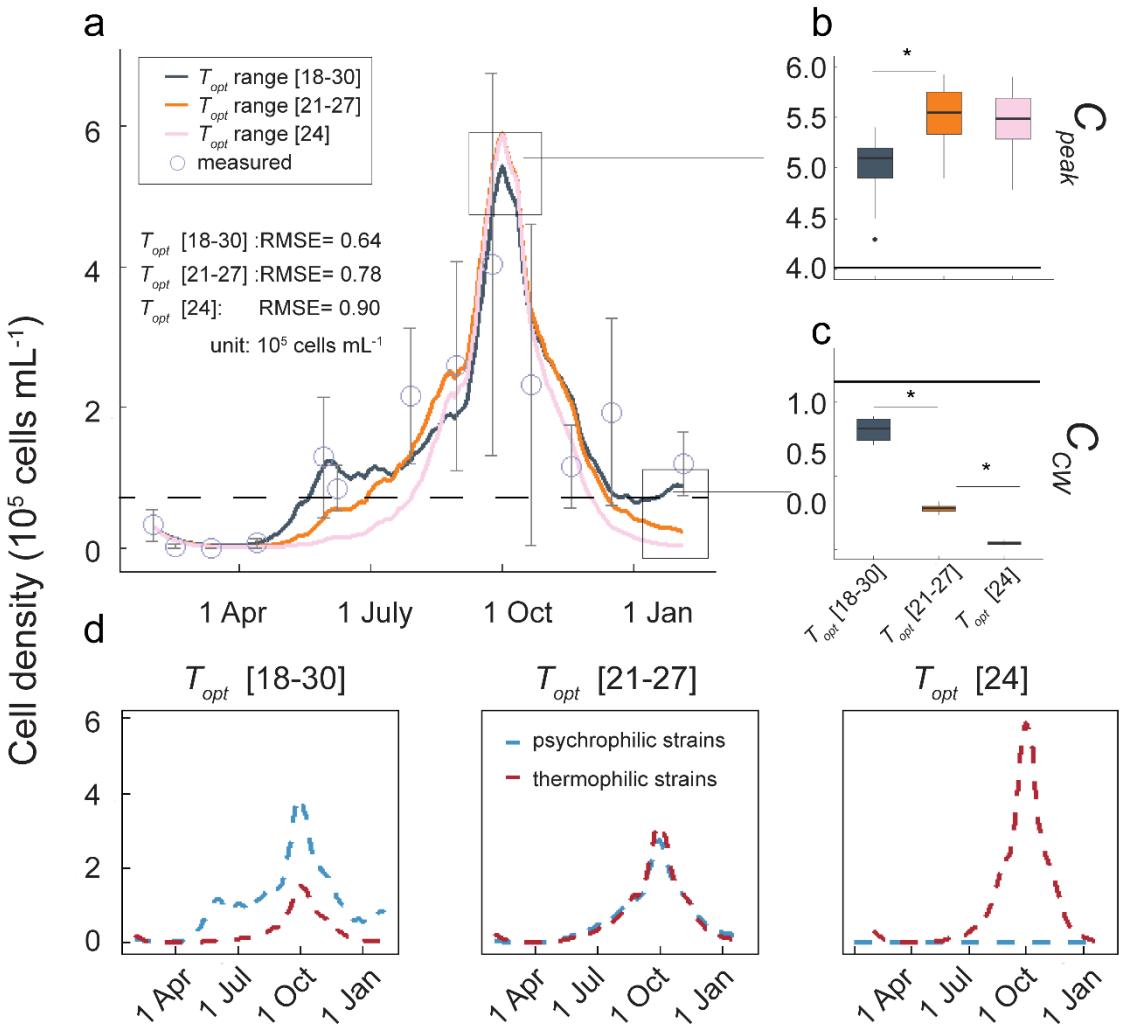

Fig. 3. (a) Time series of measured (open symbols) and simulated (solid lines) cell densities of cyanobacterial populations. The depth-integrated simulation results represent different ranges of optimum growth temperature (T_{opt}, see the color assignments for solid lines). The errors bars on the measured data represent cell density and RMSE denotes the root mean square error between simulated and observed cell densities. The dashed horizontal line marks a threshold for bloom formation (0.8 $\times 10^5$ cell mL^{-1}). (b) Box plots of simulated cell densities of the three different populations during the peak bloom (C_{peak}, 17 Sep to 7 Oct, 2023), and (c) during the representative cold-water period (C_{CW}, 10 Jan to 30 Jan, 2024). The black horizontal solid line in panel (b) panel (c) indicates the measured cell densities during peak bloom period and cold-water periods, respectively. * indicates significant differences in cell density between different T_{opt} ranges during peak blooms period (ANOVA, n=63, df =2, F value= 17.3, p <0.01) and cold-water periods (Kruskal-Wallis, n=63, df=2, H=55, p <0.01). (d) Time series of simulated cell densities of psychrophilic ($T_{opt} \leq 21$°C) and thermophilic ($T_{opt} > 21$°C) cyanobacteria within populations with different ranges of T_{opt} (see different horizontal panels).

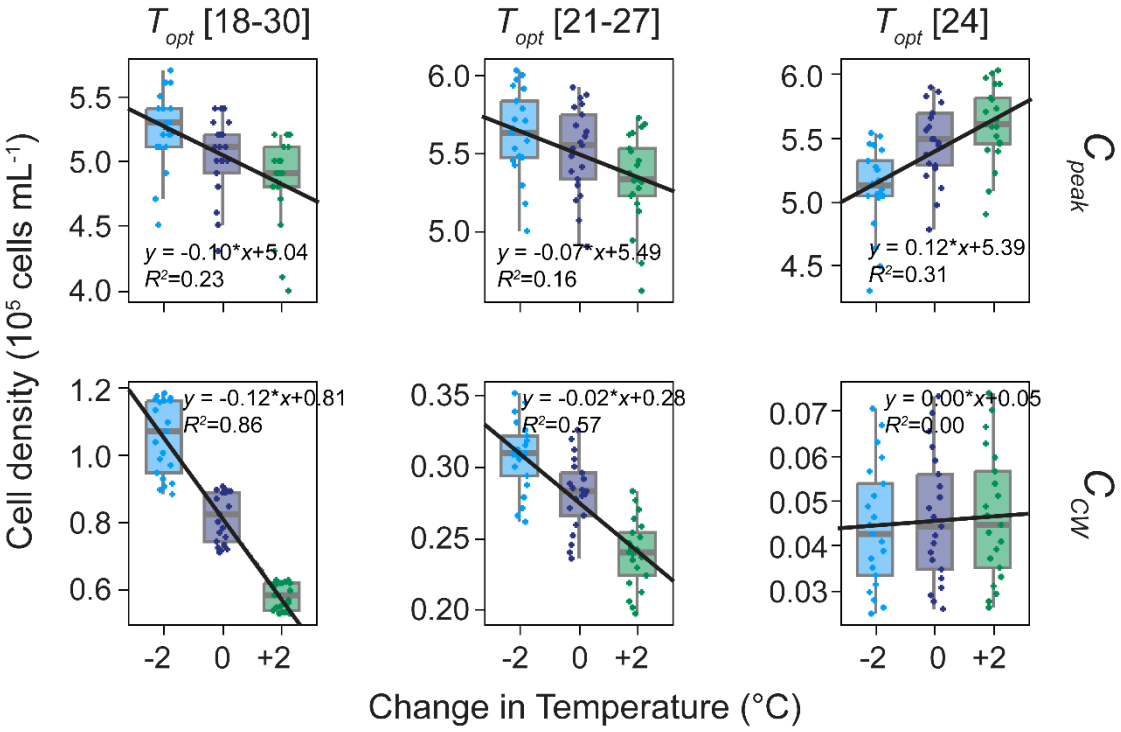

Fig. 4. Boxplots of cell densities during the peak bloom period (C_{peak}, upper rows) and during the cold-water period (C_{CW}, lower rows) for populations with different ranges of optimum growth temperature (see different columns) under varying summer temperature conditions. Grey lines represent linear regressions of all data versus the temperature change. The regression equations, coefficients of determination (R^2) and p-values (indicating the slope is significantly different from zero) Expect for the C_{CW} of single-trait population, all other regressions are significant ($p < 0.01$).

Supporting Information

Intraspecific competition can promote cold-water cyanobacterial blooms: Revisiting cyanobacteria-temperature relationships based on traits

Yanxue Zhang[a,c,e,1], Huaming Wu[b,1], Xingqiang Wu[a], Hans-Peter Grossart[c, d] , Andreas Lorke[b]

[a]*Key Laboratory of Algal Biology of Chinese Academy of Sciences, Institute of Hydrobiology, Chinese Academy of Sciences, Wuhan 430072, China*

[b]*Institute for Environmental Sciences, University of Kaiserslautern-Landau (RPTU), Landau 76829, Germany*

[c]*Department of Plankton and Microbial Ecology, Leibniz Institute of Freshwater Ecology and Inland Fisheries, Stechlin 16775, Germany*

[d]*Institute of Bicochemistry and Biology, Potsdam University, Potsdam 14469, Germany*

[e]*University of Chinese Academy of Sciences, Beijing 100049, China*

[1] These authors contributed equally to this work.

Text

Text S1: Measurements of physical, chemical and biological properties in Lake Dianchi

In-situ measurements of pH were conducted using a Yellow Springs Instruments (YSI) 6600 multi-sensor sonde (Zhang *et al*., 2024). Concentrations of TP and TN were determined using a combined persulfate digestion method after thawing (Ebina *et al*., 1983).

Phytoplankton samples were preserved with Lugol's iodine solution (2% final concentration) and allowed to settle for 48 hours. Cell density was measured with an optical microscope (BX43, Olympus Corporation) at 400X magnification using a phytoplankton counting plate (MPC-200, Matsunami Glass,

Japan) and a hemocytometer. Phytoplankton species were identified according to the method described by Hu *et al*., (1980). Water temperature at the depth of 1.5 and 3 m were measured using temperature sensor in LISST-HAB following the protocol by Zhang *et al*. (2024).

Chlorophyll-a (Chl *a*) concentrations were determined using 47 mm Whatman GF/F glass fiber filters and 90% (v/v) acetone extraction (Hagerthey *et al*., 2006). After 24 hours in darkness at 4°C, the extracts were centrifuged for 10 minutes at 4000 rpm, and the absorbance was measured at wavelengths of 630, 663, 750, and 645 nm Zhang *et al*. (2024).

Text S2: Population-averaged temperature-limitation function

The population-averaged temperature-limitation function i.e. $\overline{f(T)}$ was calculated by the following equation:

$$\overline{\overline{f(T)}} = \frac{\sum_{i=1}^{n} \bar{C}_i \cdot f_i(T)}{\sum_{i=1}^{n} \bar{C}_i} \quad \text{(S1)}$$

where n is the number of trait groups in each population (n=13 or 7, corresponding to the number of strains in population with wide range and narrow range of T_{opt}), $\overline{C}_i$ and $T_{opt,i}$ are the mean (vertically averaged) cell density and the maximum optimum growth temperature of each strain. $f_i(T)$ is the temperature-limitation function of strain i calculated by eq. 4 in the main manuscript.

Figures:

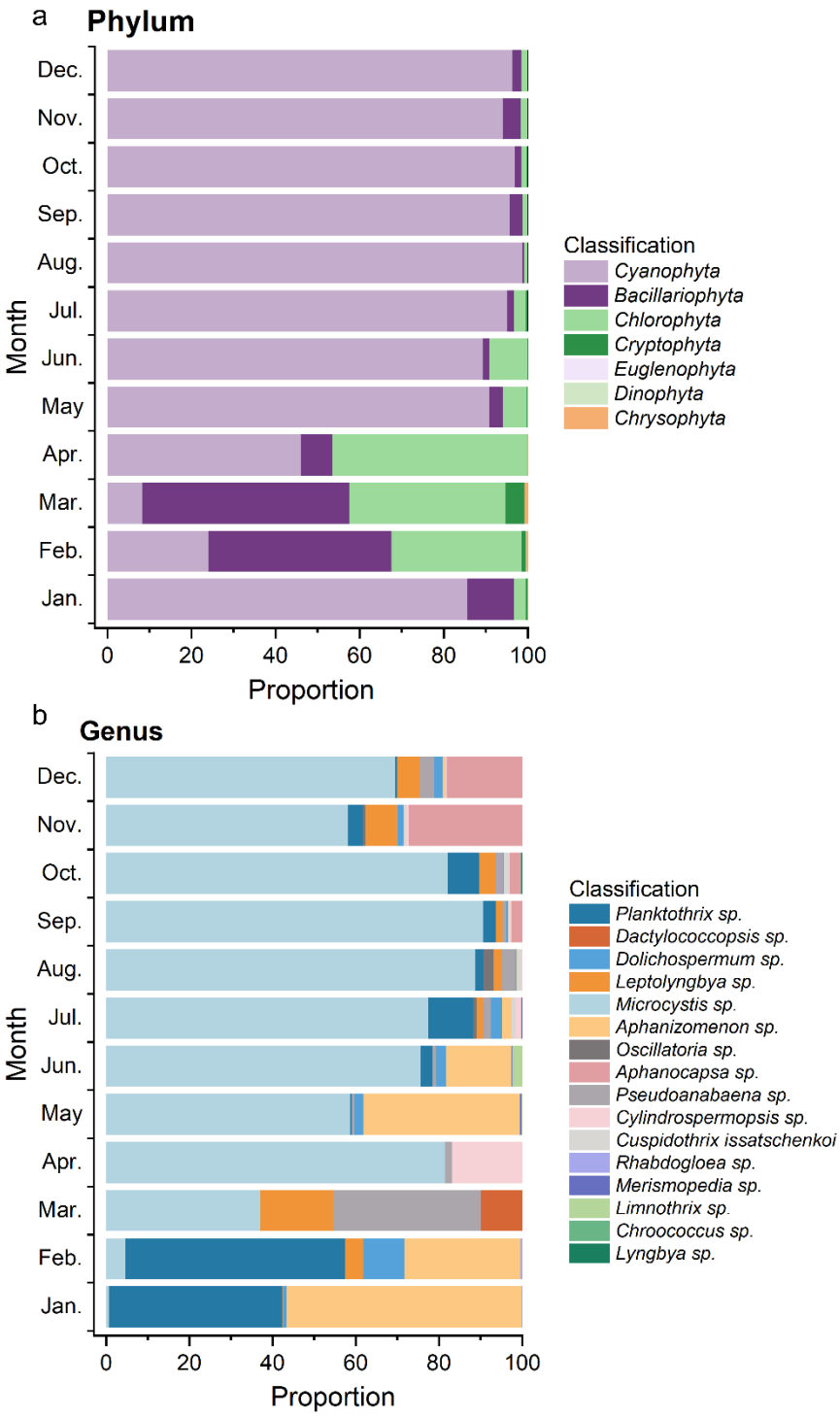

Fig. S1: The phytoplankton composition in Lake Dianchi in 2023 at the phylum level (a) and the genus level (b).

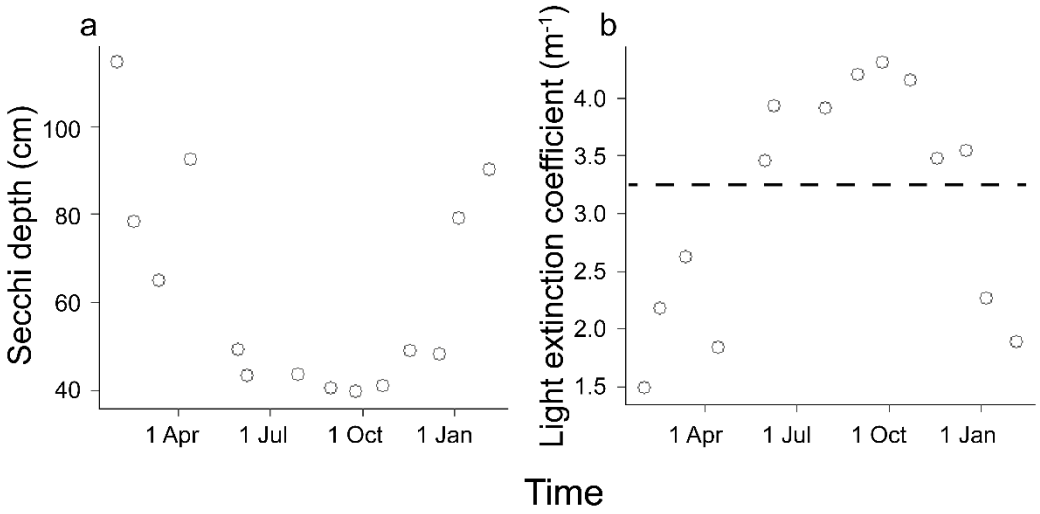

Fig. S2: The temporal dynamics of Secchi disk depth (a) and light extinction coefficient (b) in Lake Dianchi during field investigations. The dashed black line is the average light extinction coefficient (3.3 m^{-1}) in 2023.

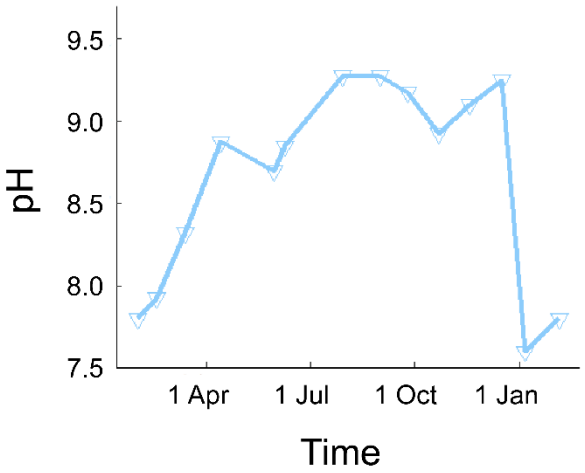

Fig. S3: The temporal dynamics of pH in Lake Dianchi during field investigations.

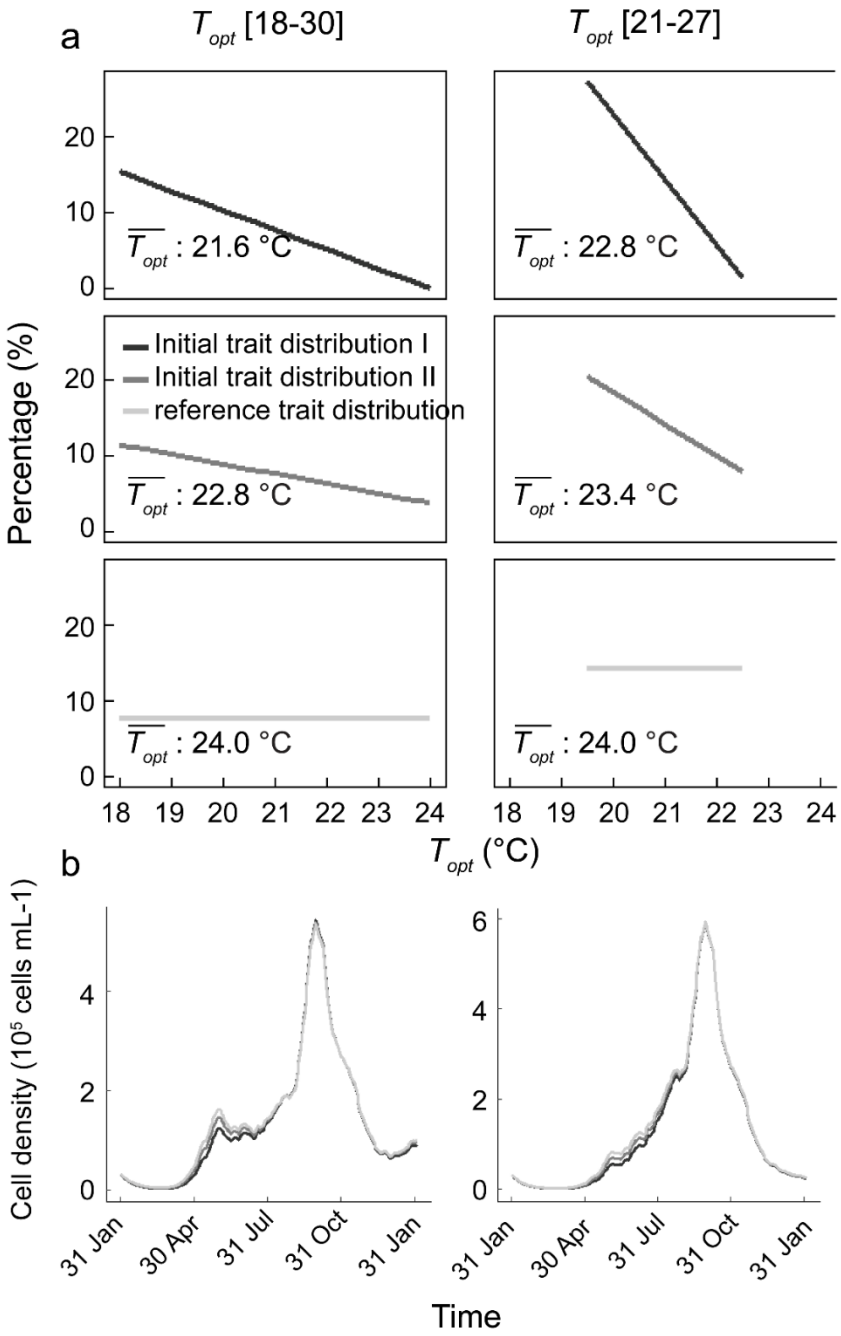

Fig. S4: Initial T_{opt} distributions for populations with wide and narrow ranges (see different columns) used in the sensitivity test (a). Temporal dynamics of cell density of populations (different columns) simulated with these initial conditions (see color assignments, b).

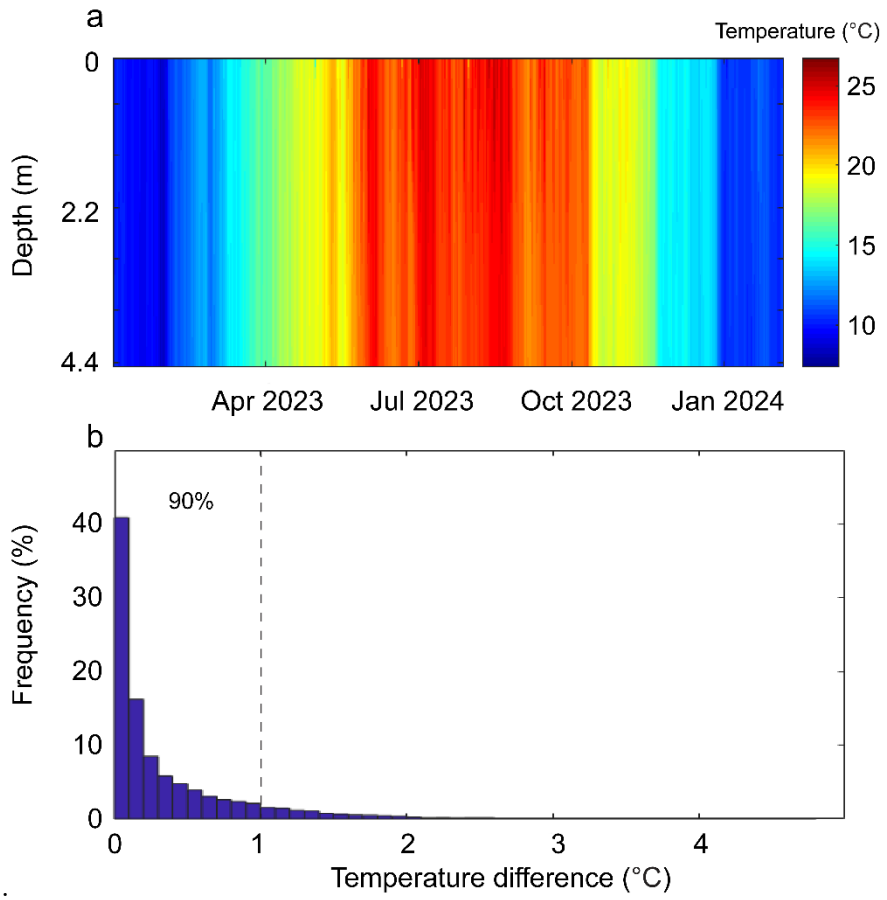

.

Fig. S5: Modeled water temperature stratification at hourly intervals throughout the simulation period (a) and histogram showing the frequency distribution of water temperature differences (defined as the difference between maximum and minimum temperature of the water column, b).

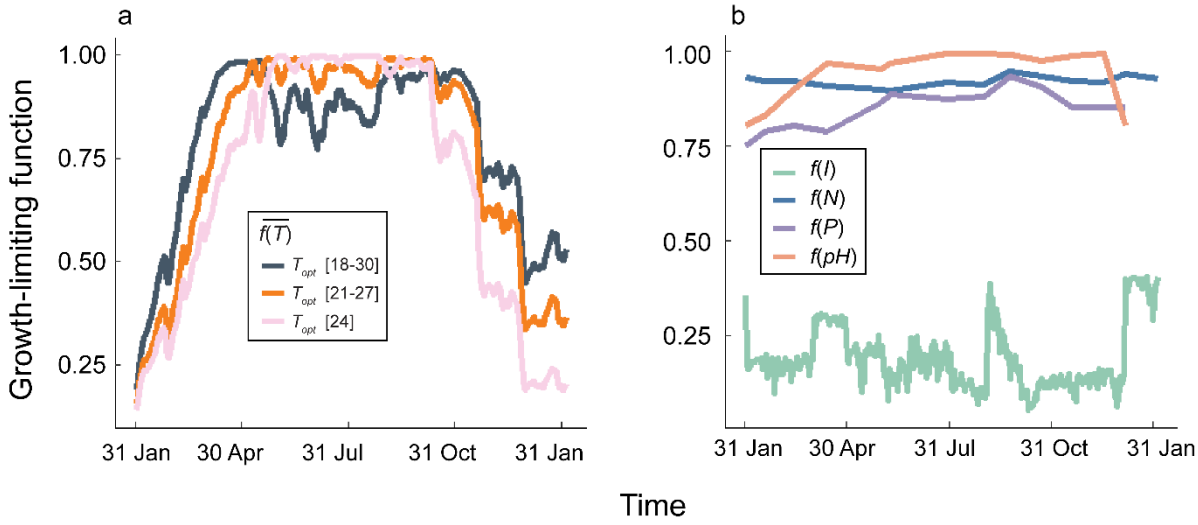

Fig. S6: Time series of the population averaged temperature-limiting functions (see eq. S1) for population with different range of optimum growth temperature (T_{opt}, see color assignment, a) and growth-limiting functions of cyanobacteria for light (I), nitrogen (N), phosphorus (P), and pH (see color assignment in the legend; cf. Eq. 3 in the main manuscript, b).

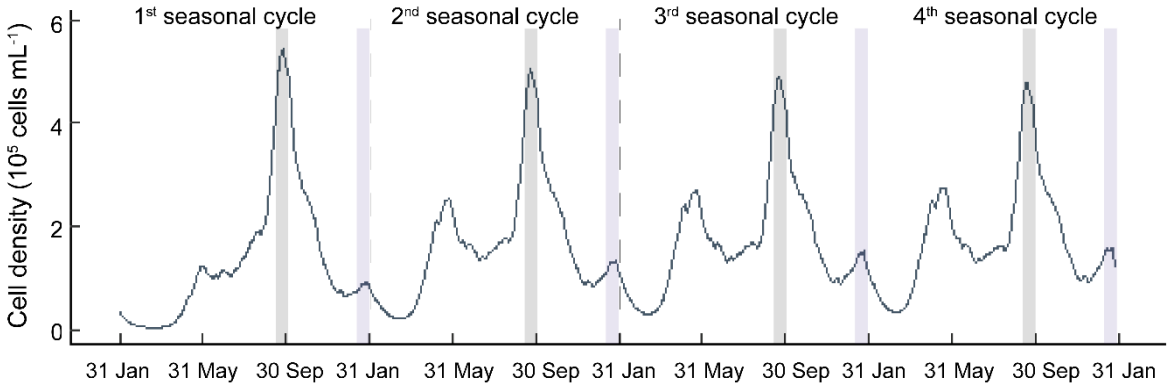

Fig. S7: Time series of cell density for a population with a wide range of optimum growth temperatures over four seasonal cycles. The periods of peak blooms and representative cold-water periods are shaded in gray and purple, respectively. The first cycle corresponds to the one analyzed in the main manuscript. In this extended simulation, the boundary and forcing conditions from the first year were also applied to the subsequent cycles.

Tables:

Table S1: Best-matching calibrated parameters for hydrodynamic model.

Parameter	Calibrated value
Scaling factors for the heat flux by shortwave radiation	1.5
The transfer of momentum from the atmosphere to lake water	1
The transfer of wind energy to seiche energy	0.001

Table S2: Definition, description, values and references of the parameters used in the model.

Symbol	Description (unit)	Value	Reference
C_k	**Kolmogorov constant**	0.076	Umlauf and Burchard, 2003
l	Loss rate of *Microcystis* (d^{-1})	0.1	Huisman *et al*., 2004
T_{tr}	**Thermal tolerance range (**°C)	16	Rossi *et al*., 2023
pH_{opt}	Optimal pH for growth	9.5	Wei *et al*., 2022
pH_{min}	**Tolerance range of pH**	4	Pham *et al*., 2023; Wei *et al*., 2022
K_N	Half-saturation constants for N (mg N L^{-1})	0.2	Baker *et al*., 2023
K_P	Half-saturation constants for P (mg P L^{-1})	0.02	Baldia *et al*., 2007
K_m	Extinction coefficient of *Microcystis* (m^2 10^{-10} $cells^{-1}$)	0.034	Huisman *et al*., 2004
K_s	Conversion factor from extinction coefficient to Secchi depth	1.7	Liu *et al*., 2010; Zhang *et al*., 2012
K_I	Half-saturation constant for light limitation (µmol m^{-2} s^{-1})	25	Kromkamp and Walsby, 1990
K_{chla}	Conversion factor from Chl*a* to light extinction coefficient (m^2 mg^{-1} Chl*a*)	0.015	Ganf *et al*., 1989
μ_{max}	maximum growth rate of cyanobacteria under ideal conditions	0.8	Xiao *et al*., 2017

Reference:

Baker, D. *et al.* (2023) Variation in resource competition traits among *Microcystis* strains is affected by their microbiomes. *mLife* **2**, 401-415.

Baldia, S. F., Evangelista, A. D., Aralar, E. V. & Santiago, A. E. (2007) Nitrogen and phosphorus utilization in the cyanobacterium *Microcystis aeruginosa* isolated from Laguna de Bay, Philippines. *J. Appl. Phycol.* **19**, 607-613.

Ebina, J., Tsutsui, T. & Shirai, T. (1983) Simultaneous determination of total nitrogen and total phosphorus in water using peroxodisulfate oxidation. *Water Res.* **17**, 1721-1726.

Ganf, G. G., Oliver, R. L. & Walsby, A. E. (1989) Optical properties of gas-vacuolate cells and colonies of *Microcystis* in relation to light attenuation in a turbid, stratified reservoir (Mount Bold Reservoir, South Australia). *Aust. J. Mar. Freshwater Res.* **40**, 595-611.

Hagerthey, S. E., William Louda, J. & Mongkronsri, P. (2006) Evaluation of pigment extraction methods and a recommended protocol for periphyton chlorophyll a determination and chemotaxonomic assessment. *Journal of Phycology* **42**, 1125-1136.

Hu, H. J. *et al.* (1980) Freshwater algae in China. *Shanghai Science and Technology Press*.

Huisman, J. *et al.* (2004) Changes in turbulent mixing shift competition for light between phytoplankton species. *Ecology* **85**, 2960-2970.

Kromkamp, J. & E.Walsby, A. (1990) A computer model of buoyancy and vertical migration in cyanobacteria. *J. Plankton Res.* **12**, 161-183.

Liu, W., Wu, R., Wu, E, Chang, Y. & Chen, W. (2010) Using water quality variables to predict light attenuation coefficient: case study in Shihmen Reservoir. *Paddy. Water Environ.* **8**, 267-275.

Pham, M. L., Askarzadmohassel, E. & Brandl, M. (2023) Growth of freshwater cyanobacterium Aphanizomenon sp. ULC602 in different growing and nutrient conditions. *Front. Microbiol.* **14**, 1220818.

Rossi, S., Carecci, D. & Ficara, E. (2023) Thermal response analysis and compilation of cardinal temperatures for 424 strains of microalgae, cyanobacteria, diatoms and other species. *Sci. Total Environ.* **873**, 162275.

Umlauf, L. & Burchard, H. (2003) A generic length-scale equation for geophysical turbulence models. *Journal of Marine Research* **61**, 235–265.

Wei, S., Zhuang, G., Cheng, L. & Wang, S. (2022) The proliferation rule of Microcystis aeruginosa under different initial pH conditions and its influence on the pH value of the environment. *Environ. Sci. Pollut. Res. Int.* **29**, 13835-13844.

Xiao, M., Adams, M. P., Willis, A., Burford, M. A. & O'Brien, K. R. (2017) Variation within and between cyanobacterial species and strains affects competition: Implications for phytoplankton modelling. *Harmful Algae* **69**, 38-47.

Zhang, Y. *et al.* (2024)Assessment of in-situ monitoring and tracking the vertical migration of cyanobacterial blooms using LISST-HAB. *Water Res.* **257**, 121693.

Zhang, Y., Liu, X., Yin, Y., Wang, M. & Qin, B. (2012) Predicting the light attenuation coefficient through Secchi disk depth and beam attenuation coefficient in a large, shallow, freshwater lake. *Hydrobiologia* **693**, 29-37.